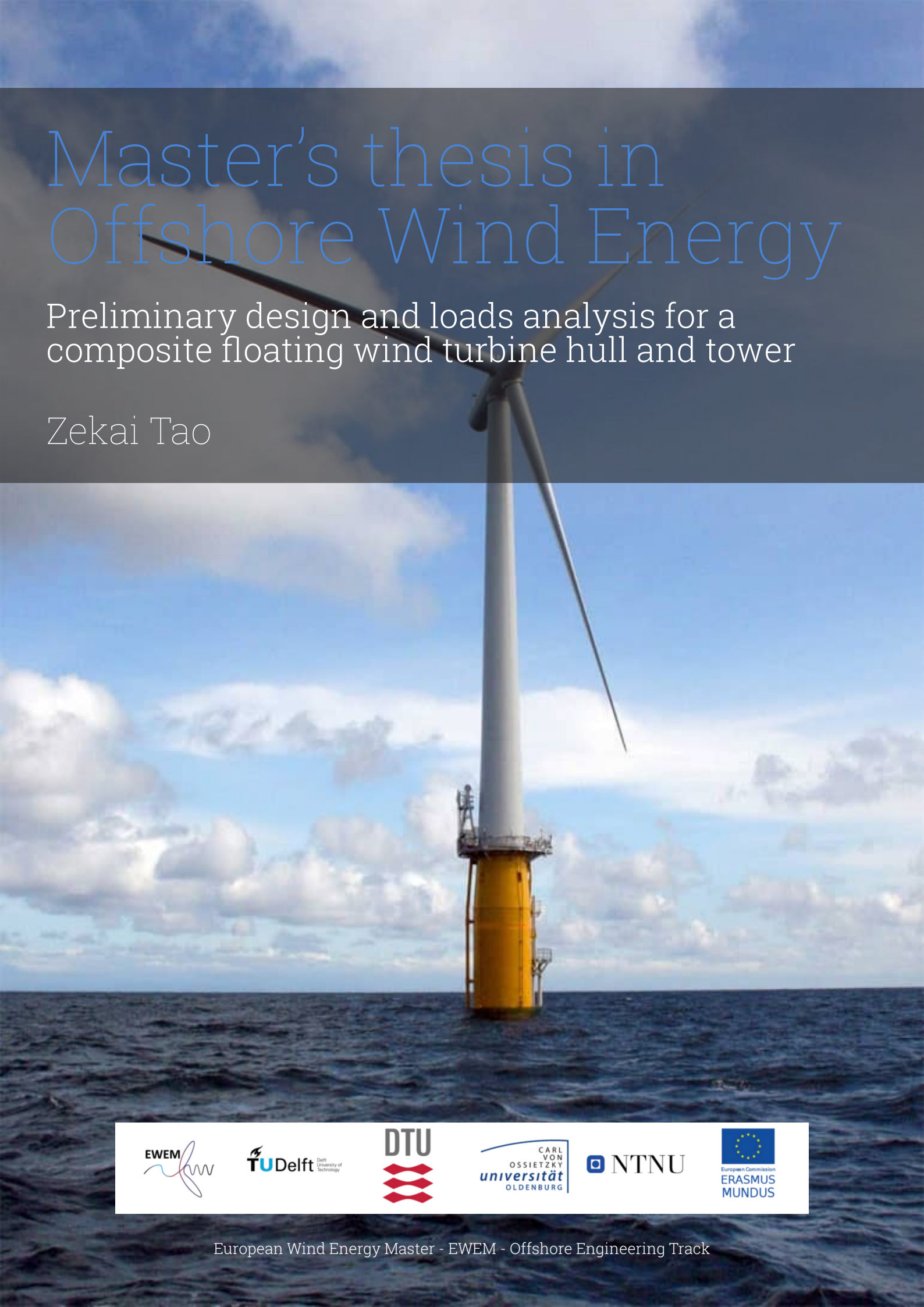

Master's thesis in Offshore Wind Energy

Preliminary design and loads analysis for a composite floating wind turbine hull and tower

Zekai Tao

European Wind Energy Master - EWEM - Offshore Engineering Track

Zekai Tao

Preliminary design and loads analysis for a composite floating wind turbine hull and tower

Master's thesis in Offshore Wind Energy
Supervisor: Erin Bachynski-Polić, Zhaolong Yu, George Lavidas, Vaibhav Raghavan
Co-supervisor: Hallvard Ellingsen Tyldum

Norwegian University of Science and Technology & Delft University of Technology
Department of Marine Technology & Faculty of Mechanical Engineering

Abstract

A design methodology for a monolithic composite spar-buoy platform supporting a 15 MW floating offshore wind turbine is developed and demonstrated. The concept originates from the need to explore composite alternatives to steel structures, with geometry and material choices initially informed by literature on comparable designs and the WindCrete reference model. The structural layout was parametrized in Grasshopper and coupled to a Python-based workflow integrating aero-hydro-servo-elastic simulations (OpenFAST, BModes, HAMS), post-processing (MExtremes, MLife), and optimization (OpenMDAO), enabling automated updates of simulation inputs from parametric geometry changes.

Extreme and fatigue design load cases (DLC6.1, DLC6.3, DLC1.2) following IEC 61400-3 were simulated to assess yielding, buckling, and fatigue performance. Due to the high computational cost of flexible spar simulations, a rigid spar approach was employed, focusing on the tower base as the critical section. Initial assessments revealed that the filament-wound layer was insufficient under extreme loads, which was addressed by increasing its thickness.

An optimization using 10,000 sampled designs identified a configuration with reduced composite thicknesses and an increased tower base diameter, lowering capital expenditure (CAPEX) to 22.67 million € while meeting structural and stability constraints. The optimized CAPEX lies within the reported range for steel spar and tower designs, indicating economic competitiveness. Further improvements, such as a tapered thickness distribution, are expected to enhance cost-effectiveness. The results demonstrate the technical feasibility and economic potential of composite spar-buoy platforms for large-scale FOWTs.

Preface

The idea and inspiration for this master's thesis project were proposed by John Bugge, whose patience and encouragement have been invaluable. I am deeply grateful for his willingness to listen to my explanations and for the positive feedback he has provided during each meeting.

The supervision of this project involved three parties: NTNU, TU Delft, and an external expert in composite materials recommended by John. My supervisors were Erin Bachynski-Polić and Zhaolong Yu from NTNU, George Lavidas and Vaibhav Raghavan from TU Delft, and Hallvard Tyldum from Spilka Industri AS. Each of them has provided valuable guidance when I faced challenges, insightful feedback on the project, and practical instructions on the use of various software tools. I sincerely thank them for their support and expertise.

It has been a challenging yet rewarding experience to complete the European Wind Energy Master's program, spending two years at three universities in three different countries. I am profoundly thankful to my family for their unwavering support and to all the friends I have met over these two years, who have made this journey both enriching and memorable.

In working on this master thesis, I have used artificial intelligence (AI) tools in the following ways: I used ChatGPT to assist with paragraph refinement, language improvements, and the development of the optimization workflow code used in this project. ChatGPT was also used to extract and restructure content from referenced literature to improve the clarity and coherence of the thesis. All content generated with AI assistance has been critically reviewed, edited, and academically assessed by me. AI was not used to generate entire paragraphs or to answer the assignment in its entirety. I have also not uploaded personal data or sensitive information into the AI tool. I am solely responsible for the academic content of the assignment.

Zekai Tao
China, August 2025

Contents

List of Figures

List of Tables

Nomenclature

Abbreviations

Abbreviation	Definition
FOWT(s)	Floating Offshore Wind Turbine(s)
LCOE	Levelized Cost of Energy
MWh	Megawatt-hour
CAPEX	Capital Expenditure
OPEX	Operational Expenditure
DLC(s)	Design Load Case(s)
IEC	International Electrotechnical Commission
ULS	Ultimate Limit State
FLS	Fatigue Limit State
WEC(s)	Wave Energy Converter(s)
COREWIND	Cost REduction and increase performance of floating WIND technology
TLP	Tension Leg Platform
CoG	Center of Gravity
CoB	Center of Buoyancy
CLPT	Classical Laminated Plate Theory
RTM	Resin Transfer Molding
VARTM	Vacuum-Assisted Resin Transfer Molding
ATL	Automated Tape Laying
AFP	Automated Fiber Placement
1P	Rotor's Rotational Frequency
3P	Blade-Passing Frequency
RNA	Rotor-Nacelle Assembly
DoF(s)	Degrees(s) of Freedom
FEA	Finite Element Analysis
FE	Finite Element
ODE(s)	Ordinary Differential Equation(s)
HAMS-MREL	Hydrodynamic Analysis of Marine Structures developed by the Marine Renewable Energies Lab
RAO	Response Amplitude Operator
F-K	Froude–Krylov
KC	Keulegan–Carpenter
CFD	Computational Fluid Dynamics
JONSWAP	Joint North Sea Wave Project
LRFD	Load and Resistance Factor Design
S–N	Stress-Life
RCC	Rainflow Cycle-Couting
WISDEM	Wind-Plant Integrated System Design and Engineering Model
NREL	National Renewable Energy Laboratory
SWL	Still Water Level
PSD	Power Spectral Density
IFFT	Inverse Fourier Transform
RK4	fourth-order Runge–Kutta
AB4	fourth-order Adams–Bashforth

Abbreviation	Definition
ABM4	fourth-order Adams–Bashforth–Moulton
LFEM	Linear Frame Finite Element Formulation
C-B	Craig–Bampton
SIM	Static-Improvement Technique
3D	Three-Dimensional
2D	Two-Dimensional
BEM	Blade Element Momentum
MDAO	Multidisciplinary Design, Analysis, and Optimization
CAID	Computer-aided Industrial Design
CDF	Cumulative Distribution Function
COBLA	Constrained Optimization BY Linear Approximations

Symbols

Symbol	Definition	Unit
g	Gravity acceleration	[m/s^2]
$W_{turbine}$	Turbine weight	[N]
$W_{foundation}$	Foundation weight	[N]
$F_{mooring}$	Mooring pre-tension in z-direction	[N]
M_R	Restoring moment	[N·m]
$\overline{GZ}$	Righting lever	[m]
$\overline{GM_C}$	Distance between metacenter and CoG	[m]
$\overline{BM_C}$	Distance between metacenter and CoB	[m]
$\overline{GB}$	Distance between CoB and CoG	[m]
z_B	Vertical position of CoB	[m]
z_G	Vertical position of CoG	[m]
I_x	Water-Plane second moment of area	[m^4]
K_R	Initial rotation restoring stiffness	[N·m]
T_{max}	Maximum thrust	[N]
E	Young's Modulus	[Pa]
G	Shear Modulus	[Pa]
V	Volume	[m^3]
u	Tower Deflection	[m]
q	Mode shape weight factor	[-]
$\overline{K}$	Generalized stiffness matrix	[N/m] [N/rad] [Nm/m] [Nm/rad]
$\overline{M}$	Generalized stiffness matrix	[kg]
m_{RNA}	Mass of RNA	[kg]
J_{RNA}	Rotation inertia of RNA	[m^4]
L	Length	[m]
I_T	Tower moment of inertia	[m^4]
A_T	Tower sectional area	[m^2]
D_{Tb}	Tower base diameter	[m]
A_{Tb}	Tower base area	[m^2]
I_{Tb}	Tower base moment of inertia	[m^4]
k_{rot}	Rotational stiffness between floater and tower base W_b	Virtual Work [J]
f_i	The natural frequency of the i^{th} DoF	[Hz]
C_{ii}	Hydrostatic stiffness matrix of the i^{th} DoF	[N/m] [N/rad] [N·m/m] [N·m/rad]
A_{ii}	Zero-Frequency added mass matrix of the i^{th} DoF	[kg]
M_{ii}	Mass matrix of the rigid floating platform of the i^{th} DoF	[kg]
p	Water pressure	[Pa]

Symbol	Definition	Unit
k	Wave number	[-]
C_m	Added mass coefficient	[-]
C_p	Dynamic pressure coefficient	[-]
C_d	Drag coefficient	[-]
KC	Keulegan–Carpenter number	[-]
T_w	Wave period	[s]
H	Wave height	[m]
A_j	Individual wave amplitude	[m]
$S(\omega)$	Wave spectrum	[m^2/Hz]
T_p	Wave peak period	[s]
f_p	Wave peak frequency	[Hz]
H_s	Significant wave height	[m]
F^e	External loadings	[N] [N·m]
P_{cr}	Critical structural resistance	[-]
P_{des}	Design load	[-]
M_x	Bending moment along x-axis	[N·m]
M_y	Bending moment along y-axis	[N·m]
M_{xy}	Sum bending moment at x-y plane	[N·m]
M_z	Bending moment along z-axis	[N·m]
N_x	Axial force along x-axis	[N]
N_y	Axial force along y-axis	[N]
N_z	Axial force along z-axis	[N]
T	Torsion moment	[N·m]
R	Cylinder shell outer diameter	[m]
r	Cylinder shell inner diameter	[m]
A	Cross-sectional area	[m^2]
I	Moment of inertia	[m^4]
P_{cr}	Euler's buckling load	[N]
K	Column effective length factor	[-]
L	Unsupported length of column	[m]
D	Total fatigue damage	[-]
n_i	Number of observed stress cycles	[-]
N_i	Number of cycles to failure at the i^{th} stress level	[-]
L_i^{RF}	The i^{th} cycle's load range about a fixed load-mean value	[N] [N·m]
L^{ult}	Ultimate design load	[N] [N·m]
L_{MF}	Fixed mean load	[N] [N·m]
L_i^R	The range of the i^{th} load cycle	[N] [N·m]
L_i^M	The mean load of the i^{th} load cycle	[N] [N·m]
f_{1p}	Rotor loading frequency	[Hz]
f_{3p}	Blade passing frequency	[Hz]
V_{wind}	Hub-height Wind Speed	[m/s]
X_T	Longitudinal tensile strength	[MPa]
X_C	Longitudinal compression strength	[MPa]
Y_T	Transverse tensile strength	[Mpa]
Y_C	Transverse compression strength	[Mpa]
S_{LT}	In-plane shear strength	[Mpa]
E_L	Longitudinal modulus	[Gpa]
E_T	Transverse modulus	[Gpa]
G_{LT}	Shear modulus	[Gpa]
H_{tower}	Tower Height	[m]
$D_{\text{tower base}}$	Tower Base Diameter	[m]
$D_{\text{tower top}}$	Tower Top Diameter	[m]
D_{Spar}	Spar Diameter	[m]
L_{cone}	Cone part length	[m]
V_{50yr}	50-year extreme wind speed	[m/s]

Symbol	Definition	Unit
V_{10yr}	10-year extreme wind speed	[m/s]
V_{in}	Turbine cut-in extreme wind speed	[m/s]
V_{out}	Turbine cut-out extreme wind speed	[m/s]
U_{FW}	Tsai–Wu failure index of filament wound layer	[-]
$U_{material}$	Material failure index of pultruded panel layer	[-]
U_{Buckle}	Buckling failure index of pultruded panel layer	[-]
S_{xy}	The maximum allowable in-plane shear strength	[Pa]
b	The width of panel measured on arc	[m]
r	The radius of curvature	[m]
U_F	Fatigue utilization factor	[-]
J	Polar moment of inertia	[-]
$f(\vec{x})$	Objective function	[€]
m_f	Filament wound layer mass	[kg]
m_p	Pultruded panel mass	[kg]
P_f	Filament wound layer material unit price	[€/kg]
P_p	Pultruded panel layer material unit price	[€/kg]
f_{tower}	Tower first bending frequency	[Hz]
$f_{1P,max}$	The maximum of rotor loading frequency range	[Hz]
$f_{3P,min}$	The minimum of blade passing frequency range	[Hz]
ρ	Water density	[kg/m^3]
∇	Displaced water volume	[m^3]
ν	Poisson's ratio	[-]
ϕ	Mode shape function	[-]
ω	Frequency	[Hz]
Φ	Wave potential	[m^2/s]
ξ	Wave elevation	[m]
$\hat{\zeta}$	Complex response amplitude	[-]
ζ_0	Incident wave amplitude	[-]
θ	Rotation angle	[°]
ϵ	Wave steepness	[-]
λ	Wave length	[m]
η	Wave elevation	[m]
ϵ_i	Individual wave phase angle	[°]
σ	Spectral width parameter	[-]
γ	Peak enhancement factor	[-]
γ_s	Partial safety factor	[-]
γ_l	Partial load factor	[-]
σ_{max}	Maximum normal stress	[Pa]
τ_{max}	Maximum shear stress	[Pa]
λ_{2s}	Wave length for wave period of 2s	[m]
σ_d	The allowable maximum stress for the design	[Pa]
σ_u	The material ultimate strength	[Pa]
γ_m	Material Factor	[-]
σ_x	In-plane normal stress along x direction	[Pa]
σ_y	In-plane normal stress along y direction	[Pa]
σ_{xy}	In-plane shear stress	[-]
σ_{yield}	In-plane yielding normal stress	[Pa]
τ_{yield}	In-plane yielding shear stress	[Pa]
R	Rayleigh-Ritz quotient	[Hz^2]
M	Mass matrix	[kg]
C	Damping matrix	[N·s/m] [N·s/rad] [N·s·m/m] [N·s·m/rad]

Symbol	Definition	Unit
K	Stiffness matrix	[N/m],[N/rad] [N·m/m] [N·m/rad]
$[N]$	CLPT resulting forces from membrane loadings	[N]
$[M]$	CLPT resulting forces from bending loadings	[N]
$[\epsilon^0]$	In-plane strain matrix	[-]
$[\kappa]$	Curvature matrix	[-]
$[A]$	Stiffness matrix of in-plane loads-strain	[N/m] [N/rad],[N·m/m] [N·m/rad]
$[D]$	Stiffness matrix of bending loads to curvatures	[N/m] [N/rad] [N·m/m] [N·m/rad]
$[B]$	Membrane-Bending coupling matrix	[N/m] [N/rad] [N·m/m] [N·m/rad]

1

Introduction

Floating wind energy is increasingly recognized as a critical technology for advancing the energy transition, particularly in Europe. However, despite the potential benefits, the high costs associated with the manufacturing and maintenance of current floating foundations pose significant barriers to large-scale deployment, in particular with the goal of reaching 270GW global capacity of floating offshore wind turbines (FOWT) by 2050, which is equivalent to installing more than 700 units of 15MW FOWT annually, according to [1].

As of 2024, the Levelized Cost of Energy (LCOE) for floating offshore wind turbines in Europe remains higher than that of fixed-bottom offshore wind [2]. According to DNV's 2024 Energy Transition Outlook, the global average LCOE for floating offshore wind is approximately USD 290 per megawatt-hour (MWh), compared to USD 133/MWh for fixed-bottom offshore wind. To achieve the goal of decreasing the LCOE for FOWT to around USD 96/MWh by 2050, one important way is to decrease the cost of the production.

Among the existing floating wind turbine components, the supporting platform and the floater structure account for a considerable proportion of the capital expenditure (CAPEX) [3].

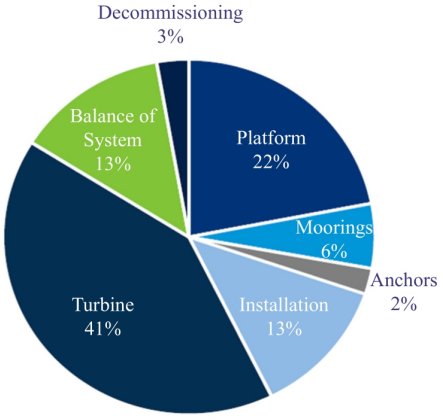

Figure 1.1: 2022 CAPEX Breakdown of Floating Wind Turbine [3]

As the offshore wind industry seeks to reduce both costs and environmental impact, novel materials have been proposed as alternatives to traditional steel or concrete for constructing floating platforms and towers. Among these alternatives, composite materials are particularly promising due to their potential for significant weight reduction and potential lower production costs. When combined with automated manufacturing techniques such as pultrusion and filament winding, composite structures may offer a viable path to reducing the weight and cost of large-scale floating wind substructures.

However, the use of composites typically necessitates specialized manufacturing processes. This study is inspired by the CorPower ocean wave energy converter [4], which utilizes filament winding to manufacture its main structural components—an approach that enhances production efficiency and reduces costs through automated fabrication. Building on this concept, the present work aims to explore the application of composite materials in the design of floating wind turbines to achieve similar advantages.

Pultrusion and filament winding—two automated and efficient manufacturing techniques for producing continuous profile structures—are proposed as suitable methods for fabricating spar-type floaters and towers as a single, integrated unit using composite materials. This integrated approach not only simplifies the manufacturing process but also enhances the structural integrity of the platform. Moreover, composite materials offer significant advantages over steel in marine environments, such as superior corrosion resistance and reduced maintenance requirements [5].

Given the limited number of existing floating wind turbine designs utilizing composite substructures, this study aims to address the following research questions:

1. What are the optimal geometric configurations of a composite spar and tower designed to support the IEA 15MW wind turbine, considering structural performance, hydrodynamic stability, and manufacturing constraints?
2. Compared to steel, what is the economic feasibility of using composite materials for spar buoys in terms of CAPEX?

To address the above research questions, the project is structured into four main phases:

1. Preliminary Design: An initial design of the composite spar and tower was developed, including specification of geometric parameters to satisfy basic hydrostatic stability requirements.
2. Parametric Modeling: The geometry and material properties were parameterized using Grasshopper, enabling flexible model definition and automation. The resulting model was then converted into input files compatible with OpenFAST via a Python-based workflow.
3. The coupled system was simulated in OpenFAST under selected Design Load Cases (DLCs), as defined in international standards IEC 61400-3-1 [6]. This phase evaluates the structural loading and dynamic behavior of the composite spar and tower under extreme weather conditions and operational conditions. The simulation results were stored and subsequently used for both Ultimate Limit State (ULS) and Fatigue Limit State (FLS) analysis.
4. The simulation results were post-processed to extract critical load responses and design conditions. Based on these insights, the structural geometry was optimized with the objective of minimizing the CAPEX. Strength and tower frequency constraints were enforced throughout the optimization process. After completing the optimization, a comparative assessment of CAPEX was performed between the proposed composite design and conventional steel-based spar FOWTs.

2

Literature Review and Background

2.1. Composite application in large scale structure

Composite materials are widely utilized in manufacturing, particularly for small objects, due to their cost-effectiveness, convenience, and excellent performance. However, the anisotropic mechanical behavior, heterogeneous microstructure, and sensitivity to manufacturing defects of composite materials present significant challenges for their large-scale adoption in advanced engineering applications, such as wind turbine blades and aircraft fuselage components [7, 8]. Despite these limitations, numerous trials have been conducted in civil engineering applications, such as bridges and pedestrian pathways, as well as in aerospace for satellite components.

One of the fastest-growing industries utilizing composites for large-scale structures is wind turbine blade manufacturing. The operational conditions of wind turbines impose stringent requirements on the materials including high stiffness to survive extreme weather conditions and sustain the optimal aerodynamic performance, light weight, and long fatigue life.

Wood and composites are two potential candidates for these applications. However, while wood is more environmentally friendly, it has low stiffness and challenges in quality control. As a result, composites remain the state-of-the-art materials for blade manufacturing. The main components of composites are the fiber and matrix. Glass fiber is the most widely used type of fiber, offering moderate stiffness, high strength, moderate density, and excellent cost performance. Carbon fiber, on the other hand, is gaining increasing attention due to its high stiffness-to-density ratio. However, its cost remains prohibitively high compared to glass fiber, limiting its application in turbine blades. The matrix, typically made of thermosetting or thermoplastic polymers, are rather soft and flexible for the purpose of binding the fibers together and transferring the loads between them. The connection techniques used between composite blades and the nacelle, as well as between blade sections presented in Figure 2.1, can be studied and adapted for connecting the composite foundation to the nacelle and for connecting foundation sections to one another [9].

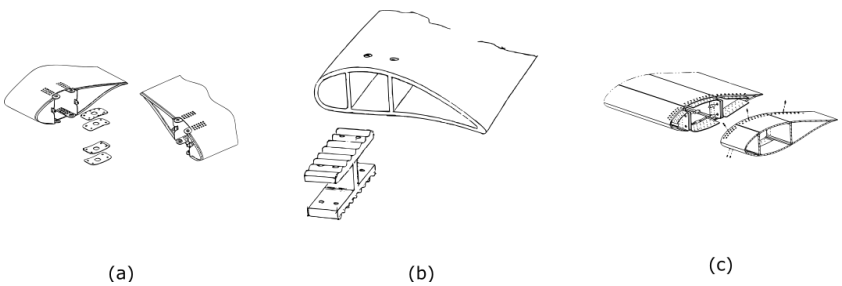

Figure 2.1: Blade section connections [9]

Another interesting application of composites in large-scale structures is ship hulls [10]. Similar to blade

applications, the unique marine operating conditions impose specific requirements on material properties. A particularly notable advantage is the superior corrosion resistance of composites compared to traditional metal materials, making them highly suitable for harsh marine environments. Additionally, their lightweight nature reduces fuel consumption, thereby improving operational efficiency.

Building on the experience of applying composite materials to ship hulls, composites have also been utilized in the renewable energy sector, particularly in wave energy converters (WECs). CorPower Ocean, in collaboration with the composite manufacturing company AUTONATIONAL, developed a composite point absorber wave energy converter [4]. The WEC is produced using filament winding as shown in Figure 2.2, an automated process in which composite materials are precisely wound along a mandrel in predefined directions. This automated process enables on-site fabrication at dock locations, significantly simplifying transportation logistics. Furthermore, automation reduces reliance on manual labor, thereby lowering manufacturing costs and enhancing production efficiency. This serves as an inspiration for this project, aiming to leverage similar automated manufacturing processes to reduce the high transportation and labor costs associated with floating wind turbines.

Figure 2.2: Filament winding application to fabricate the CorPower WEC [4]

These examples demonstrate the potential of composite materials for application in large-scale structures.

2.2. Design of new material application in offshore wind

O'Leary et al. [11] investigated an innovative offshore wind turbine tower design using composite materials to support a NREL 5 MW reference turbine. The proposed design incorporates a combination of filament winding and pultrusion for tower fabrication as depicted in Figure 2.3, based on a comprehensive literature review of similar studies. This review identifies filament winding, combined with an additional process enabling longitudinal fiber placement, as the most suitable method for constructing composite offshore wind turbine support structures.

The study focuses on developing an optimization framework to refine preliminary design geometries, which are largely constrained by manufacturing and transportation considerations. The optimization process employs gradient-based algorithms, using FAST as the numerical tool for loading assessment, ensuring compliance with criteria for buckling, fatigue, ultimate strength, and natural frequency.

With the optimized geometries of the composite tower, the study further investigates LCOE for the design. The analysis reveals that, with an extended operational lifetime and appropriate financing strategies, the LCOE of a composite tower could be economically competitive with that of a conventional steel tower.

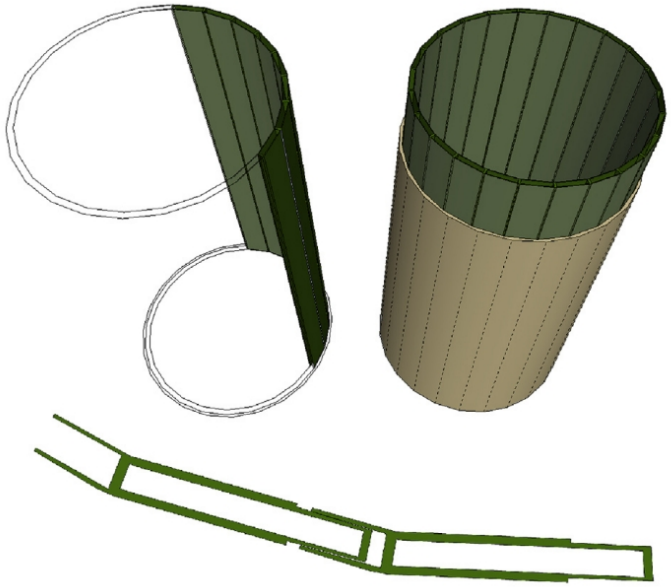

Figure 2.3: Pultruded double wall panel sections (green) bound together by filament wound laminate (light brown) [11]

.

Van der Zee et al. [12] investigated a conceptual composite tower design to support a DTU 10 MW offshore wind turbine. The study evaluates loading conditions based on IEC 61400-3 design standards and North Sea environmental conditions. Initial geometries are set to match those of a reference steel tower, and two preliminary composite tower designs are developed based on equivalent stiffness and strength characteristics compared to the steel tower. Both designs were proposed to be filament wound sandwich composite structure, with materials selected as glass-fiber and reinforced epoxy resin.

The designs are categorized as the ”soft-stiff” tower, with a natural frequency located between the 1P and 3P excitation frequency ranges, and the ”soft-soft” tower, with a natural frequency below 1P and between the wind and wave excitation frequency ranges. The ”soft-stiff” tower was found to be over-dimensioned for equivalent stiffness, resulting in a heavier structure than the steel tower, making it uncompetitive compared to traditional steel tower designs. In contrast, the ”soft-soft” tower is significantly more flexible and aligns with the project’s goal of achieving a lightweight design. Therefore, this concept was further developed to ensure sufficient strength to withstand extreme design loads while maintaining its lightweight characteristics.

Similarly, the C-Tower project [12] developed an optimization framework utilizing FOCUS6 software as the simulation tool. To minimize computational effort while maintaining optimization accuracy, the wall thickness was chosen as the sole design variable, with other geometric parameters preliminarily defined to ensure that the tower’s eigenfrequency falls within the 1P range. To address potential issues arising from the simplified optimization approach, a comprehensive load case analysis and fatigue load assessment were performed as validation checks.

After the optimization process is finished, the largest tower top deflection in the ultimate load cases was found less than 3°. The final optimized geometries show a 34% mass reduction compared to the reference steel tower.

One concern of the C-Tower project is it’s assumed that the tower is manufactured as a single piece using filament winding. In contrast, other studies propose fabricating the tower in multiple sections, enabling more practical transportation and easier assembly at the dockside. This assumption may overlook the geometric limitations of filament winding manufacturing, potentially leading to feasibility issues. This could be a contributing factor to why phase 2 of the project, which proposed creating a 1:10 prototype for experimental testing, did not proceed since 2017.

Instead of using composite materials, the EU Horizon 2020 project COREWIND (Cost REduction and

increase performance of floating WIND technology) [13] developed a conceptual design for a concrete spar buoy named WindCrete. One feature of this design is that the tower and foundation are modeled as a single rigid body and manufactured as one continuous, seamless piece. This monolithic approach is intended to optimize the construction process, extend the structure's lifetime, and reduce maintenance costs. A similar dockside construction strategy was also adopted for the Hywind Tampen spar [14], which was fabricated in one piece to minimize offshore assembly requirements and enhance structural integrity.

The WindCrete project outlines a comprehensive design process and evaluates the structure's simulated responses under selected design load cases in both static and dynamic conditions. The study presents the resulting natural frequencies obtained through free decay simulations, the static equilibrium offsets caused by nacelle center of gravity (CoG) position offsets, and the impacts of second-order hydrodynamic forces. These include contributions from mean drift, as well as difference-frequency and sum-frequency components. The second-order effects were found to be negligible in the WindCrete study, which justifies the use of only first-order wave loading in the present project without compromising the accuracy of structural response predictions.

C. Molins et al. [15] investigated the response of the WindCrete design under various load cases different from the COREWIND project. The results indicate that, under mild wave conditions, the motion responses of the 15 MW FOWT are primarily influenced by low-frequency forces. Consequently, the motions are dominated by wind forces and second-order wave forces rather than first-order wave forces. The WindCrete concept is presented in Figure 2.4.

Figure 2.4: WindCrete monolithic design with residual compounds as ballast [13]

.

Andrew C. Young et al. from the University of Maine [16] proposed a novel semi-submersible floating wind turbine design featuring a composite tower, named VolturnUS, to support a 6 MW turbine. The design process involves solving an optimization problem to develop a composite tower capable of withstanding severe weather conditions while meeting strength requirements and minimizing tower mass.

A comparison between steel towers, solid composite towers, and sandwich panel composites was conducted, demonstrating that the minimum mass is achieved with a solid shell composite configuration under reasonable design constraints.

In the preliminary design phase of VolturnUS, ANSYS shell Finite Element (FE) analysis was utilized to verify that the tower's natural frequency does not coincide with excitation frequencies from the turbine. Additionally, a linear buckling analysis was conducted to ensure the tower's structural integrity under expected loading conditions.

The design variable in the optimization process was set as the thickness of the tower, with constraints on frequency, stress, and buckling. Fatigue was excluded from the optimization iterations and checked after optimization, as it was determined not to be a design driver for the turbine tower and would significantly increase the computational time. The results revealed that the steel tower concept weighs at least 2.21 times the optimized composite tower, which is constructed using E-glass/epoxy. The concept comparison and a 1:8 model are presented in Figure 2.5 and 2.6.

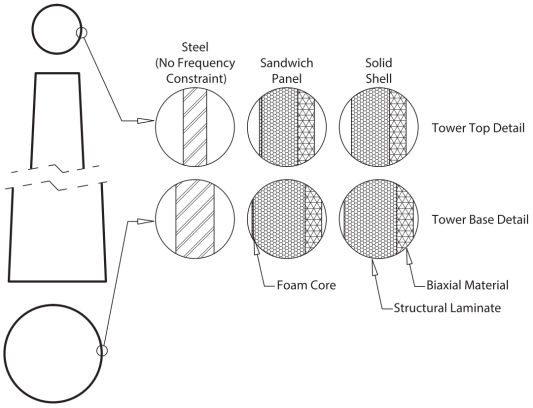

Figure 2.5: VolturnUS concepts comparison [16]

.

Figure 2.6: VolturnUS 1:8 model with composite tower [16]

2.3. Optimization strategies of offshore wind turbine

FOWTs remain an emerging technology, with high capital and operational costs posing major barriers to large-scale commercial deployment. Among these cost components, CAPEX is the most critical, representing up to 75% of the total investment [17]. The limited technological maturity, together with the pronounced variability of site-specific environmental conditions, makes it difficult to establish a universally optimal design for FOWT systems. Consequently, numerous studies have sought to reduce CAPEX by employing optimization workflows that focus on minimizing structural mass or adopting material-efficient substructure configurations. However, such mass-reduction strategies must also ensure compliance with essential design constraints, including structural integrity, stability, and platform motion limits. As a result, recent research has increasingly adopted optimization frameworks that concurrently address cost, structural reliability, and overall system performance across a wide range of operating conditions [17].

The Wind-Plant Integrated System Design and Engineering Model (WISDEM) [18], developed by the National Renewable Energy Laboratory (NREL), is a modular framework designed to support multidisciplinary analysis and optimization of wind energy systems. It couples physics-based engineering models with detailed cost estimation modules, enabling integrated assessments of both technical performance and economic viability. WISDEM has been widely adopted in wind turbine research for early-stage design studies, where design variables such as geometry, structural parameters, and control settings are optimized under techno-economic constraints. In recent years, its application has been extended to floating offshore wind systems, although its original architecture was primarily developed for fixed-bottom configurations. Within the WISDEM framework, OpenFAST is employed to simulate system dynamics, evaluate structural responses, and estimate energy production, while the optimization process is handled by OpenMDAO [19], which provides a flexible environment for implementing both gradient-based and gradient-free optimization strategies.

However, in order to ensure numerical stability and computational efficiency during the optimization process, WISDEM relies on relatively low-fidelity modeling approaches. While this simplification enables rapid evaluation over large design spaces, it can limit the accuracy of subsystem-level predictions, particularly when modeling the complex hydrodynamic responses of floating offshore wind platforms. Moreover, WISDEM does not provide analytic gradients for the coupled models, meaning that gradient-based optimization must rely on finite-difference approximations at the system level. This approach can introduce numerical noise and increase computational cost, especially when the number of design variables is large.

Conducting high-fidelity simulations for FOWTs is computationally intensive. A single time-domain simulation can take several hours or even days, particularly when modeling complex platform dynamics and aerodynamic-hydrodynamic interactions. Furthermore, design standards such as IEC 61400-3 mandate extensive load case evaluations under various environmental conditions and random seeds, resulting in hundreds or even thousands of simulations per design iteration. This computational burden presents a major obstacle to performing efficient optimization. One promising approach to address this challenge is the use of surrogate models, which approximate the behavior of high-fidelity models with significantly reduced computational effort.

To improve the computational efficiency of the optimization process, one common approach is to linearize the system dynamics and perform simulations in the frequency domain. This significantly reduces computational cost by assuming a linear relationship between system responses and external excitations. However, this linearization inherently limits model fidelity, particularly in capturing nonlinear behaviors such as large-amplitude motions, nonlinear damping, or coupling effects, which are critical in floating offshore wind applications. Therefore, caution and engineering judgment should be exercised when interpreting frequency domain results.

Hegseth et al.[20] conducted an integrated design optimization study using a linearized model of a spar-type floating wind turbine. The model encompassed key subsystems including the platform and tower, mooring lines, and the turbine's control system. The objective was to maximize a weighted sum of power quality and system cost, subject to constraints derived from both extreme and fatigue loading scenarios. Given the multidisciplinary nature of the problem, OpenMDAO was adopted as the optimization framework.

The resulting optimal design features a reduced diameter in the wave-exposed region to minimize hydrodynamic loading, and an hourglass-like shape below the waterline. This configuration increases pitch restoring moments and raises the natural frequency in pitch, thereby enhancing the system's response characteristics in low-frequency regimes. The study also concludes that, despite the simplifications inherent in frequency-domain modeling, the linearized approach remains sufficiently accurate in capturing key design trends when compared to full time-domain simulations.

Kalimeris [21] developed a surrogate-assisted optimization framework based on a linearized frequency-domain model of a semi-submersible floating wind turbine. The study focused on the trade-off between platform CAPEX and power quality, proposing two surrogate modeling strategies to improve computational efficiency: the End-to-End approach and the PyHAMS approach. The former replaces the entire RAFT-based simulation workflow with a surrogate model trained to predict key outputs for optimization, such as power quality objectives and constraint variables. The latter targets only the potential flow analysis module within RAFT—specifically the generation of the wetted surface mesh and the solution of potential flow equations—by approximating the added mass matrix A, hydrodynamic damping matrix B, and excitation force vector X.

The optimization results reveal that improvements in power quality are generally associated with increased substructure cost. While the End-to-End approach yields substantial reductions in simulation time, it introduces greater approximation errors. In contrast, the PyHAMS surrogate achieves a more favorable balance between accuracy and efficiency, requiring fewer training samples while producing results comparable to the full simulation. This work illustrates the potential of hybrid surrogate-assisted workflows to support tractable and scalable FOWT design optimization, particularly under computational constraints.

As offshore wind turbines are deployed in increasingly deep waters, the geometries of turbines and floating substructures have become larger and more complex, posing challenges for design workflows—particularly in managing parametric variations and ensuring clarity in geometry definition. To address these issues, integrating parametric modeling tools with simulation platforms has been explored to streamline the design process and enhance visual feedback.

Deng et al.[22] proposed a modular framework that links Grasshopper, used for parametric geometry definition and real-time visualization, with the FAST aeroelastic simulation tool. Applied to a 10MW blade optimization, the framework demonstrates how Grasshopper can serve as an effective front-end for geometry control (see Figure 2.7), while FAST performs physics-based performance evaluation. This approach enables efficient parameter exploration and improves transparency in the design process, particularly for structures with complex geometries.

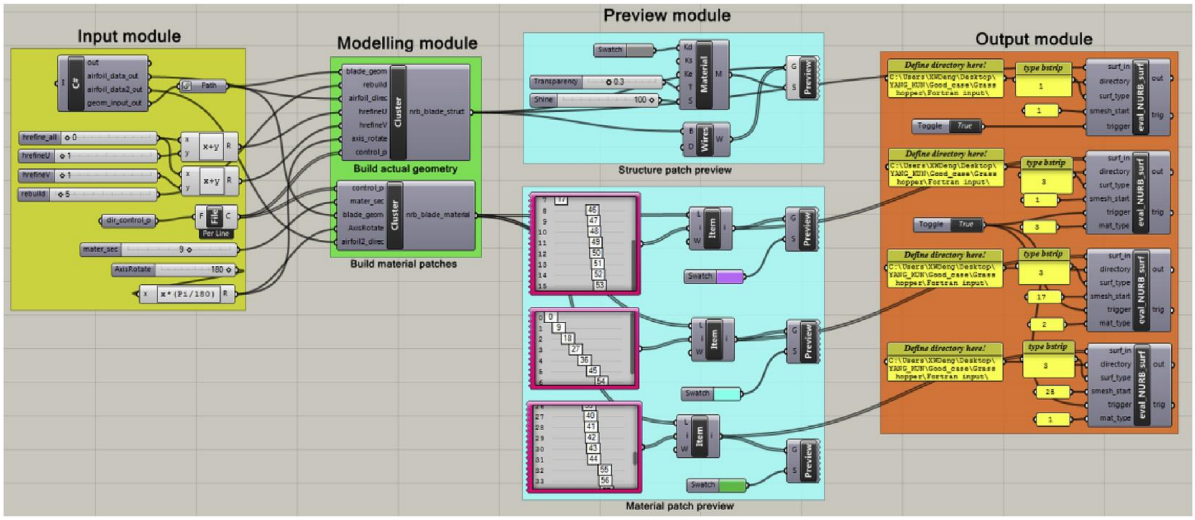

Figure 2.7: . Framework of 3D modeling by using Grasshopper [22]

To achieve higher simulation accuracy, nonlinear time-domain analysis is typically required. In a formal

FOWT design workflow, structural feasibility must be verified in accordance with engineering standards such as IEC 61400-3. This involves conducting time-domain simulations across a comprehensive set of DLCs, which represent various operational and extreme conditions. However, such simulations are computationally intensive and can impose significant burdens on the optimization process.

In the study by O'Leary et al.[11] as mentioned previously, structural responses were evaluated using nonlinear time-domain simulations rather than frequency-domain analysis. Several selected DLCs from IEC 61400-3 were employed to cover both ULS and FLS conditions. Due to the high level of wind field discretization required for operational conditions such as DLC 1.2, it was deemed impractical to simulate every generated design in each optimization iteration. Moreover, re-running time-domain simulations at each step could introduce variability into the optimization process, potentially leading to divergence from the true optimum as the algorithm adapts to inconsistent responses.

To address these challenges and reduce computational cost, the framework relied on FAST simulation results from the initial baseline design and applied them to subsequent geometry updates without re-simulating each variation. While this approximation significantly improved computational efficiency, it introduced inaccuracies that could affect the reliability of the optimization outcomes. Nevertheless, the authors concluded that the achieved level of accuracy was acceptable for a preliminary design study.

2.4. Summary

In conclusion, existing literature highlights the significant potential of composite materials for large-scale structural applications, particularly in floating offshore wind turbines. Owing to their lightweight characteristics, high specific strength, corrosion resistance, and versatility in manufacturing, composites offer new opportunities for the design of both turbine towers and floating substructures. Demonstration projects such as VolturnUS, featuring an optimized composite tower, illustrate how alternatives to steel can satisfy structural strength requirements while reducing overall mass.

Furthermore, advances in manufacturing techniques—such as continuous filament winding—and the optimization of key design parameters, including wall thickness and natural frequency tuning, have demonstrated that composite-based structures can withstand extreme loading conditions while maintaining competitive cost performance. Collectively, these studies confirm the technical feasibility and economic viability of composites as a robust alternative to conventional steel structures, thereby motivating the investigation of composite spar platforms and towers in the present study.

In addition to supporting the use of composite materials, the literature also offers valuable methodological insights for structural optimization. These include guidance on constructing the overall optimization workflow, selecting appropriate objective functions, choosing suitable optimization algorithms, and implementing strategies to accelerate the computational process.

3

Theory

This chapter introduces the key theoretical foundations adopted in this project. Section 3.1 presents the derivation of the initial stability calculation for the floating platform design. Section 3.2 outlines the equations used to characterize composite materials, incorporating both material properties and the influence of the selected manufacturing processes. Modal analysis is presented in Section 3.3, with emphasis on avoiding resonance between the tower's natural frequencies and the turbine's 1P and 3P frequencies, as well as dominant excitations from wind and wave loading. The hydrodynamic force calculations are addressed through potential flow theory and Morison equation in Section 3.4. Section 3.5 describes the wave models employed in the study and their applicable conditions. Section 3.6 introduces how the equations of motions are established in the time-domain for floating structures. Structural assessment methods, including yield, buckling, and fatigue criteria, are detailed in Section 3.7. Finally, the Section 3.8 outlines the formulation of the optimization problem.

3.1. Hydrostatics and stability of FOWT

The most popular FOWT concepts are categorized into three main types: spar buoy, semi-submersible and tension leg platform (TLP) depicted in Figure 3.1.

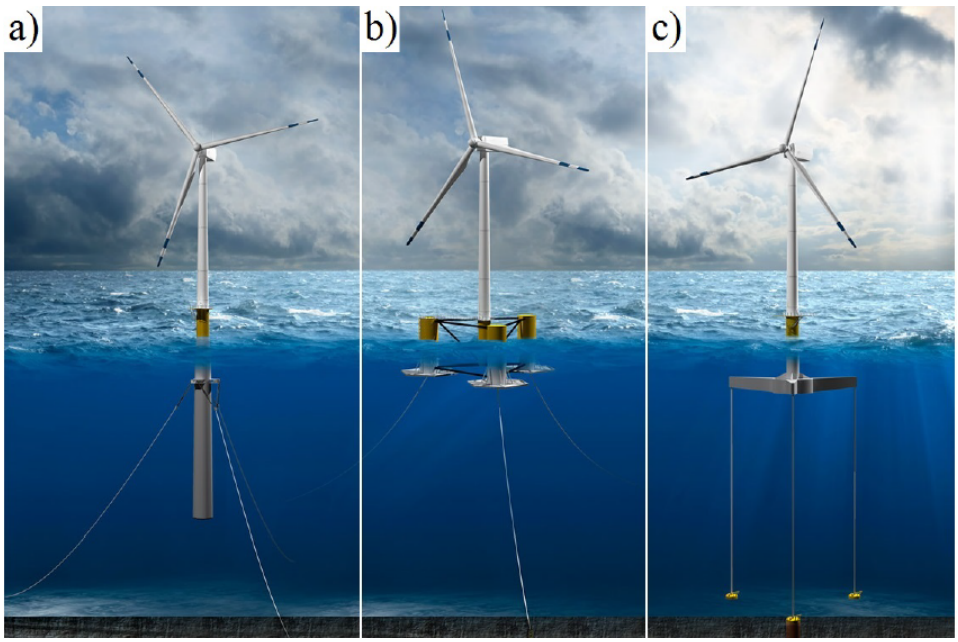

Figure 3.1: Three main floating wind concepts. a) spar buoy, b) semi-submersible, c) TLP [23]

The motion coordinate system of a FOWT system is defined by 6 DoFs, which include translations along the x, y, and z axes, referred to as surge, sway, and heave, respectively, as well as rotations around the x, y, and z axes, known as roll, pitch, and yaw. A typical motion coordinate system of a FOWT is illustrated in Figure 3.2. With this motion system defined, the stability of a FOWT can be understood as its ability to maintain or restore equilibrium when subjected to external environmental forces such as wind, current, and waves. This includes the system's capacity to minimize excessive motions and effectively utilize restoring forces to return to a stable state.

The classification of the three types of FOWT presented in Figure 3.1 arises from three primary stabilizing mechanisms: ballast-stabilized, water-plane-stabilized, and mooring-stabilized. Rather than relying exclusively on one stabilizing method, FOWT designs typically incorporate elements of all three, forming a hybrid system where one mechanism dominates. For this project, the spar buoy type was chosen due to its simple geometry and compatibility with the selected composite manufacturing process, as will be discussed in the following section. For the selected spar buoy type, high-density materials such as concrete are typically used as ballast to lower the center of gravity of the structure, thereby enhancing the ballast-stabilized restoring moment.

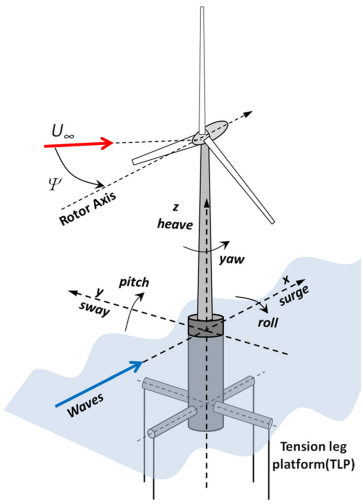

Figure 3.2: FOWT 6 DoFs coordinate system [24]

To maintain the stability of a floating system, the first fundamental requirement is to ensure flotation. This means that the weight of the system must equal the buoyant force and the vertical component of mooring pre-tension acting on it. With Archimedes' law to calculate the buoyancy, this relationship can be expressed as shown in Eq.3.1.

$$\rho_w \nabla g = W_{turbine} + W_{foundation} + F_{mooring} \tag{3.1}$$

where ρ_w, ∇, $W_{turbine}$, $W_{foundation}$, $F_{mooring}$ stand for the sea water density, displaced water volume, turbine weight, foundation weight and mooring pre-tension in z-direction. While every object has a center of gravity (CoG) representing the point where gravitational force is concentrated, a floating object also has a center of buoyancy (CoB), which represents the point where the buoyant force, acting upward could be assumed to be concentrated. CoB is thus defined as the center of the submerged body.

For a stable floating object, when a small rotational displacement θ in pitch or roll is applied to the system, CoG remains fixed relative to the local coordinate system, while the CoB may shift. The first two stabilizing mechanisms, ballast-stabilized and water-plane-stabilized, can be better understood by examining changes in the CoB position. In contrast, the third stabilizing mechanism, mooring-stabilized, is governed by the stiffness of the mooring lines attached to the system. Since the mooring system acts as an external stabilizing system, the first two mechanisms represent the inherent or initial stability of the floating body, which can be quantitatively evaluated through the restoring moment M_R.

The first two mechanisms can be illustrated in Figure 3.3 and are expressed as a restoring moment M_R. From the figure it shows that the shift of CoB introduces the restoring moment M_R which could be expressed as Eq.3.2. If the floating object is a FOWT, by introducing Eq.3.1 this could be further expressed as Eq.3.3.

$$M_R = \rho_w g \nabla \overline{GZ} \tag{3.2}$$

$$M_R = (W_{turbine} + W_{foundation}) \overline{GZ} \tag{3.3}$$

To evaluate the righting lever $\overline{GZ}$, the concept of metacenter position M_C is introduced. The metacenter M_C as presented in Figure 3.3, is typically assumed to be located at a fixed point defined as the intersection between the centerline of the cross-section containing the CoG and the original CoB, and the vertical line passing through the new CoB resulting from a small angular displacement θ of the body. This definition gives:

$$\overline{GZ} = \overline{GM_C} \sin\theta \tag{3.4}$$

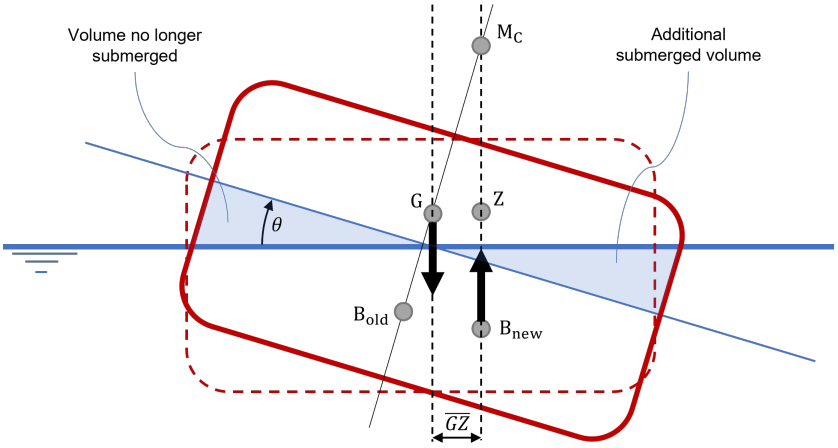

Figure 3.3: The formed restoring moment from new CoB and old CoG [25]

To calculate $\overline{GM_C}$, as observed from the figure it could be expressed as:

$$\overline{GM_C} = \overline{BM_C} - \overline{GB} \tag{3.5}$$

where $\overline{GB}$ is the distance between CoB and CoG, and could be thus defined as:

$$GB = z_B - z_G \tag{3.6}$$

while $\overline{BM_C}$ is the distance between CoB and M_C. For small angle displacement, BM_C could be calculated as:

$$\overline{BM_C} = \frac{I_x}{\nabla} \tag{3.7}$$

where I_x is the water-plane second moment of area and could be expressed as an integration assuming small angle displacement:

$$I_x = \iint x^2 dS \tag{3.8}$$

Combining these equations, the initial restoring moment M_R equation is:

$$M_R = \overline{GM_C} \sin\theta = \rho_w g \nabla \left(\frac{I_x}{\nabla} + (z_B - z_G) \right) \sin(\theta) \tag{3.9}$$

From this, it can be observed that the initial stability provided by the first two stabilizing mechanisms is determined by the distance $\overline{GM_C}$, known as the metacentric height. This distance indicates that increasing the water-plane area enhances the restoring moment, representing the water-plane-stabilized mechanism, while increasing the distance $\overline{GB}$ enhances the restoring moment, representing the ballast-stabilized mechanism. These factors underscore the importance of the metacentric height in evaluating the stability of the floating body, as it directly governs the magnitude of the restoring moment.

As this definition of metacenter is only applicable for small angle displacements, the restoring moment could be further simplified as:

$$M_R = \rho_w g \nabla \overline{GM_C} \theta \tag{3.10}$$

This gives the initial rotation restoring stiffness K_R for a small angle displacement θ as:

$$K_R = \rho_w g \nabla \overline{GM_C} \tag{3.11}$$

In the preliminary design of a FOWT, it is essential to ensure that the initial restoring moment is sufficient to maintain stability. To achieve this, the rotation angle is typically limited to no more than 10 degrees under rated performance conditions, which corresponds to the maximum thrust force T_{max} acting on the turbine plane at the hub height h_t [26]. This could be expressed by the following equation:

$$K_R = \rho_w g \nabla (\frac{I_x}{\nabla} + (z_B - z_G)) \geq \frac{T_{max} \cdot h_t}{\theta_{max}} \tag{3.12}$$

Here θ_{max} is considered as 10 degrees and applied in the preliminary design of this project with 1 DoF approximation.

3.2. Composite Material Property and Manufacturing Process

3.2.1. Composite Material

Compared to traditional materials like steel used in marine engineering applications, most engineering composites exhibit anisotropic properties due to their composition of at least two distinct materials. These materials form the reinforcement and matrix components of the composite. The reinforcement provides stiffness and strength, while the matrix binds the material together and transfers loads between the reinforcements. For example, an epoxy resin reinforced with continuous graphite fibers demonstrates this anisotropy by exhibiting very high strength and stiffness along the direction of the fibers, while showing significantly lower mechanical properties in the transverse or normal directions [27].

This anisotropy results in a greater number of parameters needed to describe the material properties of composites compared to isotropic materials like steel. For steel, the mechanical properties can be fully characterized by just two engineering constants: Young's Modulus E and Poisson's Ratio ν. In contrast, a single ply of composite material requires at least four constants for a complete description: the longitudinal Young's Modulus E_L, transverse Young's Modulus E_T, major Poisson's Ratio ν_{12}, and Shear Modulus G_{12}. The ply coordinate system refers to Figure 3.4.

With this anisotropy property, composite plies can be stacked together with fibers oriented at various angles θ to form a laminate. This stacking configuration allows the mechanical properties of the composite material to be tailored and improved, optimizing its performance for specific loading conditions and applications. The laminate coordinate system and the variations in modulus with respect to ply angles are illustrated in Figure 3.5 and Figure 3.6 [27].

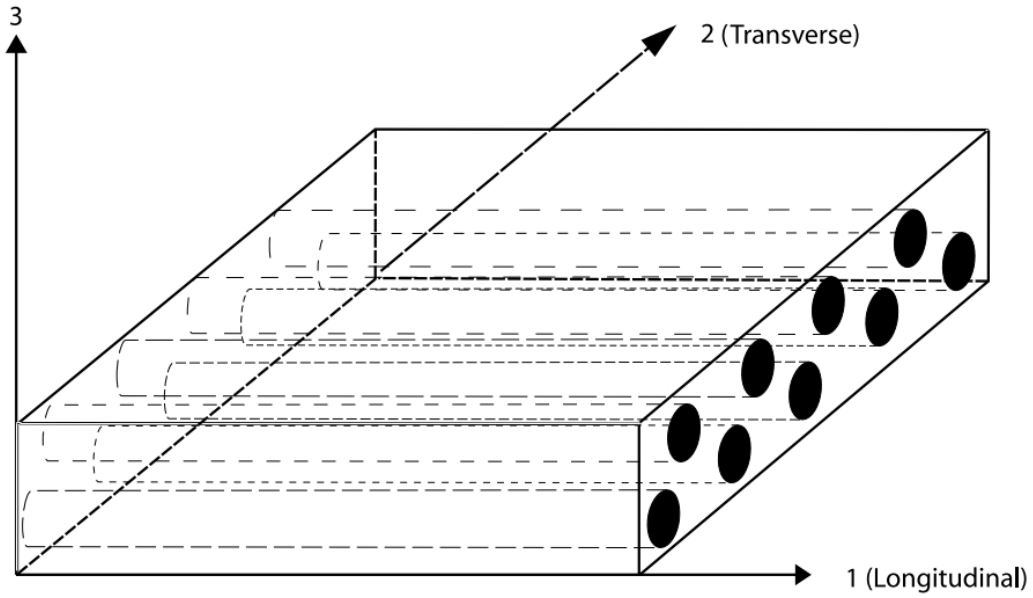

Figure 3.4: Ply coordinate system [27]

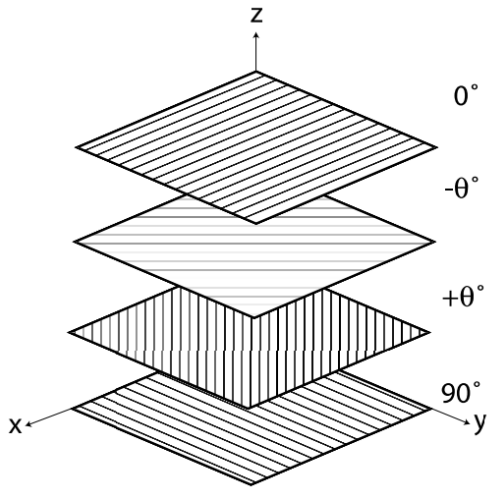

Figure 3.5: Laminated composite coordinate system

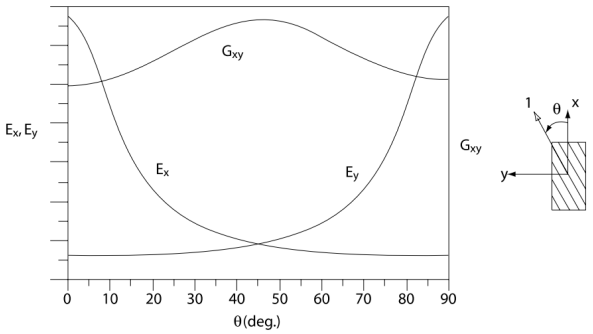

Figure 3.6: Laminate modulus as a function of ply angle

3.2.2. Classical Laminated Plate Theory (CLPT)

To address the complex properties of laminates, CLPT is employed. By utilizing the properties of each ply, the ply angles, and the laying sequence, the effective properties of the laminate can be determined. Typical laminate analysis software, such as CompositePro, ESAComp, HyperSizer, Laminator, and V-Lab, utilizes CLPT to facilitate this process. Users input and define these parameters, and the software outputs key results such as the stiffness matrix, engineering properties, and the corresponding stresses and strains [27].

A typical laminate is subjected to both membrane (in-plane) and bending loads as presented in Figure 3.8. CLPT assumes that the resulting strains and curvatures are uniform throughout the laminate. However, since the plies are oriented in all directions, the stresses are continuous only within a single ply. This is presented in Figure 3.8.

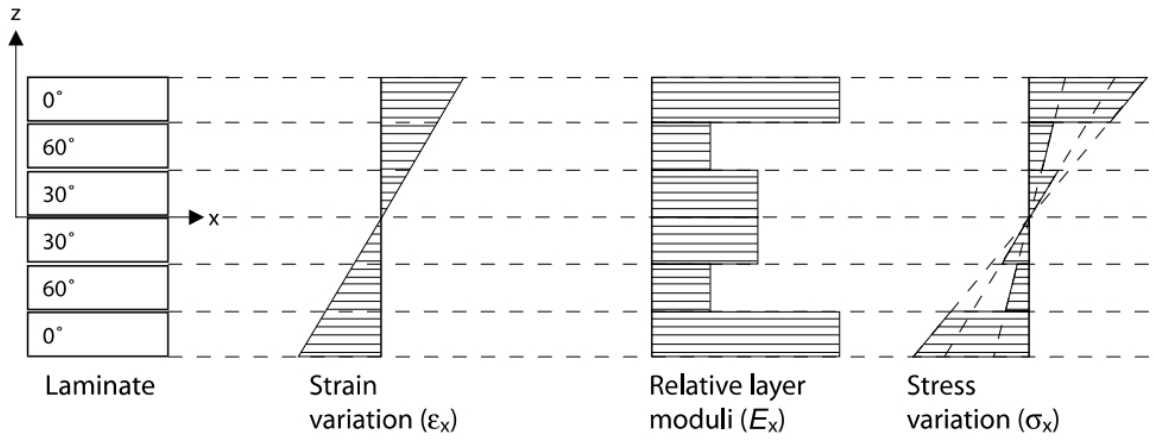

Figure 3.7: Variation of strain, modulus and stress in a laminate subjected to bending [27]

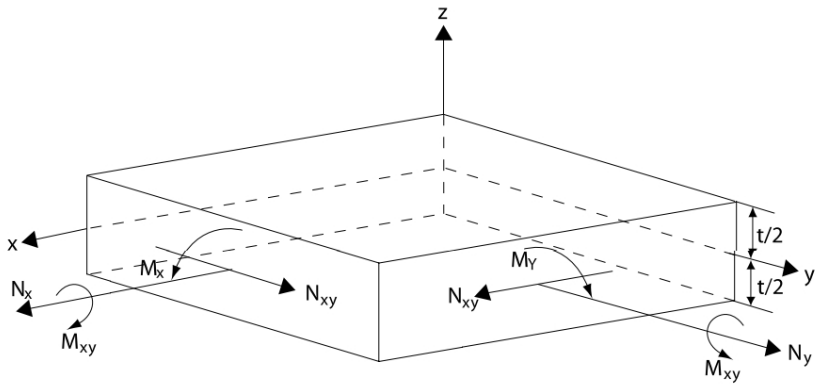

Figure 3.8: Resulting forces and moments on an element, membrane – [N_x, N_y, N_{xy}], bending – [M_x, M_y, M_{xy}] [27]

The general form of the laminate stress-strain [27] is given by:

$$\left[\begin{array}{c} N_x \\ N_y \\ N_{xy} \\ \hline M_x \\ M_y \\ M_{xy} \end{array}\right] = \left[\begin{array}{ccc|ccc} A_{11} & A_{12} & A_{16} & B_{11} & B_{12} & B_{16} \\ A_{12} & A_{22} & A_{26} & B_{12} & B_{22} & B_{26} \\ A_{16} & A_{26} & A_{66} & B_{16} & B_{26} & B_{66} \\ \hline B_{11} & B_{12} & B_{16} & D_{11} & D_{12} & D_{16} \\ B_{12} & B_{22} & B_{26} & D_{12} & D_{22} & D_{26} \\ B_{16} & B_{26} & B_{66} & D_{16} & D_{26} & D_{66} \end{array}\right] \left[\begin{array}{c} \varepsilon_x^0 \\ \varepsilon_y^0 \\ \gamma_{xy}^0 \\ \hline \kappa_x \\ \kappa_y \\ \kappa_{xy} \end{array}\right] \tag{3.13}$$

and could be written in a simplified form:

$$\begin{aligned} [N] &= [A]\left[\varepsilon^0\right] + [B][\kappa] \\ [M] &= [B]\left[\varepsilon^0\right] + [D][\kappa] \end{aligned} \tag{3.14}$$

where the matrix $[N]$ and $[M]$ represent the resulting forces from membrane and bending loadings, respectively. The term $[\epsilon^0]$ denotes the in-plane strain, where the superscript 0 specifies that the strain is referenced to the laminate's mid-plane, and $[\kappa]$ represents the curvature. The stiffness matrices $[A]$, $[B]$, and $[D]$ characterize the laminate's mechanical behavior. Specifically, $[A]$ relates in-plane loads to in-plane strains, while $[D]$ relates bending loads to curvatures. The coupling matrix $[B]$, known as the membrane-bending coupling matrix, describes the interaction between in-plane loads and bending moments. This coupling indicates that, under appropriate conditions, a purely in-plane load can induce warping in the laminate, or a pure bending moment can result in stretching of the laminate.

For a symmetric laminate, which means that each ply on one side of the laminate mid-plane, there is a corresponding ply on the other side of the mid-plane at the same distance and of the same material, thickness and orientation, in this case the coupling matrix $[B]$ is 0 and the stress-strain relation could be further simplified as:

$$\begin{aligned}[N] &= [A]\left[\varepsilon^0\right] \\ [M] &= [D][\kappa]\end{aligned} \tag{3.15}$$

3.2.3. Rule of mixture

Unlike laminated composites, homogeneous composites with uniform composition and unidirectional fiber configurations, such as pultrusion panels, use the rule of mixtures rather than CLPT to calculate their mechanical properties. This is because their behavior is dominated by the continuous, aligned fibers and matrix, whereas laminated composites consist of multiple plies with different orientation angles, resulting in more complex mechanical interactions.

For a composite like this, assuming it is composed of reinforcement fibers with properties ρ_f, E_f, G_f, ν_f, and an epoxy resin matrix with corresponding properties ρ_m, E_m, G_m, ν_m, the effective properties of the composite can be expressed using the rule of mixtures as follows:

$$E_L = E_f V_f + E_m V_m \tag{3.16}$$

$$E_T = \left(\frac{V_f}{E_f} + \frac{V_m}{E_m}\right)^{-1} \tag{3.17}$$

$$G_{12} = \left(\frac{V_f}{G_f} + \frac{V_m}{G_m}\right)^{-1} \tag{3.18}$$

$$\nu_{12} = \nu_f V_f + \nu_m V_m \tag{3.19}$$

$$\rho_c = \rho_f V_f + \rho_m V_m \tag{3.20}$$

Where: V_f and V_m are the volume fractions of the fibers and matrix, respectively, with $V_f + V_m = 1$. These equations assume perfect bonding between the fibers and matrix and uniform distribution of the fibers within the matrix.

These simplified equations provide a straightforward way to predict the overall properties of homogeneous, unidirectional composites. However, they are not suitable for describing the more complex interactions present in laminated composites with varied ply orientations.

3.2.4. Manufacturing Process

Composite manufacturing processes can be broadly categorized into five major classes based on their methodologies and applications, which provides a comprehensive framework for selecting appropriate composite manufacturing techniques based on application-specific requirements:

1. The first category is Open Molding Processes, such as hand lay-up and spray-up, which are widely used for producing large and simple structures. These methods are cost-effective but labor-intensive, with limited automation capabilities.
2. The second category is Closed Molding Processes, including Resin Transfer Molding (RTM) and Vacuum-Assisted Resin Transfer Molding (VARTM). These processes offer enhanced quality control, superior surface finishes, and are particularly suited for medium to high production volumes such as turbine blades.
3. The third category is Continuous Processes, exemplified by pultrusion and filament winding. These methods are highly automated and specialized for manufacturing long, uniform profiles with consistent properties.
4. The fourth category is Prepreg and Autoclave Processes, such as prepreg lay-up, Automated Tape Laying (ATL), and Automated Fiber Placement (AFP). These processes are characterized by their high precision and are primarily used in aerospace and high-performance applications.
5. Finally, the Additive and Specialized Processes category encompasses techniques like 3D printing, injection molding, and vacuum bagging.

Continuous manufacturing processes are selected for their compatibility with the continuous profile of the spar buoy and tower. As highlighted in the literature, filament winding, particularly when combined with an additional process, is considered the most suitable method for producing composite offshore wind turbine support structures. Additionally, the automation inherent in these processes significantly reduces labor costs compared to other methods. For this reason, filament winding and pultrusion are chosen as the primary manufacturing techniques for the floating support structure, illustrated in Figure 3.9 and Figure 3.10.

Filament winding involves the continuous winding of resin-impregnated fibers around a rotating mandrel. The fibers, impregnated with thermosetting resin in a resin bath, are passed through a nip roller to ensure consistent resin distribution before being wound onto the mandrel at specific angles. Once the desired thickness is achieved, the structure is cured to form a rigid composite. This process is particularly effective for manufacturing cylindrical or tubular components such as spar buoys and wind turbine towers.

Pultrusion, on the other hand, is a continuous process for creating constant cross-section composite profiles. In this process, unidirectional rovings, multi-directional mats, and surface veils are impregnated with thermosetting resin and pulled through a heated die, where they are shaped and cured under heat and pressure. The finished profiles are continuously pulled and cut to specified lengths, making this method ideal for structural components such as beams and panels.

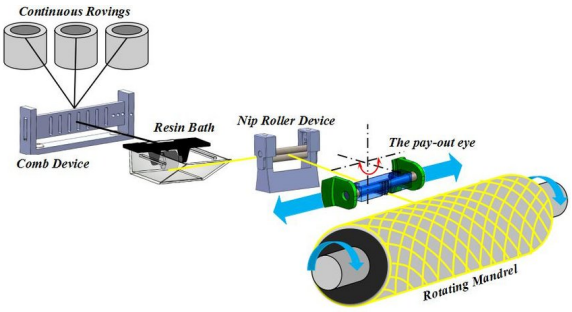

Figure 3.9: Filament Winding Process [28]

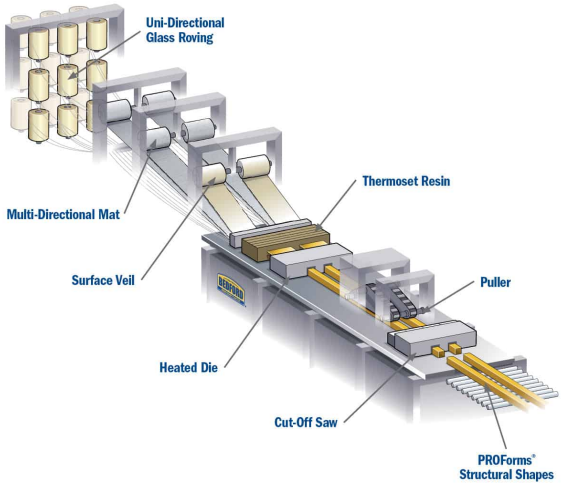

Figure 3.10: Pultrusion Process [29]

According to [30], which studies the effects of the fibre orientations and the number of piles on the overall performance of a floating tidal energy converter structure, the optimum filament wind angle was found as $\pm 60^{\circ}$ relative to the float system.

In summary, filament winding and pultrusion are combined as the manufacturing processes to fabricate the monolithic design of this project. Due to the differences in composition and structure between filament wound components and pultrusion panels, CLPT is used to calculate the mechanical properties of filament wound components, while the rule of mixtures is applied to determine the properties of pultrusion panels. This distinction ensures relatively accurate property prediction for each type of composite structure in the preliminary design stage.

3.3. Modal Analysis and Natural Frequencies

In structural design, a fundamental requirement during the preliminary phase is to avoid resonance, as it can greatly amplify vibration amplitudes and potentially lead to structural failure. For floating offshore wind turbines, the natural frequencies of the system must be carefully tuned to avoid overlapping with dominant excitation frequency bands. These include the rotor's rotational frequency (1P), the blade-passing frequency (3P), and environmental excitations caused by wind and wave loading [31]. The

key structural modes that require frequency separation include the tower bending modes and the six rigid-body DoFs of the floating platform.

Modal analysis is conducted to determine the corresponding natural frequencies and mode shapes, which characterize the system's dynamic response and guide the frequency separation strategy during the design process.

For the tower, which exhibits bending in both the fore-aft and side-to-side directions, modal analysis assumes that the tower deflection $u(x)$ could be expressed as a superposition of linear independent modes $\phi_i(x)$ with corresponding weight q_i:

$$u(x) = \sum_{i=1}^{N} q_i \phi_i(x) \tag{3.21}$$

where the individual mode shape ϕ_i has the orthogonal property:

$$\begin{aligned} \phi_i \phi_j &= 0 \quad (i \neq j) \\ \phi_i \phi_j &\neq 0 \quad (i = j) \end{aligned} \tag{3.22}$$

In the Rayleigh–Ritz approach, the Rayleigh principle states that a system vibrates at certain mode shapes with corresponding frequencies when it achieves an equilibrium between its potential energy U and kinetic energy T. When the method is used to calculate eigen-frequencies, it is based on a known mode shape or a good approximation. The downside of this method is that the mode shapes must be known to start with.

The Rayleigh-Ritz quotient R is given as:

$$\mathbf{R} = \omega^2 = \frac{U_{max}}{T_0} \tag{3.23}$$

where ω is the vibration frequency, U_{max} is the maximum of potential energy and T_0 is defined as $T_0 = T_{max}/\omega^2$ where T_{max} is the maximum kinematic energy.

Through minimizing the Rayleigh quotient:

$$\frac{\partial \mathbf{R}}{\partial q_i} = (\frac{U_{max}}{q_i} - \omega^2 \frac{T_0}{q_i}) = 0 \tag{3.24}$$

an eigenvalue problem equation could be obtained to solve the eigenfrequency ω_i and the corresponding mode weight q_i:

$$(\overline{\mathbf{K}} - \omega^2 \overline{\mathbf{M}})\mathbf{q} = 0 \tag{3.25}$$

where $\overline{\mathbf{K}}$ and $\overline{\mathbf{M}}$ denote the generalized stiffness and mass matrices, respectively. For Rayleigh-Ritz method, mode shapes are firstly assumed and combined, the matrices $\overline{\mathbf{K}}$ and $\overline{\mathbf{M}}$ are then derived from the terms $\frac{U_{\max}}{q_i}$ and $\omega^2 \frac{T_0}{q_i}$, and their accurate computation typically requires the establishment of a finite element model. In the context of wind turbine tower bending analysis, they characterize the dynamic behavior of the structure. The first bending mode eigenfrequency is specifically designed to remain outside the excitation ranges of the rotor's 1P and 3P frequencies, which is essential for avoiding resonance and ensuring structural integrity.

Zhaolong Yu et al. [32] proposed analytical formulations for estimating the generalized stiffness and mass matrices used to compute eigen-frequencies and mode shapes of taped towers, which could be applied to both land based turbine and floating wind turbine. The configuration of the tower model employed in their analysis is illustrated in Figure 3.11, where m_{RNA} and J_{RNA} are the mass and rotation inertia of the rotor-nacelle assembly (RNA), L_T, E_T, $I_T(x)$, $A_T(x)$ and t_T are the length, modulus, moment of inertia, cross section area and thickness of the tower, and D_{Tb}, A_{Tb}, I_{Tb} are the tower base diameter, tower base cross section area and tower base moment of inertia. For FOWT model, the floater is treated as a rigid body and the connection between the floater and the tower introduces a

finite rotational stiffness k_{rot} To simplify the calculation with accuracy, a 2^{nd} order polynomial and a 1^{st} order polynomial are used to approximate and describe the variation of $I_T(x)$ and $A_T(x)$ respectively. These are expressed as:

$$\frac{I_T}{I_{Tb}} = b_0 + b_1\frac{z}{L} + b_2(\frac{z}{L})^2 \tag{3.26}$$

$$\frac{A_T}{A_{Tb}} = c_0 + c_1\frac{z}{L} \tag{3.27}$$

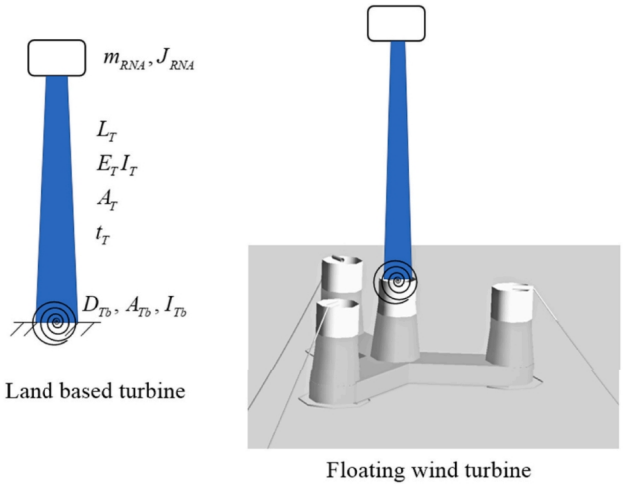

Figure 3.11: Simplified floating wind turbine taped tower model for modal analysis [32]

With the above structural parameters defined and coefficients b_0, b_1, b_2, c_0 and c_1 found, the generalized mass matrix and stiffness could be calculated. The matrix forms are presented in Appendix A. With these matrix, the modal frequencies and mode shapes could be calculated with Eq.3.25.

The other approach employed in this study for performing modal analysis is the use of BModes [33], a tool developed by NREL to compute the mode shapes and natural frequencies of beam-like structures in wind turbine models, such as blades and towers.

In BModes, the tower model is discretized into a series of Euler–Bernoulli beam elements. Each element consists of two boundary nodes and three internal nodes, collectively contributing to a total of 15 degrees of freedom (DoFs). These DoFs include axial deflections (u_1, u_2, u_3, u_4), flapwise deflections and slopes (w_1, w_1', w_2, w_2'), edgewise deflections and slopes (v_1, v_1', v_2, v_2'), and elastic twists $(\varphi_1, \varphi_2, \varphi_3)$, as presented in Figure 3.12.

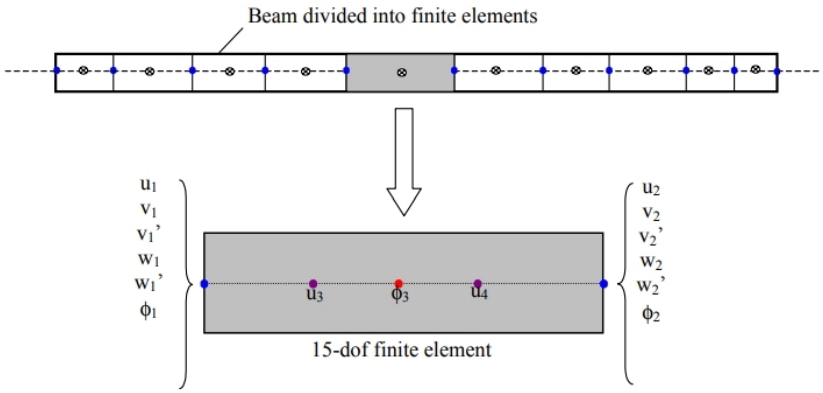

Figure 3.12: BModes beam discretization [33]

The nonlinear equations of motion for the finite element model are derived using Hamilton's principle, which is expressed as:

$$\int_{t_1}^{t_2} [\delta W_e + \delta T - \delta U] \, dt = 0 \tag{3.28}$$

Here, W_e denotes the virtual work performed by external forces acting on the beam. In the context of the tower, these external forces may include gravitational loads from the rotor-nacelle assembly, reactions from the mooring system, and hydrodynamic forces induced by waves and currents. Finite Element Analysis (FEA) is employed to spatially discretize the nonlinear equations of motion, reducing them to a set of ordinary differential equations (ODEs) in time. Subsequently, analytical linearization is applied, transforming the system into a modal analysis problem in the form of Eq.3.25.

In addition to avoiding the 1P and 3P frequency ranges, the tower bending natural frequency should also be designed to steer clear of the dominant frequencies in the wind and wave spectra. This helps avoid the resonance between the tower and environment excitations. All the frequencies mentioned in this section are demonstrated in Figure 3.13.

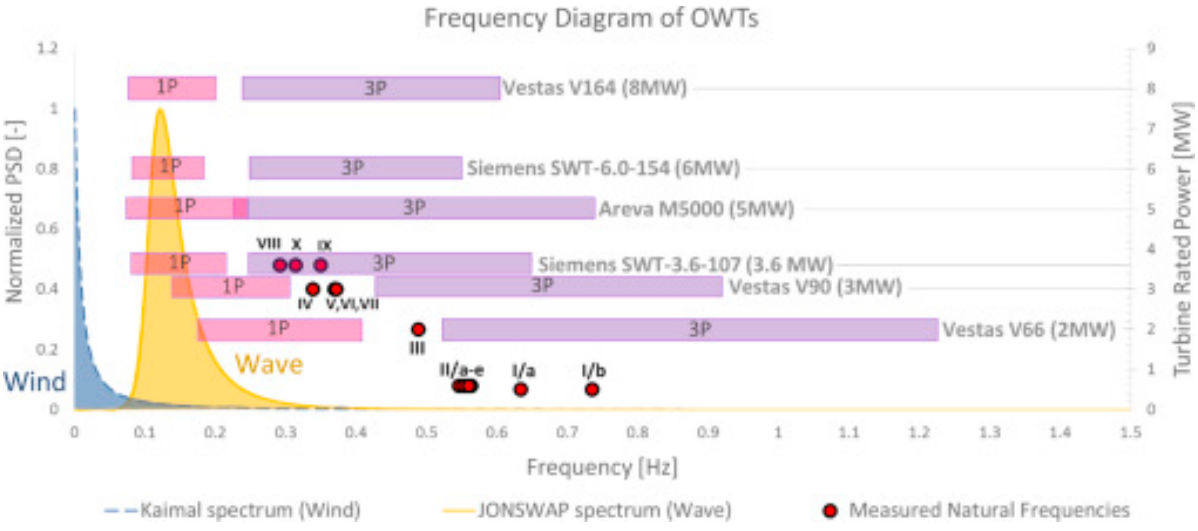

Figure 3.13: Typical wind and wave spectra, 1P and 3P frequency bands of six commercial turbines [31]

In addition to the tower, the floating platform also requires a frequency assessment during the preliminary design stage to ensure that its natural frequencies do not coincide with dominant wave excitation frequencies. This is essential for maintaining structural stability and avoiding excessive platform motions. By providing the hydrostatic stiffness matrix C_{ii}, zero-frequency added mass A_{ii}, mass matrix M_{ii} of the rigid floating platform, the natural frequency of the i^{th} DoF could be calculated:

$$f_i = \frac{1}{2\pi} \sqrt{\frac{C_{ii}}{M_{ii} + A_{ii}(\omega_{n,i})}} \tag{3.29}$$

This calculation can also be performed using BModes.

However, due to the complexity of fluid–structure interactions in floating systems, frequency identification through free-decay simulations is often preferred over traditional modal analysis. In this approach, a displacement offset is applied to the degree of freedom of interest, and the natural frequency is determined by measuring the time interval between two successive peaks in the time-domain response.

Although BModes is capable of estimating the natural frequencies for the six rigid-body degrees of freedom of a floating platform, in this study, free-decay simulations are conducted for each degree of freedom to ensure consistency between BModes predictions and results obtained from time-domain simulations.

3.4. Floater hydrodynamic loadings

For a FOWT system, hydrodynamic loading is typically modeled using one of three approaches: potential flow theory, the Morison equation, or a hybrid method that combines elements of both.

Faltinsen [34] proposed a classification framework to guide the selection of appropriate hydrodynamic force models based on wave conditions and body characteristics. This framework is illustrated in Figure 3.14, which shows the relative importance of wave diffraction, inertial (mass-related) forces, and viscous drag. Each region in the figure corresponds to conditions where different force calculation approaches, such as potential flow theory, Morison's equation, and hybrid methods, provide different levels of accuracy.

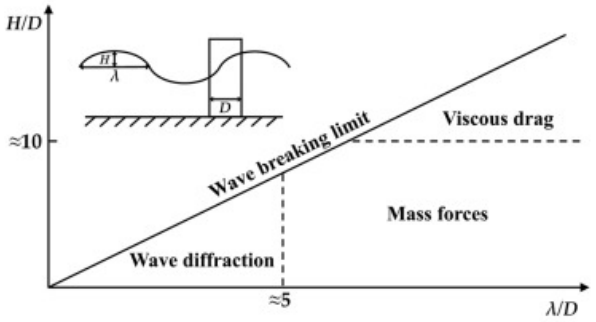

Figure 3.14: Wave forces relative importance [34]

Potential flow theory is generally well-suited for analyzing large-volume structures, particularly when assessing wave diffraction and radiation effects. However, a primary limitation of this approach is its inability to capture viscous and nonlinear effects, which may become significant under certain flow conditions or for specific geometries. This is especially true in regions with sharp edges or in turbulent environments influenced by strong currents. Moreover, achieving accurate frequency-dependent hydrodynamic coefficients requires detailed mesh discretization of the wetted surface, which can increase computational cost and complexity.

The Morison equation, in contrast, is a semi-empirical formulation typically applied to slender, cylindrical structures. Its main advantage lies in its simplicity and relatively low computational cost, making it well-suited for preliminary design and real-time applications. However, one of its underlying assumptions is that the undisturbed wave kinematics remain valid at the location of the structure. This assumption breaks down when the characteristic size of the structure becomes comparable to the incident wavelength. In such cases, near-field wave diffraction effects become significant, and the interaction between the incident wave field and the structure can no longer be neglected. These effects must be accounted for using potential flow theory or a hybrid approach.

3.4.1. Potential Flow Theory

For the analysis of submerged components in FOWTs, potential flow theory is commonly employed to evaluate unsteady hydrodynamic pressures, wave-induced loads, body motions, and the resulting pressure and velocity fields in the surrounding fluid domain. This theory assumes an incompressible, inviscid, and irrotational fluid, allowing the hydrodynamic problem to be described by a boundary value problem governed by Laplace's equation.

In this project, an old version of compiled Hydrodynamic Analysis of Marine Structures developed by the Marine Renewable Energies Lab (HAMS-MREL) [35] is used to calculate the hydrodynamic coefficients of the submerged portion of the floating platform. HAMS is based on three-dimensional potential flow theory and applies panel methods to discretize the wetted surface of the structure. It computes key frequency-domain hydrodynamic parameters, including added mass, radiation damping, and wave excitation forces, which are later used as inputs for dynamic response simulations in HydroDyn module of OpenFAST.

In potential flow theory, hydrodynamic forces are derived by integrating the pressure over the wetted

surface of the body. The pressure field, in turn, is obtained from the unsteady Bernoulli equation:

$$p - p_a = \underbrace{-\rho g z}_{\text{static}} - \underbrace{\rho \frac{\partial \Phi}{\partial t}}_{\substack{\text{dynamic} \\ \text{linear}}} \underbrace{- \frac{1}{2} \rho |\nabla \Phi|^2}_{\substack{\text{dynamic} \\ \text{quadratic}}} \tag{3.30}$$

where Φ is the velocity potential. The first term represents the hydrostatic pressure, the second term and the third term refer to the induced linear and quadratic hydrodynamic pressure. In linear potential flow theory, only the static and linear dynamic terms are retained, while the quadratic term is omitted to simplify the analysis.

Then the hydrodynamic forces in linear potential flow theory are calculated as follows:

$$F_j(t) = \int_{S_{0B}} -\rho \frac{\partial \Phi}{\partial t} \mathbf{n} \, dS + \int_{S_B} -\rho g z \mathbf{n} \, dS \qquad j = 1, \ldots, 6 \tag{3.31}$$

where j denotes DoFs, and the wave potential Φ is to be solved with the following steps.

With the assumption of linear potential flow theory, the wave body interaction problem could be divided into the diffraction problem: the body is fixed and interacting with incident waves, and radiation problem: the body is forced to oscillate in its six degrees of freedom without incident wave. This is visualized in Figure 3.15.

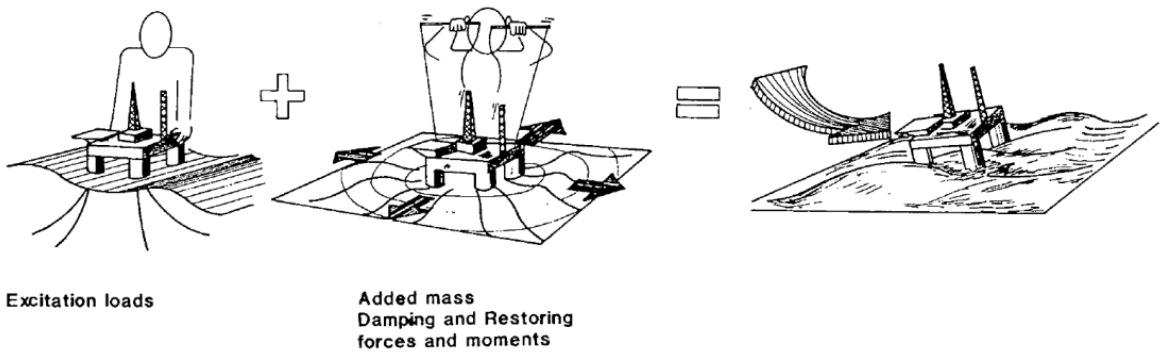

Figure 3.15: Linear Potential Flow [36]

This allows the wave potential linear decomposition:

$$\Phi = \Phi_0 + \Phi_S + \Phi_R = \Phi_D + \Phi_R \tag{3.32}$$

where Φ_0, Φ_S, Φ_D, Φ_R represent the potential of incident wave, scattered potential, diffraction potential and radiation potential. It should be noted that the diffraction is the combination of scattering and incident wave potential. In HAMS, the first order potential for the wave-body interaction can be expressed by a sum of components having circular frequency $\omega_j > 0$:

$$\Phi(\mathbf{x}, t) = \mathrm{Re} \sum_j \phi_j(\mathbf{x}) e^{i\omega_j t} \tag{3.33}$$

This allows to avoid the time dependence from the problem and solve the problem only dependent on ω (frequency domain analysis).It should also be noted that the radiation potential is a linear combination of the components corresponding to 6 degrees of freedom such that:

$$\Phi_R(x, y, z, t) = \Re\{\sum_{j=1}^{6} \underbrace{\dot{\eta}_j}_{\text{velocity in mode } j} \underbrace{\varphi_j}_{\text{potential per unit velocity}} \} \tag{3.34}$$

Each wave potential is subjected to the governing Laplace Equation:

- Laplace Equation:

$$\nabla^2\Phi = 0 \tag{3.35}$$

and the following boundary conditions:

- Body Surface:

$$\frac{\partial\Phi}{\partial n} = \mathbf{U}, \quad \mathbf{n} \text{ on mean body surface} \tag{3.36}$$

- Linearized Dynamic+Kinematic Free Surface (dispersion relationship):

$$\frac{\partial^2\Phi}{\partial t^2} + g\frac{\partial\Phi}{\partial z} = 0, \quad \text{on z=0} \tag{3.37}$$

- Seabed:

$$\frac{\partial\Phi}{\partial z} = 0, \quad \text{on z=-H} \tag{3.38}$$

The moving body generates radiated waves associated with the radiation velocity potential and it is subjected to hydrodynamic loads identified as added-mass, damping, and restoring terms. The restoring terms are connected with the variation of the buoyancy due to the body motions. The added-mass and damping terms are connected with the dynamic pressure caused by the body motions. In HAMS, added-mass A_{ij} and damping coefficients B_{ij} are defined by:

$$A_{ij} - \frac{i}{\omega}B_{ij} = \rho\iint_{S_b}\Phi_i n_i dS \tag{3.39}$$

Therefore, added mass and damping coefficients are calculated as:

$$A_{ij}(\omega) = \Re[\rho\int_{S_b}\varphi_j n_i dS] \tag{3.40}$$

$$B_{ij}(\omega) = -\omega\Im[\rho\int_{S_b}\varphi_j n_i dS] \tag{3.41}$$

For the free surface wave elevation ξ, it's calculated by the linearized dynamic boundary condition:

$$g\xi + \frac{\partial\Phi}{\partial t} = 0 \tag{3.42}$$

In the linear potential flow wave model, the Response Amplitude Operator (RAO) is widely used to describe the dynamic characteristics of the system. The RAO is defined as a transfer function that relates the system's outputs or responses, such as motions or forces, to known inputs like wave frequency and wave height. It provides a clear measure of how the system responds to waves of varying frequencies, facilitating the analysis of wave-body interactions. The RAO of each DoF referring to Figure 3.2 is defined by:

$$RAO_i(\omega) = \left|\frac{\hat{\xi}_i}{\zeta_0}\right| \quad \text{for} \quad i = 1,2,3 \quad \text{and} \quad RAO_i(\omega) = \left|\frac{\hat{\xi}_i}{k\zeta_0}\right| \quad \text{for} \quad i = 4,5,6 \tag{3.43}$$

where $\hat{\zeta}$ is the complex response amplitude, ζ_0 is the incident wave amplitude and $k\zeta_0$ is the wave slope amplitude.

By plotting the transfer function RAO with respect to the input frequency ω, the natural frequency of each DoF can be identified. This is achieved by locating the peak value of the RAO curve and determining the corresponding frequency, which indicates the system's resonance condition for that particular DoF. If this frequency coincides with the dominant frequencies of the wave spectrum, the structural geometry should be redesigned to shift the natural frequency away from the wave spectrum to avoid resonance.

3.4.2. Morison Equation

Morison equation describes the hydrodynamic loadings in three terms: drag force, hydrodynamic mass force, and the F-K (Froude–Krylov) force introduced from wave pressure field. The sum of F-K force and hydrodynamic mass force is referred as inertia force. For a cylindrical element as presented in Figure 3.16, the equation can be expressed as:

$$dF = (\underbrace{\rho C_p A \dot{u}}_{F-K\ Force} + \underbrace{\rho C_m A(\dot{u}-\dot{v})}_{Hydrodynamic\ Mass\ Force} + \underbrace{\frac{1}{2}\rho C_d D(u-v)|u-v|)dz}_{Drag\ Force} \tag{3.44}$$

where ρ is the water density, A is the cross-sectional area, D is the cross-section diameter, C_m is the added-mass coefficient, C_p is the dynamic pressure coefficient, C_d is the drag coefficient, u is the water particle velocity and v is the body velocity.

To evaluate whether the hydrodynamic loading is dominated by inertia or drag forces, the Keulegan–Carpenter number (KC) [37] is commonly used, defined as

$$KC = \frac{uT_w}{D} \tag{3.45}$$

where T_w is the wave period. The KC number represents the relative importance of drag versus inertia effects in oscillatory flows. For K«20, the hydrodynamic response is primarily inertia-dominated, while for KC»20, drag forces become dominant.

As illustrated in Figure 3.14, when the diameter of a structural member exceeds approximately one-fifth of the incident wavelength, applying the pure Morison equation will be inaccurate and tend to overestimate the wave-induced excitation forces. To account for diffraction effects under such conditions, the McCamy–Fuchs correction [38] offers a practical solution by modifying the coefficient associated with the inertia force term. An alternative approach involves replacing the inertia component in the Morison equation with the corresponding force obtained from potential flow theory, thereby capturing diffraction effects more rigorously. This method is commonly referred to as hybrid modeling in OpenFAST, as it combines viscous drag treatment from Morison theory with inertia terms derived from diffraction-based potential flow analysis.

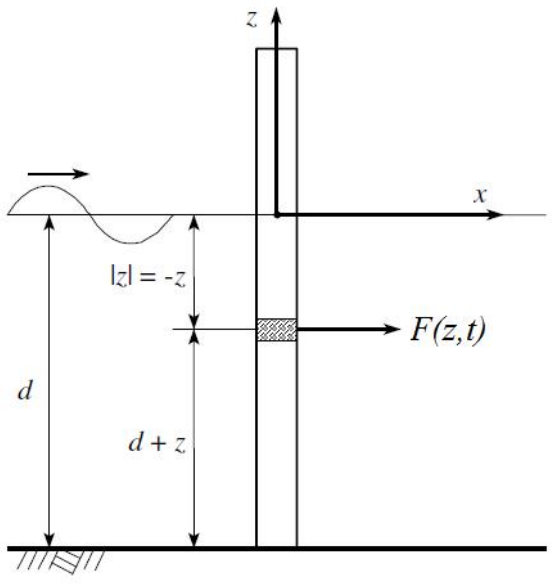

Figure 3.16: Slender cylindrical body with Morison force F [39]

While Morison-based models with McCamy–Fuchs correction are computationally more efficient than combining potential flow solutions, they still rely on empirically calibrated hydrodynamic coefficients,

such as C_p, C_m, and C_d which typically require validation through computational fluid dynamics (CFD) simulations or physical experiments to ensure modeling accuracy.

3.5. Wave Model

3.5.1. Linear wave

Under the assumption of potential flow, the wave-body interaction problem can be analyzed by introducing the parameter wave steepness ϵ expressed as:

$$\epsilon = H/\lambda \tag{3.46}$$

where H is the wave height and λ is the wave length. ϵ is used to describe the nonlinearities associated with the free-surface waves and the body motions. The wave potential ϕ and free-surface elevation ζ could then be written as:

$$\begin{aligned} \phi &= \tilde{\phi}_1\varepsilon + \tilde{\phi}_2\varepsilon^2 + \tilde{\phi}_3\varepsilon^3 + \ldots\ldots\ldots \\ \zeta &= \tilde{\zeta}_1\varepsilon + \tilde{\zeta}_2\varepsilon^2 + \tilde{\zeta}_3\varepsilon^3 + \ldots\ldots\ldots \end{aligned} \tag{3.47}$$

This approach is known as the perturbation method. Specifically, by assuming that the wave steepness ϵ is small and that terms of $O(\epsilon^n)$ (with $n > 1$) are negligible, the flow simplifies to a linear potential flow. As a consequence of this linearization, the system's responses become proportional to the inputs, such as the incident wave height. At steady states, the responses oscillate at the same frequency as the inputs.

This means that, under linear conditions, it is possible to eliminate the time dependence of the problem and solve it as a single instance that depends only on ω (frequency domain analysis). However, when nonlinearities become significant, transient conditions exist, or multiple frequencies are involved, the problem can no longer be simplified in this manner and must instead be solved in the time domain (time domain analysis).

3.5.2. Nonlinear effects

When the wave steepness ϵ becomes significant or the body motion is large, the higher-order terms in Eq. 3.47 can no longer be neglected. Under such conditions, the assumption of linearity breaks down, and nonlinear effects must be included to accurately describe the wave-body interactions.

Given a wave spectrum $S(\omega)$, which represents the composition of incident waves with different frequencies and phases (as will be explained in the next subsection), typical second-order nonlinear effects arise from both the nonlinearity of the incident wave field and the hydrodynamic interaction between the body and the waves. These effects are commonly expressed in terms of the sum-frequency and difference-frequency components, which result from the interaction between wave components of varying frequencies, leading to higher-order responses that cannot be captured by linear theory.

The sum-frequency term can induce phenomena such as ringing, particularly in floaters with shorter natural periods, such as TLPs. On the other hand, the difference-frequency term plays a significant role in freely floating structures with small water-plane areas, where the restoring forces in the vertical plane are small. This results in longer natural periods, typically on the order of $O(30\ \mathrm{s})$, which can lead to slowly-varying drift (slow-drift) motions in the vertical plane, including heave, roll, and pitch. Many of these slow-drift effects are dominated by body–wave interaction mechanisms rather than incident wave nonlinearity alone. Consequently, it is essential to investigate slow-drift forces for spar buoy platforms to ensure accurate predictions of their dynamic behavior.

3.5.3. Regular and irregular wave

A regular wave could be defined with its properties: wave height H, wave frequency ω and wave number k. For linear wave, the wave elevation could be defined as:

$$\eta(x,t) = \frac{H}{2} cos(\omega t - kx) \tag{3.48}$$

Linear irregular waves can be considered as a summation of a large number of linear regular waves with different wave characteristics. Thus, the linear irregular wave elevation can be defined as:

$$\eta(x,t) = \sum_{j=1}^{N} A_j cos(\omega_j t - k_j x + \epsilon_j) \tag{3.49}$$

where A_j is the individual wave amplitude and ϵ_i is the individual wave phase angle.

In general, a wave spectrum $S(\omega)$ is obtained by first computing the auto-correlation function of the wave elevation time series and then applying the Fourier transform, to describe the wave energy distribution with respect to frequency. However, the time series of irregular waves could be difficult to capture accurately due to the complex nature of wave interactions and variations in wave characteristics. For instance, in the North Sea, the wave spectrum is rarely fully developed. To address this, the Joint North Sea Wave Project (JONSWAP) wave spectrum is commonly used as a representative model. The JONSWAP wave spectrum is expressed as [40]:

$$S_{\text{JS}}(f) = 0.3125 \cdot H_s^2 \cdot T_p \cdot \left(\frac{f}{f_p}\right)^{-5} \exp\left(-1.25\left(\frac{f}{f_p}\right)^{-4}\right)(1 - 0.287\ln\gamma)\,\gamma \cdot \exp\left(-0.5 \cdot \left(\frac{\frac{f}{f_p} - 1}{\sigma}\right)^2\right) \tag{3.50}$$

where H_s is the significant wave height, T_p and f_p correspond to peak period and peak frequency, σ is the spectral width parameter and γ is the peak enhancement factor. Recommended by IEC 641300-3 design standard [6], σ and γ could be calculated by:

$$\sigma(\omega) = \begin{cases} 0.07 & \text{for } \omega \leq \frac{2\pi}{T_p} \\ 0.09 & \text{for } \omega > \frac{2\pi}{T_p} \end{cases} \tag{3.51}$$

$$\gamma = \begin{cases} 5 & \text{for } \frac{T_p}{\sqrt{H_s}} \leq 3.6 \\ \exp\left(5.75 - 1.15\frac{T_p}{\sqrt{H_s}}\right) & \text{for } 3.6 < \frac{T_p}{\sqrt{H_s}} \leq 5. \\ 1 & \text{for } \frac{T_p}{\sqrt{H_s}} > 5 \end{cases} \tag{3.52}$$

By dividing the wave spectrum $S(\omega)$ in N frequency intervals with Δf corresponding to N wave components in Eq.3.49, the individual wave amplitude A_j and frequency ω_j could be defined as:

$$A_j = \sqrt{2S(\omega)\Delta f} \tag{3.53}$$

$$\omega_j = \frac{2\pi}{f_j} \tag{3.54}$$

where f_j is the j^{th} frequency in the divided wave spectrum. With the phase ϵ_j given as random values and application of JONSWAP wave spectrum the irregular wave time series could be determined given significant wave height H_s and peak period T_p by Eq.3.49.

3.6. Equation of motions

A general form of equation of motion could be written as:

$$\mathbf{M}\ddot{\mathbf{x}}(t) + \mathbf{C}\dot{\mathbf{x}}(t) + \mathbf{K}\mathbf{x}(t) = \mathbf{F}(t) \tag{3.55}$$

where $\mathbf{M}$, $\mathbf{C}$ and $\mathbf{K}$ are mass matrix, linear damping matrix and linear stiffness matrix receptively, and $\vec{\mathbf{x}}$ is the motion of each DoF.

For estimating the more complex hydrodynamical responses, the motion of a floating body can be studied in the time domain by solving the Cummins [41] Eq.3.56 or in the frequency domain by solving the Ogilvie [42] Eq.3.57. These two methods are linked through the Fourier Transform.

$$\left(M_{ij} + A_{ij}^{\infty}\right) \ddot{x}_j(t) + \int_{-\infty}^{t} K_{ij}(t-\tau)\dot{x}_j(\tau)d\tau + C_{ij}x_j(t) = F_j^e(x, \dot{x}, t) \tag{3.56}$$

$$-\omega^2 \left(M_{ij} + A(\omega)\right) x_j(i\omega) + i\omega B(\omega) x_j(i\omega) + C_{ij}x_j(i\omega) = F_j^e(i\omega) \tag{3.57}$$

Here, A, B, convolution term, C, and F^e represent the added mass, linear hydrodynamic damping coefficient, radiation force, linear hydrostatic matrix, and external forces. By using HAMS, hydrodynamic coefficients, including added mass, damping coefficient, and hydrostatic restoring coefficients, could be obtained.

In particular, the Cummins equation [41] is implemented in the HydroDyn module of OpenFAST to model wave-radiation forces acting on floating substructures.

3.7. Structural Analysis

For FOWT systems deployed in deep-water ocean environments, structural integrity is of critical concern due to exposure to potential severe environmental conditions such as storms and typhoons. If the structure fails to withstand these extreme events, the consequences can be catastrophic, potentially resulting in major equipment damage or even loss of life. In addition to extreme loading events, FOWTs are designed for long operational lifetimes, typically on the order of 20-25 years. Over this period, the structure is subjected to continuous cyclic loading from wind and wave actions, as well as material degradation due to seawater corrosion. These factors can lead to fatigue-induced damage accumulation over time.

Therefore, it is essential to conduct a comprehensive structural assessment to ensure that the system can withstand both extreme loading events and long-term cyclic degradation over its service life. These two states are typically categorized as the ULS, which is related to the structural failure under extreme or accidental loads, and the FLS, which concerns cumulative damage due to repeated operational loading.

A complete structural verification involves evaluating compliance with applicable design standards and confirming that sufficient safety margins are maintained under both transient and steady-state environmental conditions.

Load and Resistance Factor Design (LRFD) [43] is a widely adopted methodology for assessing structural integrity. This approach introduces safety by applying separate partial factors to both the structural resistance and the applied loads. The design criterion can be expressed as:

$$\frac{P_{cr}}{\gamma_s} \geq \gamma_l P_{des} \tag{3.58}$$

where P_{cr} is the critical structural resistance, which may be defined in terms of yield strength, buckling limit, or fatigue capacity, depending on the failure mode under consideration. P_{des} is the representative design load associated with a specific design scenario or load case. The factor γ_s is the partial safety factor applied to the resistance side, determined by material properties, structural configuration, and uncertainties in the resistance model. The factor γ_l is the partial load factor, accounting for uncertainties in the applied loading and environmental conditions.

This formulation ensures that the design maintains an acceptable level of safety by accounting for both variabilities in material strength and uncertainties in external loading. It is particularly useful for complex systems like floating wind turbines, where load conditions can vary significantly across time and operational modes.

3.7.1. Yielding

The yield strength is a material property that defines the maximum stress a material can withstand without undergoing plastic deformation. In the case of cylindrical shell structures, such as the tower or spar sections of a floating offshore wind turbine, the onset of yielding is typically evaluated by comparing the combined normal and shear stresses within the shell to the allowable yield strength.

The normal stress may include contributions from both axial force N_z (tensile or compressive) and bending moments M_x and M_y, depending on the loading condition and location along the member. The shear stress includes components from the transverse shear force F_x, F_y and torsional moment T. For a cylindrical shell, the distribution of these loads is illustrated in Figure 3.17. The maximum normal stress σ_{max} and shear stress τ_{max} can be estimated analytically using Equations 3.59 and 3.60, respectively.

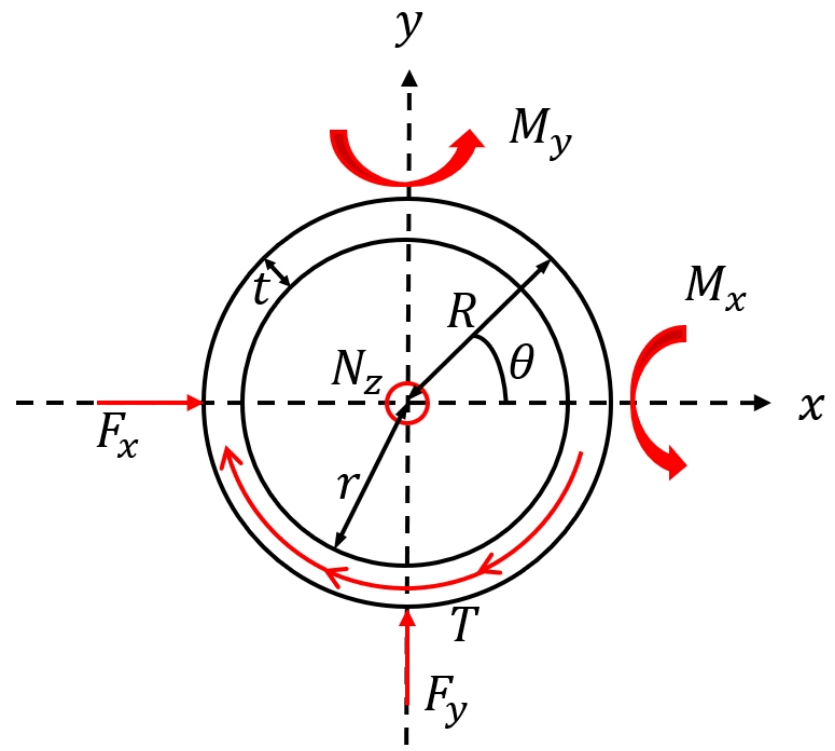

Figure 3.17: Loading components on a cylindrical shell cross-section

$$\sigma_{\text{max}} = \frac{N_z}{A} + \frac{\sqrt{M_x^2 + M_y^2}}{I} R \tag{3.59}$$

$$\tau_{\text{max}} = \frac{2\sqrt{F_x^2 + F_y^2}}{A} + \frac{TR}{2I} \tag{3.60}$$

where R and r denote the outer and inner radius of the cylindrical shell, respectively; A is the cross-sectional area, and I is the moment of inertia, which could by calculated by:

$$A = \pi(R^2 - r^2) \tag{3.61}$$

$$I = \frac{\pi}{2}(R^4 - r^4) \tag{3.62}$$

3.7.2. Buckling

Buckling refers to a sudden structural deformation under load, such as the bowing of a column under axial compression or the wrinkling of a panel under shear forces.

For a beam element subjected to axial tension, the resulting tensile stress is typically compared against the material's yield strength to evaluate structural failure. However, when subjected to axial compression, local or global buckling may occur before the material reaches its yield strength, making buckling the critical failure mode in such cases.

Typically, for a slender column, Euler's buckling load is used to determine the maximum axial compressive load that the column can withstand before buckling occurs:

$$P_{cr} = \frac{\pi^2 EI}{(KL)^2} \tag{3.63}$$

where K is the column effective length factor, L is the unsupported length of the column, and E and I represent the Young's modulus of the column material and the minimum second moment of area of the cross-section, respectively. The value of K is selected based on the end conditions and corresponding buckled shape, as illustrated in Figure 3.18.

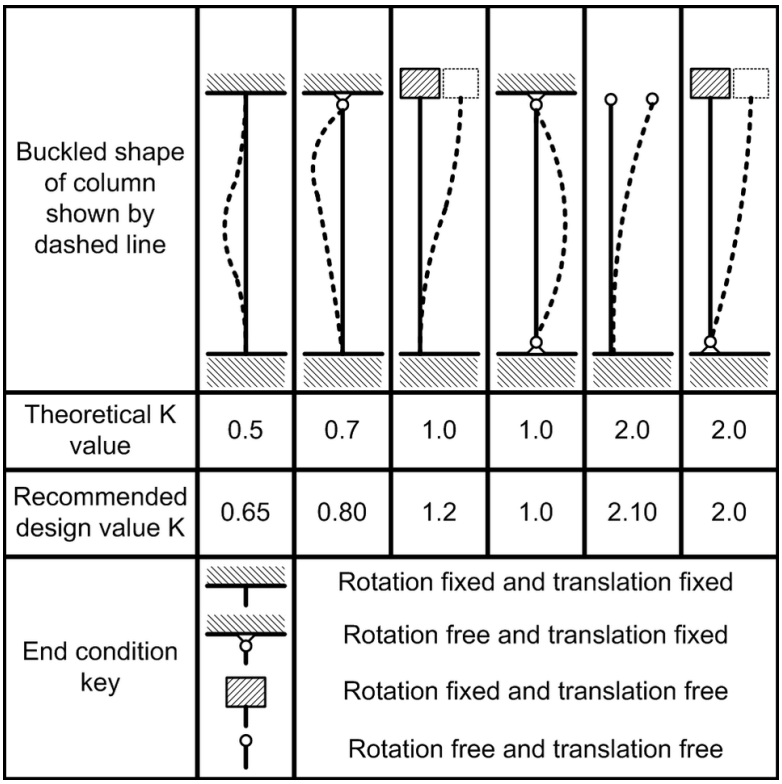

Figure 3.18: Effective length factors K for typical buckling modes, redrawn based on Table C.1.8.1 in [44]

However, since this project uses composite materials, the buckling failure criterion is evaluated using the formulation presented in [27], the calculation will be discussed in detail with the defined material properties in the methodology section.

3.7.3. Fatigue

Fatigue refers to the process by which cracks initiate and gradually propagate in a material subjected to repeated or fluctuating loading. After the initial formation of a fatigue crack, it advances incrementally with each load cycle, often leaving behind visible striations on portions of the fracture surface.

To assess the fatigue strength of the structure over its operational lifetime, the material's S–N curve (stress–life curve) is first established. Based on time-domain simulation results, the stress range and the corresponding number of load cycles at various stress levels are recorded using Rainflow Cycle-Counting (RCC) method [39], as illustrated in Figure 3.19.

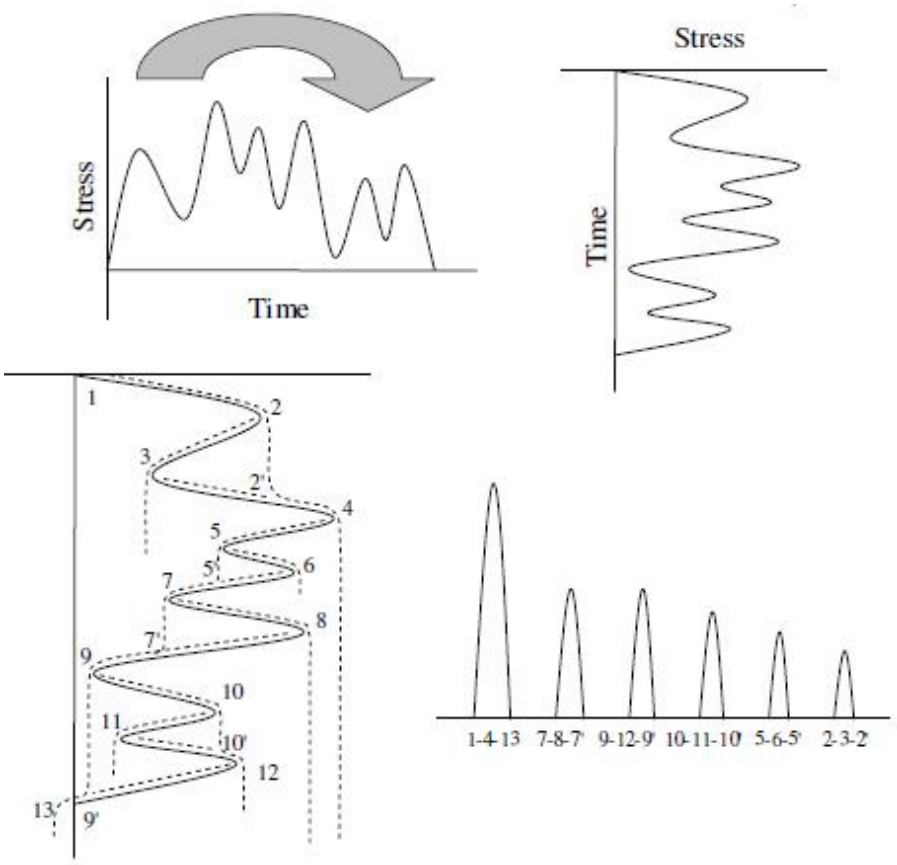

Figure 3.19: Rain Flow Counting method overview [39].

In this project, fatigue assessment is carried out using MLife [45], a post-processing tool developed by NREL for fatigue analysis of wind turbine components. MLife will be described in more detail in the Methodology section. The total fatigue damage D is computed using the Palmgren–Miner linear damage accumulation rule:

$$D = \sum_i \frac{n_i}{N_i(L_i^{RF})} \tag{3.64}$$

where n_i denotes the number of observed stress cycles at the i^{th} stress level, and N_i represents the number of cycles to failure at that stress level, as determined from the S–N curve, and L_i^{RF} represents the cycle's load range about a fixed load-mean value. According to this criterion, fatigue failure is considered to occur when the cumulative damage $D \geq 1$.

In MLife, the S–N curve for a given structural component is characterized by specifying the ultimate design load ^{ult} and the Wöhler exponent m. With these parameters, the number of cycles to failure N_i at a given load range L_i^{RF} and a fixed load mean L_{MF} is estimated using the following relationship:

$$N_i = \left(\frac{L^{\text{ult}} - L_{MF}}{L_i^{RF}} \right)^m \tag{3.65}$$

While the above two formulations assume that all fatigue cycles are counted with respect to a fixed load mean L_{MF}, this simplification does not accurately reflect real-world loading conditions, where cycles occur over a spectrum of load means. To account for the influence of varying mean loads on fatigue life, the Goodman correction is applied. The corrected load range L_i^{RF} is calculated as:

$$L_i^{RF} = L_i^R \left(\frac{L^{ult} - |L^{MF}|}{L^{ult} - |L_i^M|} \right) \tag{3.66}$$

where L_i^R is the range of the i^{th} load cycle, L_i^M is the mean load of that cycle,

3.8. Optimization approach

The design of a floating wind turbine is inherently complex, involving numerous interdependent variables arising from its multi-physics nature. Among these variables, geometric parameters are particularly critical, as they influence both the dynamic response of the system and its overall cost. A widely adopted engineering approach begins with a baseline configuration, followed by the optimization of selected geometric parameters—such as diameter, draft, and wall thickness—with the objective of reducing structural mass and, more broadly, minimizing the LCOE.

A general optimization problem can be decomposed into four essential components: the design variables, the objective function(s), the constraints, and the optimization algorithm. During each iteration of the optimization loop, the selected design variables are evaluated using numerical models or simulations to generate output responses. Some of these outputs are required to satisfy predefined constraints—such as structural strength and global stability—while others serve as objective functions to be either minimized or maximized [46].

The goal of the optimization process is to identify the optimal set of design variables that yields the minimum (or maximum) value of the objective function(s), subject to specified input bounds and output constraints. These bounds often reflect practical considerations such as manufacturability, material limitations, or regulatory requirements. The mathematical formulation of such an optimization problem can be expressed as:

$$\begin{aligned} &\text{Given:} && \vec{x} = \{x_1, x_2, \ldots, x_n\} \\ &\text{Minimize/maximize:} && f(\vec{x}) \\ &\text{Subject to:} && g_1(\vec{x}) \leq b_1 \\ & && g_2(\vec{x}) \leq b_2 \\ & && \vdots \\ & && g_m(\vec{x}) \leq b_m \\ & && lb_i \leq x_i \leq ub_i \end{aligned} \tag{3.67}$$

where $\vec{x}$ denotes the vector of design variables, f is the objective function to be minimized or maximized, and $g_i(\vec{x}) \leq b_i$ represents the m inequality constraints applied to the system. The terms lb_i and ub_i define the lower and upper bounds for each design variable. The overview of an optimization workflow is presented in Figure 3.20.

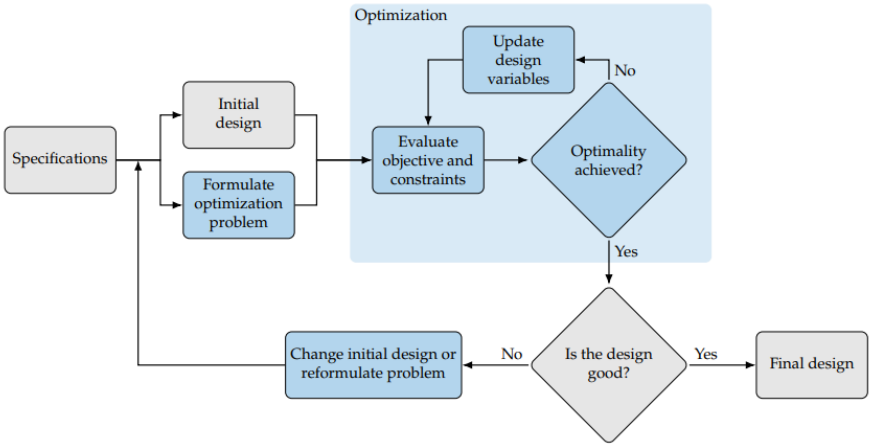

Figure 3.20: General Optimization Process Overview [47]

The choice of optimization strategy depends on various factors, including the nature of the objective function, the dimensionality of the design space, and the presence of nonlinearity or discontinuities [19]. Broadly, these strategies can be categorized into gradient-based and gradient-free methods. Gradient-based approaches are efficient for problems with smooth, differentiable objective functions and well-defined gradients. In contrast, gradient-free methods—such as genetic algorithms and particle swarm optimization—are more robust in handling non-convex design spaces, discontinuities, or multiple local optima, characteristics frequently encountered in the design of offshore floating wind structures.

4

Methodology

4.1. IEA 15MW wind turbine parameters

To reduce LCOE, one of the most effective strategies is to employ turbines with higher rated power. Accordingly, a clear trend in floating offshore wind turbine development is the design of larger-scale systems. In line with this trend, the present study adopts the IEA 15MW reference wind turbine [48] as the baseline. This turbine has been widely studied and validated in numerous research efforts related to floating wind applications. Key parameters of the IEA 15MW turbine, including rotor dimensions and overall turbine height, have been well established and are therefore suitable for use in preliminary design. The rotor specifications employed in this study are summarized in Table 4.1, and are adopted as default inputs.

Table 4.1: IEA 15MW Wind Turbine Parameters [48]

Parameter	Value
Mass [kg]	1.02×10^{6}
Rotor diameter [m]	240
Rated thrust [MN]	2.4
J_{RNA} [kg·m^2]	3.52×10^{8}
Cut-in wind V_{in}[m/s]	3
Rated wind V_{rated}[m/s]	10.59
Cut-out wind V_{out}[m/s]	25
Turbine class [-]	IEC class 1B
Turbine height [m]	145

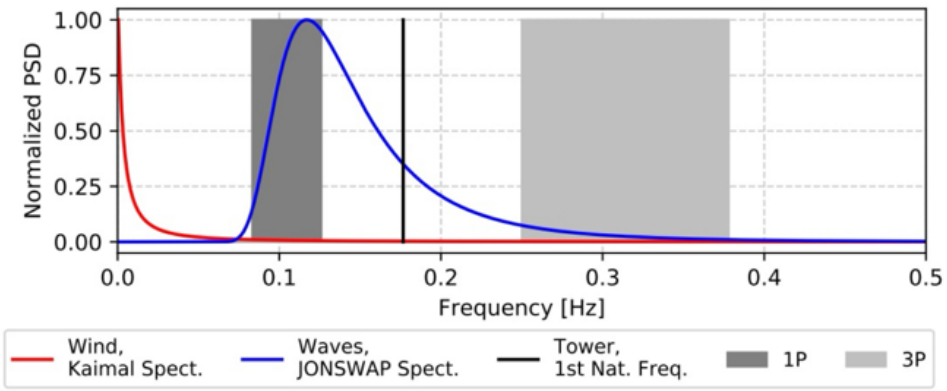

Figure 4.1: IEA 15MW wind turbine frequency bands [48]

Other key information include the rotor frequency bands, controller regulation curve and thrust/power curve, which are essential for the simulation initial settings in the aerodynamics and servo-dynamic modules [49]. These are presented in Figures 4.1, 4.2 and 4.3.

According to the above Figure 4.1, the turbine 1P and 3P frequency ranges are set as:

$$0.083\text{[Hz]} \leq f_{1P} \leq 0.126\text{[Hz]} \tag{4.1}$$

$$0.25\text{[Hz]} \leq f_{3P} \leq 0.378\text{[Hz]} \tag{4.2}$$

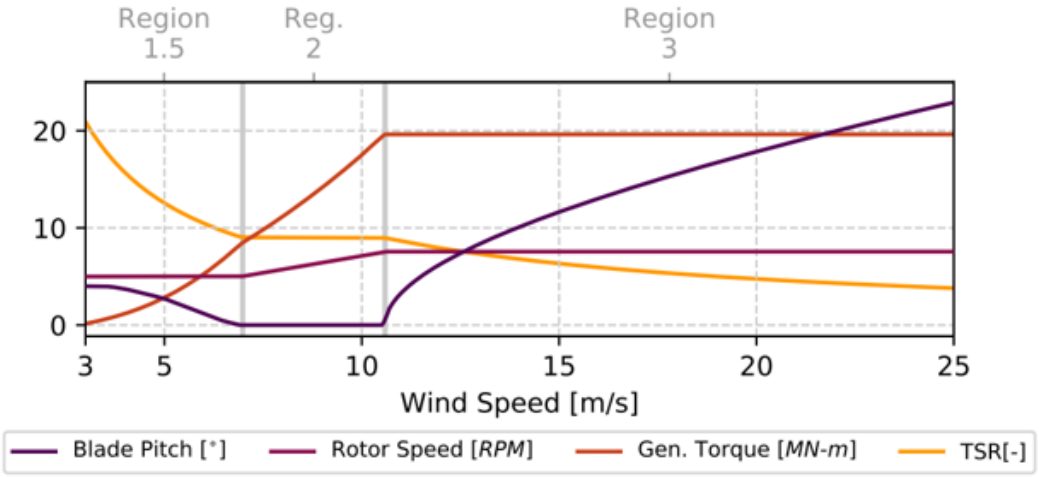

Figure 4.2: IEA 15MW wind turbine controller regulation curve [48]

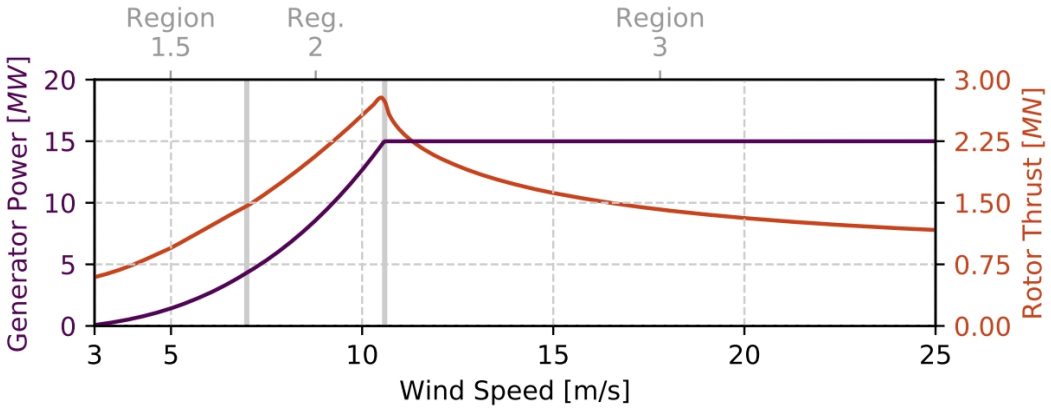

Figure 4.3: IEA 15MW wind turbine power and thrust curve [48]

4.2. Mooring System

The mooring system employed in this project is a catenary mooring system, which is commonly used for spar-buoy-type floating wind turbines as depicted in Figure 4.4. The configuration is adopted from the WindCrete concept [15], as its global geometry is comparable to that of the present design. Furthermore, the redesign of a dedicated mooring system is considered beyond the scope of this study. Therefore, it is deemed acceptable to directly apply the WindCrete mooring configuration in this project.

The details of the adopted mooring system including fairlead attachment positions and anchor positions can be found in the OpenFAST MoorDyn module input file, which is provided in the appendix F. At this initial design stage, the mooring line pre-tension is of particular interest and is found to be approximately 7.37×10^5 N.

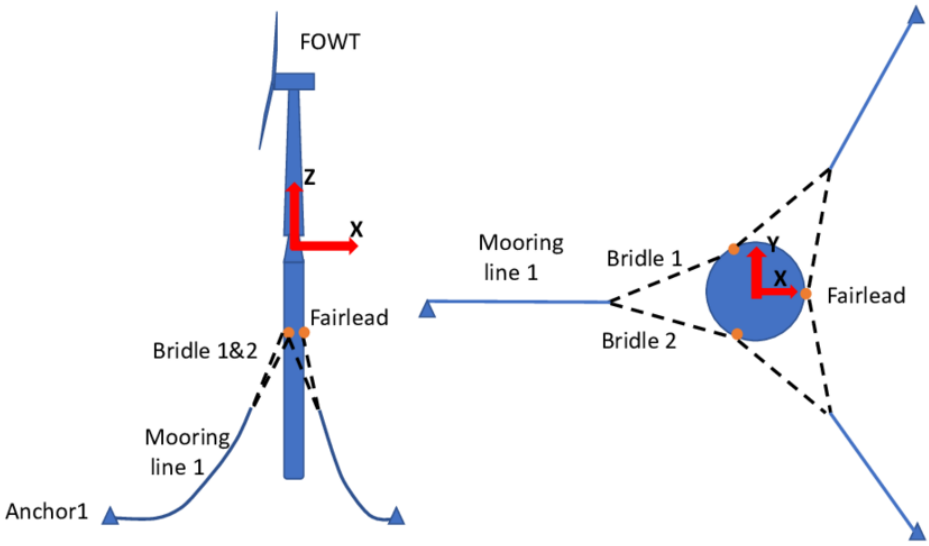

Figure 4.4: Mooring Configuration [50]

4.3. Environment Conditions

The reference site is selected as the North Sea, where the Hywind Tampen spar buoy floating wind farm is also located [14]. Due to limited sources, the location of the former Stevenson Weather Station in Figure 4.5 is chosen to collect environmental conditions including wind and wave characteristics [51]. The statistics of the wind and wave are presented in Table 4.2, and water depth is assumed to be 200m.

Table 4.2: Wave and wind statistics for 1-Year and 50-Year Recurrence Periods

Parameter	1-Year Recurrence	50-Year Recurrence
Significant Wave Height, H_s (m)	10.8	17.6
Peak Spectral Period, T_p (s)	15.5–19.7	19.1
Hub-Height Wind Speed, V_{wind} (m/s)	40	50

Figure 4.5: Reference site location

4.4. Material Properties

As there is limited existing literature on composite floating wind turbine hull design, the material properties and the layer configuration are initially set to match those applied in [11] as a starting point. It is important to note that while the referenced design was developed for a floating wind turbine tower, a floating hull is subject to additional hydrostatic and hydrodynamic pressures. As a result, a detailed stress check is required, and the hull geometry may need to be significantly modified to account for these conditions, potentially diverging from the original tower design.

The reference configuration is shown in Figure 2.3, which illustrates the composite tower design for the floating wind turbine. The structure consists of an external filament-wound layer and an internal double-walled pultruded panel layer.

In this preliminary design study, the configuration is simplified to a single-wall pultruded panel, as also explored in [11]. This simplification facilitates manufacturability and reduces structural complexity while maintaining the essential load-bearing function of the composite tower. The resulting composite layer configuration is illustrated in Figure 4.6, based on a parametric model developed in Grasshopper, which will be introduced in a later subsection.

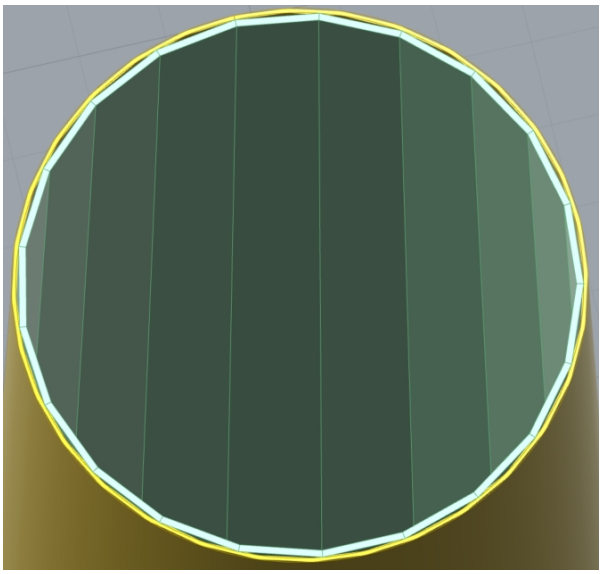

Figure 4.6: Sectional view of material configuration, green part is the pultruded panel, yellow part is the filament wound layer.

Silenka Eglass 1200 tex and MY750/HY917/DY063 epoxy [52] is selected as the composite material for the filament wound layer, as they are widely used for filament winding process with its high stiffness and strength.

In this project, the filament-wound layer adopts a ply angle of 45°, which has been identified as the optimal angle according to [53]. This ply orientation results in approximately equal in-plane elastic moduli in both principal directions, as shown in Table 4.3, and illustrated in Figure 3.6.

This quasi-isotropic behavior is particularly advantageous for OpenFAST implementation, since the ElastoDyn module is primarily designed for isotropic materials. Therefore, the use of a symmetric $\pm 45^\circ$ laminate configuration improves the fidelity of structural modeling within the OpenFAST framework.

CLPT as mentioned in the theory chapter is used to determine the orthogonal moduli and shear modulus of the filament wound layer, as presented in Table 4.3.

A composite of glass fiber reinforced epoxy resin [54] is chosen for the pultrusion panel material due to its combination of cost-effectiveness and high strength. The rule of mixtures is used to determine the pultrusion panel properties, as presented in Table 4.4.

Table 4.3: Filament Wound Layer Properties

Property	Value
Orthogonal moduli E [GPa]	17.6
Shear modulus G_{LT} [GPa]	13.6
Poisson Ratio [-]	0.278
Longitudinal tensile strength X_T [MPa]	1280
Longitudinal compression strength X_C [MPa]	800
Transverse tensile strength Y_T [MPa]	40
Transverse compression strength Y_C [MPa]	143
In-plane shear strength S_{LT} [MPa]	73
Density [kg/m^3]	2000

Table 4.4: Pultruded Panel Properties

Property	Value
Longitudinal modulus E_L [GPa]	40
Transverse modulus E_T [GPa]	5
Shear modulus GLT G_{LT} [GPa]	3
Poisson Ratio [-]	0.3
Maximum Stress [MPa]	414
Density [kg/m^3]	1942

4.5. Geometries

With the initialized material properties, the geometries are designed to satisfy the criteria outlined in Sections 3.1 and 3.3, which include the initial stability check and the tower frequency check. Since these characteristics depend on the geometries, it is challenging to derive the final geometries directly from the criteria. Therefore, an iterative design approach is adopted, starting with an initial geometry guess, which is then evaluated and refined against the specified criteria.

The initial guessed geometries are based on the IEA 15 MW WindCrete spar-buoy concept [15] and a previously optimized composite floating wind turbine tower design [11]. These geometries are subsequently adjusted and evaluated against the initial stability criteria and the frequency check criteria introduced earlier, in order to arrive at a feasible initial configuration. Additionally, a specific design parameter: the number of surrounding pultruded panels, is introduced to determine the panel width and curvature based on the panel layer diameter. These geometric characteristics play a critical role in the buckling resistance of the pultruded panels, as will be further discussed in subsection 4.10.2. In this study, the number of panels is set to 20, following the optimized design of a composite turbine tower presented in [11].

The WindCrete monolithic spar-tower serves as a reasonable starting point for the global geometry definition, as it is also designed to support the IEA 15MW reference turbine. For this monolithic design, where the tower and the spar floater are assumed to be rigidly connected, the tower base is positioned at the still water level (SWL). Based on the WindCrete configurations and the specifications of the IEA 15MW turbine, the global geometric parameters are initially defined as follows:

- Tower height H_{tower}=145m,
- Tower base outer diameter $D_{tower\ base}$=13m,
- Tower top outer diameter $D_{tower\ top}$=6.5m,
- Spar cylinder outer diameter D_{spar}=18.6m,
- Draft=150m,
- Length of the tapered connection part between spar floater and tower L_{cone}=10m

Considering the monolithic design strategy, the thicknesses of both the spar floater and the tower are

initially set to be the same for the pultruded panel layer and the filament-wound layer. In [10], the optimal thicknesses for a single-wall pultruded panel and a filament-wound layer were identified as 20 mm and 73 mm, respectively. Taking into account the manufacturing limitations discussed in that study, the thickness values adopted in this project are carefully selected and subject to verification through the subsequent design steps. The initial thickness design process is illustrated in the flowchart shown in Figure 4.7.

As described in Section 3.1, the initial stability of the structure is governed by the static equilibrium equation (Eq. 3.1) and the metacentric height criterion (Eq. 3.12). The ballast material is assumed to be concrete with a density of $2300\,\text{kg/m}^3$, which is commonly used in spar-buoy applications. Based on the initial geometry, including the estimated thickness values and the defined material densities, Eq. 3.1 is first applied to compute the required ballast volume to satisfy the static equilibrium condition. After the ballast volume is determined, the key parameters contributing to the initial restoring stiffness in Eq. 3.12 are evaluated. These include the water-plane second moment of area I_x, as well as the vertical positions of the center of buoyancy z_B and the center of gravity z_G. Based on a prescribed maximum allowable heel angle of $\theta_{\text{max}} = 10^\circ$, the initially estimated thickness were found to satisfy the metacentric height criterion defined by Eq. 3.12, thereby ensuring adequate initial static stability.

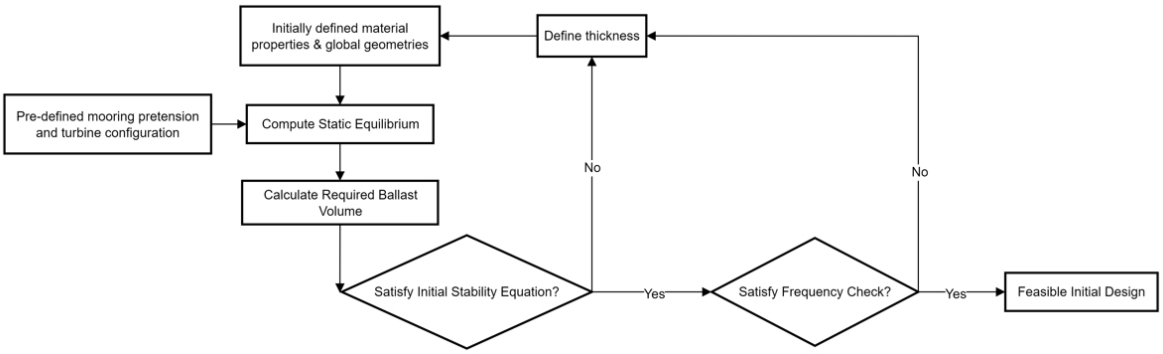

Figure 4.7: Initial design process diagram

After the geometries are checked against the initial stability criteria, the tower configurations are further validated to ensure that their natural frequencies satisfy the requirements outlined in Section 3.3, specifically by avoiding resonance with the 1P and 3P excitation frequencies, as well as dominant wind and wave spectral components. In this step, the thickness is iteratively adjusted to satisfy the tower frequency constraints.

Using the general mass and stiffness matrices defined in Appendix A, the Rayleigh–Ritz method is employed to estimate the fundamental natural frequency of the tower. The corresponding Python implementation is provided in Appendix B. The first modal frequency is calculated to be 0.174 Hz, which lies between the 1P and 3P excitation frequency bands defined in Eq.4.1 and Eq.4.2, indicating that the tower operates within the soft–stiff frequency regime.

At a later stage of the project, a detailed tower modal analysis is carried out using BModes to validate the Rayleigh–Ritz results. BModes predicts a slightly higher first natural frequency of 0.2 Hz. This discrepancy is attributed to the simplifications inherent in the Rayleigh–Ritz model, such as limited degrees of freedom and idealized boundary conditions, which may lead to conservative estimations.

Given that the wave spectrum peak frequency is typically around 0.13 Hz [40] and the wind peak frequency is significantly lower, this frequency is considered acceptable for the design.

After these two design checks, the resulting geometries of tower part and floater part are presented in Table 4.5 and Table 4.6.

For clarity, the design proposed in this study is referred to as 'CSpar', denoting a composite spar-buoy floating wind turbine concept. The initial geometric configuration of CSpar, derived from the iterative

Table 4.5: Taped Tower Geometries

Parameter	Value [m]
Outer Diameter (Base)	13
Outer Diameter (Hub)	6.5
Filament wound layer thickness	0.05
Pultruded panel layer thickness	0.08
Height	145

Table 4.6: Spar Floater Geometries

Parameter	Value [m]
Outer Diameter	18.6
Filament wound layer thickness	0.05
Pultruded panel layer thickness	0.08
Draft	150
Tapered part length	10
Ballast body length	59.14

stability-based design process, is compared with the WindCrete reference design in Figure 4.9 and Figure 4.8.

With the geometries and material properties defined and validated against both the initial stability criteria and the tower frequency requirements, the Preliminary Design phase of the project is considered complete.

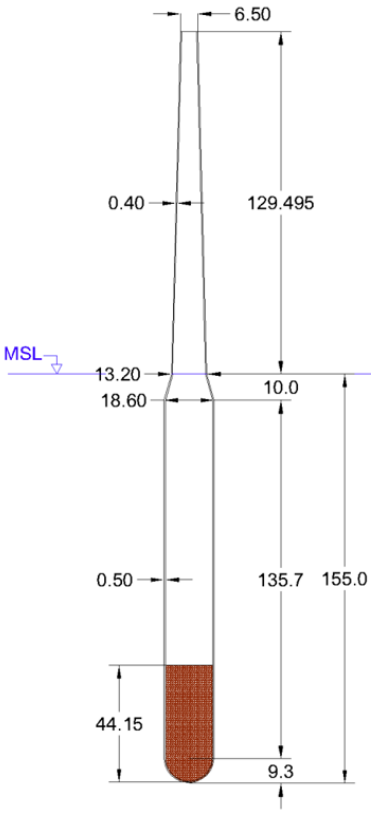

Figure 4.8: WindCrete Spar Buoy Geometries

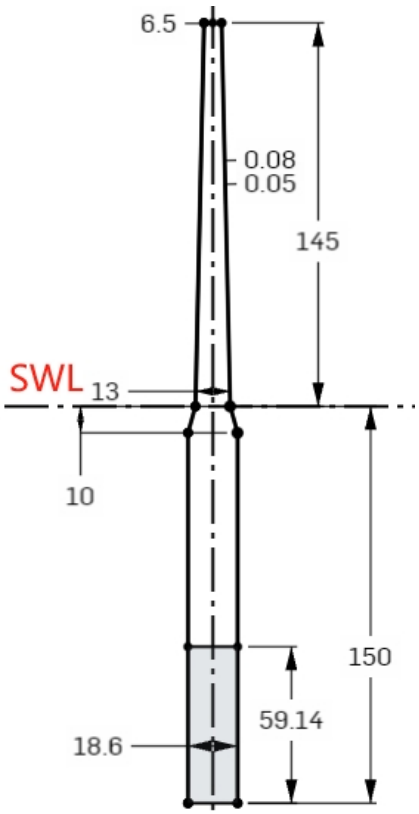

Figure 4.9: CSpar initial design geometries

4.6. Modeling with Computational Tools

4.6.1. HAMS

After defining the environmental conditions and the initial substructure geometry, the added mass, hydrodynamic damping coefficients, and wave excitation forces acting on the structure can be computed using HAMS.

In HAMS, the first step involves generating the wetted surface panel mesh. Based on the previously defined geometry and the meshing considerations, which will be further discussed in the HydroDyn module of OpenFAST, the resulting wetted surface panel model is shown in Figure 4.10.

The computed frequency range is specified in terms of wave periods as -1 s, 0 s, and the interval [2 s, 19.5 s]. The values -1 s and 0 s are required by the OpenFAST HydroDyn module for numerical consistency, while 19.5 s is selected to ensure coverage of the peak period corresponding to the 50-year return period wave.

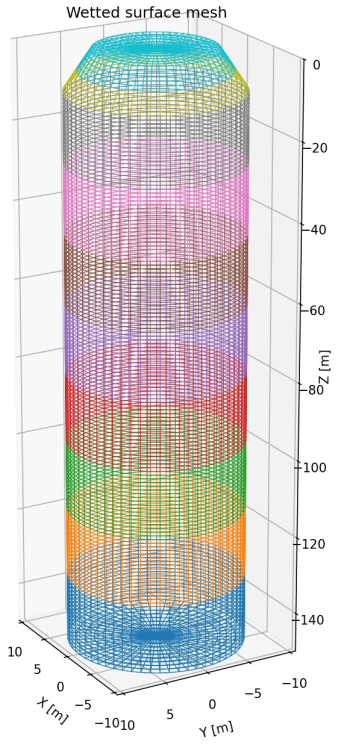

Figure 4.10: Wetted surface mesh panels with panel size=1m

From rules of thumb, generally it is good to have around 6 elements per wavelength. For wave period of 2 s, the corresponding wavelength could be calculated using linear wave theory:

$$\lambda_{2s} = \frac{gT^2}{2\pi} \approx 6.24m \tag{4.3}$$

This corresponds to a mesh size of approximately 1 m, which results in a simulation time of about half a day per run. Consequently, the minimum wave period used in the analysis was set to 2 s. For shorter wave periods, achieving sufficient accuracy would require a finer mesh resolution, which would significantly increase the computational cost and render the simulation impractical within the scope of this study.

To further confirm the proper mesh size to be used, two additional mesh sizes of 1.5 m and 2 m were tested as part of a mesh convergence study. The added mass results of three DoFs computed by HAMS for each mesh configuration were compared, and the maximum deviation from the 1 m mesh

results is indicated in the corresponding figure labels. The added mass values in the surge, heave and pitch DoFs are provided in Appendix D.

Based on the comparison plots, the mesh size of 1.5 m produces results that are sufficiently close to those obtained with the 1 m mesh. Therefore, using a mesh size of 1.5 m is considered acceptable for subsequent analyses.

4.6.2. InflowWind and Turbsim

TurbSim is a stochastic, full-field turbulent wind simulator developed by the NREL [55]. In this study, TurbSim is utilized to generate site-specific turbulent wind field data as input for aeroelastic simulations. The InflowWind module of OpenFAST is then employed to process and integrate the wind-inflow data generated by TurbSim into the simulation framework, specifically passing it to the AeroDyn module for aerodynamic load calculations. This workflow is presented in Figure 4.11.

In Turbsim, the three-component wind speed vectors simulated in a two-dimensional vertical rectangular grid that is fixed in space, as shown in Figure 4.12. TurbSim computes winds in a coordinate system aligned with the direction of the mean velocity vector at each point in space. The velocities are rotated to the inertial reference frame coordinate system before they are written to output files.

To generate turbulent wind fields using TurbSim, it is first necessary to define the wind speed power spectral density (PSD) and the spatial coherence function. TurbSim applies the inverse Fourier transform (IFFT) to convert wind speed spectra from the frequency domain to the time domain. Based on the specified coherence model, it generates three-dimensional turbulent wind fields across multiple spatial points.

The TurbSim input file requires a range of model specifications, including the grid dimensions, wind turbine geometry, analysis duration, and the random seed number for turbulence realization. In addition, key characteristics of the wind profile are defined in the Meteorological Boundary Conditions section of the input file, such as the mean wind speed, reference height, and turbulence intensity.

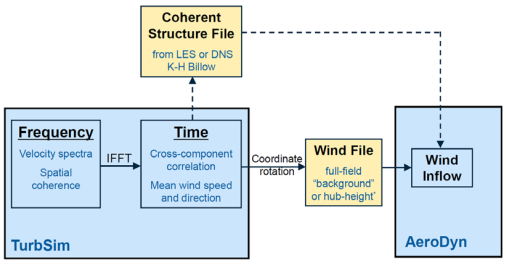

Figure 4.11: TurbSim workflow overview [55]

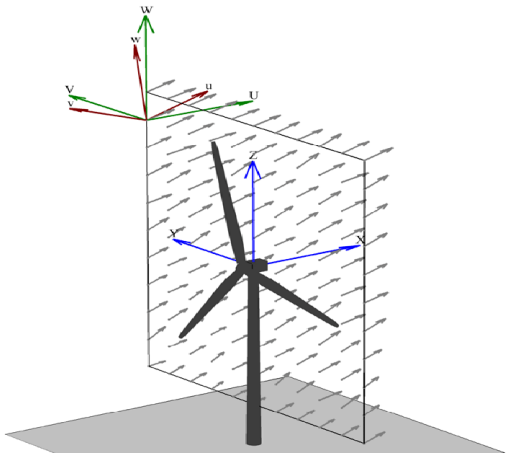

Figure 4.12: Coordinates of a TurbSim wind field with 15° horizontal and 8° vertical mean flow angles [55]

4.6.3. BModes

BModes is a software tool developed by NREL for performing modal analysis of beam-like structures [33]. It computes the natural frequencies and corresponding mode shapes of the structure. In the context of offshore wind turbines, BModes supports two types of beam configurations: blade and tower. In this study, BModes is used to verify that the fore-aft and side-to-side natural frequencies of the tower do not interfere with the turbine's 1P and 3P excitation frequency ranges. Additionally, the mode shape coefficients obtained from BModes are used as inputs to the ElastoDyn module, which will be introduced in a later subsection.

As a standalone tool external to the OpenFAST framework, BModes is executed prior to running Open-

FAST. Its input file primarily requires the tower geometry, node locations, and associated structural properties such as mass density and stiffness distributions. Furthermore, by supplying a mooring stiffness matrix, platform mass matrix, and hydrostatic restoring matrix, BModes can also be used to compute the natural frequencies of the floating platform's 6 DoFs. This capability is particularly useful for validating the numerical model against free-decay test results.

4.6.4. OpenFAST

A FOWT is generally subjected to a variety of environmental loadings, as illustrated in Figure 4.13. Among these, the primary contributors are aerodynamic loads induced by turbulent wind and hydrodynamic loads resulting from waves and ocean currents.

To evaluate these coupled responses, this study employs OpenFAST [49], a modular simulation tool developed by NREL. OpenFAST provides a comprehensive framework for analyzing the multiphysics behavior of wind turbines by integrating various sub-modules, each representing a specific physical domain. These modules are dynamically coupled through a multi-body simulation architecture, enabling realistic assessment of turbine performance under complex offshore conditions.

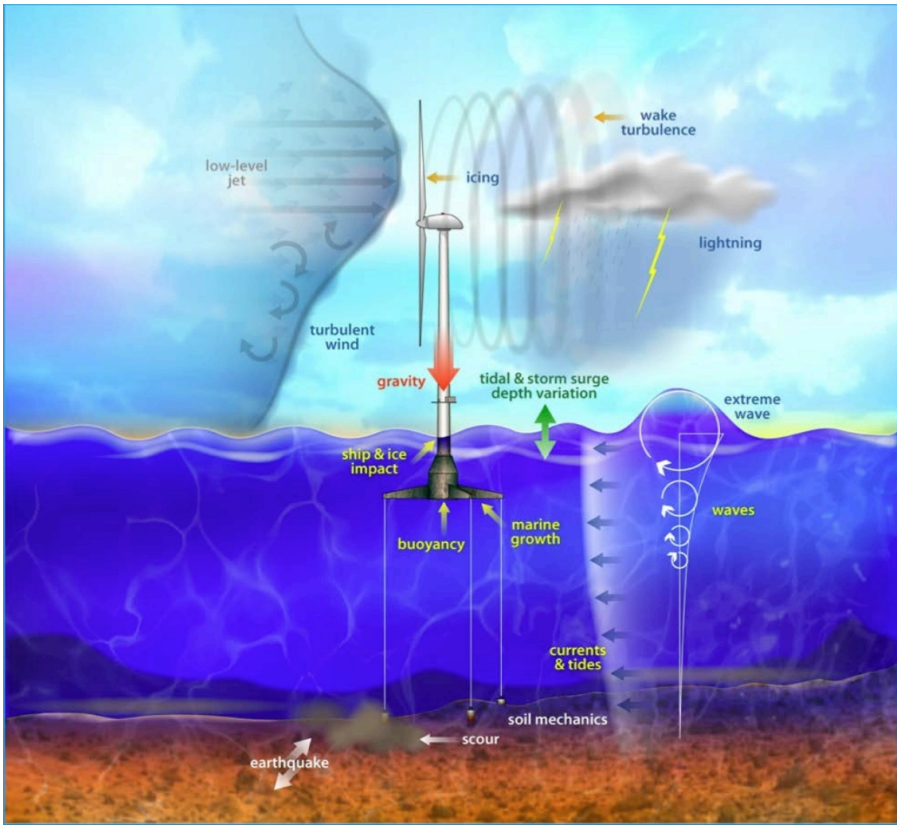

Figure 4.13: Environmental force modeling of a TLP type FOWT in OpenFAST [49]

In this work, OpenFAST is employed as the primary platform for simulating the environmental loading and structural response of the proposed composite spar-type FOWT. The external excitations are incorporated into the generalized external force vector F^e in the governing equation of motion (Eq. 3.56).

The application of composite materials to the substructure necessitates evaluation of structural loading along its length to assess strength. This analysis typically requires consideration of substructure flexibility, implemented through coupled HydroDyn, SubDyn, ElastoDyn, and MoorDyn modules [56]. In this study, only the rigid substructure simulations were performed. This dual approach was justified by the assumed load concentration at the tower base, which represents the critical location for stress analysis and strength verification. This assumption is supported by [57] with the plot shown in Figure 4.14, which conducted structural analysis of a flexible spar buoy model.

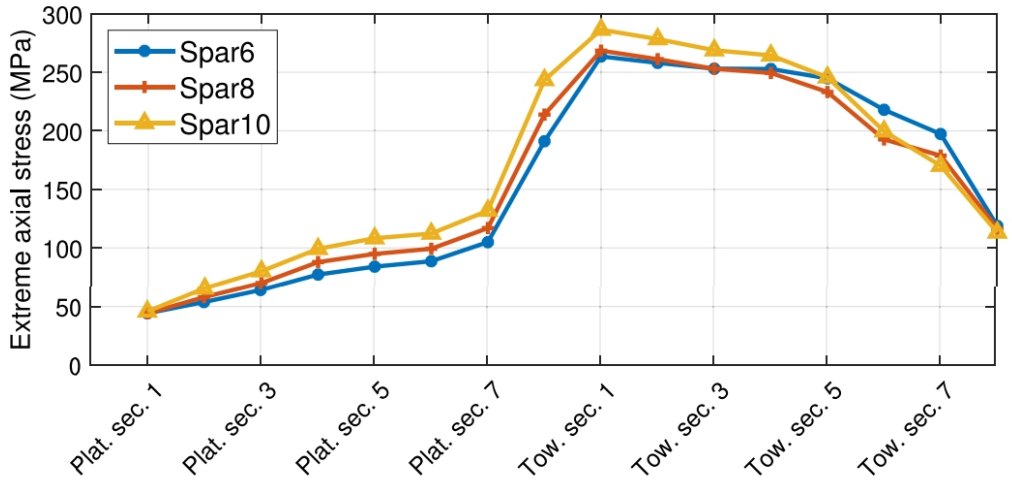

Figure 4.14: Extreme sectional load along the structure studied in [57]. The maximum was found at the tower base node (Tow. sec. 1)

Given the uniform thickness assumption from the spar to the tower, if the tower base can withstand the applied loads, the rest of the spar substructure which has a larger diameter and lower stress concentration, is also deemed sufficient neglecting the hydrostatic pressure effects. Additionally, rigid spar simulations are computationally more efficient; a DLC6.1 rigid spar simulation completes in approximately 2 hours, whereas a flexible spar simulation requires about 3.5 days.

The following subsections provide a detailed overview of the key OpenFAST modules employed in this study. A schematic representation of the relationships among these modules for modeling a flexible platform is presented in Figure 4.15.

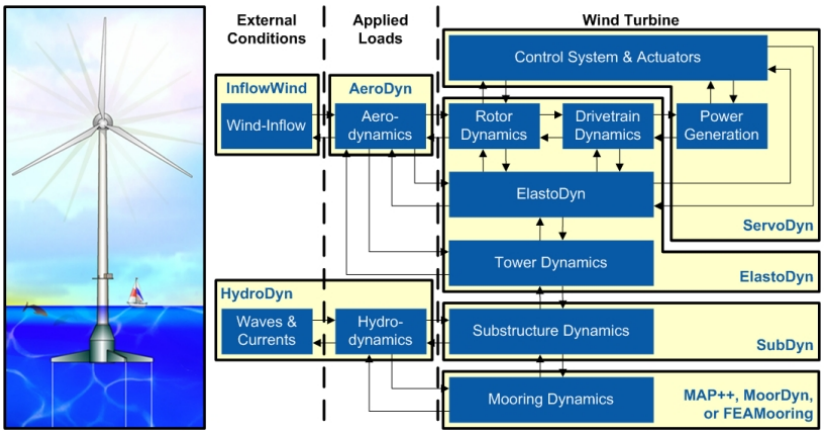

Figure 4.15: OpenFAST workflow

4.6.4.1. SeaState and HydroDyn

HydroDyn models hydrodynamic loads based on a combination of incident wave kinematics and hydrodynamic loading formulations. It supports both first-order linear Airy wave theory and an optional second-order formulation, where nonlinear wave effects are incorporated by extending the wave spectrum using first-order wave amplitudes. This enables a more realistic representation of surface wave nonlinearities, thereby improving the accuracy of hydrodynamic load predictions. Directional wave spreading can also be included to represent complex sea states. Additionally, the accuracy of the strip-theory model in short waves can be further enhanced by enabling the MacCamy–Fuchs diffraction model, which adjusts the wave excitation loads to account for diffraction effects in finite-depth water conditions [58].

By modeling the floater of the structure in HAMS as presented in Figure 4.10, the added mass and damping coefficients, excitation forces from the diffraction potential, and the hydrostatic restoring coefficients are calculated through HAMS. These results are output as .1, .3, and .hst files from HAMS, and taken as inputs for OpenFAST. Due to limited functionalities of HAMS, non-linear effects are excluded and linear potential flow model is used.

4.6.4.2. ElastoDyn

As a structural dynamics module, ElastoDyn is responsible for computing the positions, velocities, and accelerations of key structural points, starting from the platform reference point along the global Z-axis and progressing upward through the structure. When provided with an additional ElastoDyn tower input file containing the tower's sectional properties and mode shape coefficients, ElastoDyn can also compute the local nodal loads along the tower.

From a dynamics perspective, ElastoDyn defines the initial conditions for the DoFs associated with the drivetrain, nacelle, tower, blades, and platform. It also specifies which DoFs are activated during the simulation, thereby facilitating debugging and model configuration.

In a rigid platform configuration, ElastoDyn defines the mass and inertia properties of the entire platform, including the substructure and ballast.

The tower is modeled in ElastoDyn using straight Euler–Bernoulli beam theory. Its structural flexibility is represented through a reduced-order modal formulation, in which a limited number of predefined mode shapes are used to capture the tower's dynamic behavior. These mode shapes, typically obtained from BModes, are assumed to remain constant throughout the simulation and form the basis for calculating deformations and internal loads.

The time integration scheme in ElastoDyn is user-selectable among several options, including the explicit fourth-order Runge–Kutta (RK4) method, the fourth-order Adams–Bashforth (AB4) explicit multistep method, and the fourth-order Adams–Bashforth–Moulton (ABM4) predictor–corrector method. The ABM4 method is chosen in this work due to its favorable balance between accuracy and computational efficiency for multi-degree-of-freedom structural dynamic simulations. As a fourth-order predictor–corrector scheme, ABM4 provides higher accuracy than lower-order methods while requiring fewer function evaluations per time step compared to explicit Runge–Kutta methods. This makes it particularly suitable for long-duration simulations of offshore wind turbines, where stability and performance are both critical.

4.6.4.3. AeroDyn

AeroDyn is the aerodynamic module within the OpenFAST framework responsible for time-domain computation of aerodynamic loads, enabling aeroelastic simulations of horizontal-axis wind turbines. It accounts for aerodynamic forces on both the blades and the tower.

The aerodynamic formulation in AeroDyn is based on the actuator line concept, in which the three-dimensional (3D) flow around the rotor is approximated by a series of local two-dimensional (2D) flow solutions at discrete cross-sectional analysis nodes. At each node, the pressure and shear stress distributions on the airfoil surface are represented by equivalent lift, drag, and pitching moment forces. These sectional loads are calculated per unit length and subsequently integrated along the blade or tower span to obtain the total 3D aerodynamic loads. The distribution of aerodynamic analysis nodes is defined independently of the structural discretization in OpenFAST.

The actuator line model inherently assumes the structure is slender, with fully 3D effects either neglected or approximated through embedded correction models, such as tip-loss, hub-loss, or skewed-wake corrections. Rotational augmentation effects may also be accounted for via modified airfoil tables provided as input.

AeroDyn uses the quasi-steady Blade Element Momentum (BEM) method [49] to evaluate the aerodynamic loads acting on the rotor. Wake effects are incorporated through momentum theory, and unsteady airfoil behavior is captured using the Beddoes–Leishman dynamic stall model.

The rotor's initial angular velocity is initialized based on the prescribed wind speed and the corresponding rotational speed, following the baseline controller's performance curves (see Figure 4.2). In addition to blade aerodynamics, tower loading and tower shadow effects are also considered in the simulation.

4.6.4.4. Others

Other key modules in OpenFAST used in this study include BeamDyn, MoorDyn, and ServoDyn, which handle the modeling of the blades, mooring system, and control system, respectively.

Given that this work primarily focuses on the structural analysis and evaluation of the feasibility of composite materials in the floating wind turbine system—specifically in the tower and spar platform—no modifications were made to the mooring and control configurations. The mooring system is directly adopted from the WindCrete spar design due to its geometric similarity and validated strength [13]. Similarly, the control strategy implemented through the ServoDyn module is based on the publicly available controller developed for the IEA 15 MW reference turbine. For blade modeling, BeamDyn is used with its default configuration from the standard IEA 15 MW (UMain semi-submersible) OpenFAST input set.

4.6.5. MExtremes and MLife

MExtremes [59] and MLife [45] are two MATLAB-based post-processing tools developed by NREL for conducting extreme-event statistical analysis and fatigue damage assessment, respectively. These tools operate on the output files generated from one or multiple OpenFAST simulations, enabling systematic evaluation of structural loads under varying design load cases.

In MExtremes, the user specifies the output channels to be analyzed for extreme value statistics. In this study, particular attention is given to the nodal structural loadings of the spar and tower, which are critical for evaluating material strength, as well as to the platform displacements, which are assessed against operational and design limits. The tool also supports the creation of custom output channels by combining existing ones from the OpenFAST simulation results. For example, a resultant nodal axial force can be defined as the vector sum of the axial force components in the x- and y-directions.

Input channels in MLife are defined in a similar manner to MExtremes, with the distinction that only loading-related output channels are specified for fatigue analysis. In this study, the design life is set to 630,720,000 seconds, equivalent to 20 years, as defined by the DesignLife parameter in the input file. Each output channel is assigned a specific S–N curve for fatigue damage calculation, requiring the user to provide the corresponding curve parameters.

MLife computes fatigue damage using different strategies depending on the type of design load cases represented by the simulation outputs. Specifically, it distinguishes between normal operating conditions and idling scenarios under extreme environmental loads, applying separate statistical treatments appropriate to each category.

4.6.6. OpenMDAO

OpenMDAO is a widely adopted open-source framework for multidisciplinary design, analysis, and optimization (MDAO) [19]. Developed by NASA Glenn Research Center, it provides a flexible and extensible platform for integrating complex simulation models and performing gradient-based or gradient-free optimization. The framework supports features such as automatic differentiation, parallel execution, design space exploration, and constraint management, making it particularly suitable for engineering systems involving tightly coupled physics and computationally intensive analyses.

In the context of wind turbine or floating platform design, OpenMDAO enables the integration of various physics-based modules—such as structural analysis, hydrodynamics, aerodynamics, and cost models—into a unified optimization workflow. Its modular architecture facilitates communication between different simulation tools, allowing the user to efficiently evaluate and optimize design variables under multidisciplinary constraints.

In this project, OpenMDAO is used as the platform frame to combine the structural analysis results obtained with the post-processing of MExtremes and MLife, and then optimize the selected geometries for the optimization objectives while satisfying constraints of the variables.

4.6.7. Grasshopper

Grasshopper is a visual programming environment integrated with Rhinoceros (Rhino), a widely used computer-aided industrial design (CAID) software. In this project, Grasshopper is used to define the parametric geometry of the floating wind turbine's substructure and tower. By modifying key design

parameters—such as diameters, wall thicknesses, and platform draft—users can immediately visualize the resulting changes in the 3D model within the Rhino interface. This capability facilitates intuitive geometric exploration and rapid iteration during early-stage design.

Moreover, Grasshopper also supports Python scripting through its integrated components. This feature is particularly useful in this project, as the double-layer composite structure introduces significant geometric complexity. When performing sensitivity studies of geometry, manually updating OpenFAST input files becomes inefficient and error-prone. To address this, Grasshopper is used not only for geometry modeling, but also for computing key physical properties such as center of gravity, inertia of bodies. These quantities are then passed to the local Python-based simulation workflow, where OpenFAST input files are automatically generated and batch simulations are executed.

This Grasshopper workflow is structured into four main components, illustrated in the figures attached in Appendix E: (1) the definition of constants, such as material properties and environmental parameters, as illustrated in Figure E.1; (2) the specification of design variables that govern key geometric features—including diameters, wall thicknesses, and platform draft—shown in Figure E.2; (3) the execution of Python-based calculations, where essential physical quantities such as the center of gravity and submerged volume are derived. On the right side of Figure E.2, a set of Python scripting components compute these quantities and pass them to the local simulation workflow, enabling automatic generation of OpenFAST input files; and (4) the real-time 3D visualization of the resulting geometry within the Rhino interface, which displays the initial structural configuration. An example of this visualized design is shown in Figure E.3.

This modular structure enhances clarity during parametric modeling, facilitates efficient design iteration, and ensures smooth integration with the downstream simulation and optimization framework. With the model modularized through the combined use of Grasshopper and Python, changes to the geometries in Grasshopper can instantly update the corresponding geometry settings in the OpenFAST input files, making them ready for simulation. Therefore, the second phase of the project is considered complete.

4.7. Design Load Cases

The IEC 61400-3 standard [6] provides guidelines for the loading scenarios that an offshore wind turbine is expected to experience throughout its design lifetime. These guidelines aim to ensure structural safety and reliable performance under a wide range of environmental and operational conditions.

DLCs defined by the standard are essential for identifying critical loading conditions, both during extreme events and under normal operation, and serve as the basis for ultimate and fatigue load analyses. Although a complete set of DLCs is typically required for a comprehensive design study, it was found that simulating a single ultimate DLC for all seeds can take approximately seven days. Due to limitations in available time and computational resources, only a selected subset of DLCs is considered in this study, as summarized in Table 4.7.

Table 4.7: Chosen IEC 61400-3 DLCs

Load Case	**DLC 6.1**	**DLC 6.3**	**DLC 1.2**
Load Type	Ultimate	Ultimate	Fatigue
Load Factor	1.35	1.35	1.00
Status	Idling (Storm)	Idling (yaw error)	Producing
Wind	$V_{50\text{yr}}$	$V_{1\text{yr}}$	V_{in}-V_{out}
Turbulence	EWM50	EWM50	NTM
SeaState	50 yr	1 yr	$H_s, T_p = f(V_{\text{hub}})$
Yaw Error	$0°, \pm 8°$	$0°, \pm 30°$	$0°, \pm 10°$
Wind and Wave Directionality	COD, MUL (-10, 0, 10)	MIS, MUL (-30, 30)	MIS, MUL (-30, 30)
Seeds	6	6	6
Currents	ECM	ECM	No Currents
Duration [s]	5400	5400	5400

In Table 4.7, EWM50 refers to the extreme wind model with a 50-year return period, NTM denotes the normal turbulence model, COD stands for co-directional, MIS indicates misaligned, and MUL represents multi-directional environmental conditions. And the load factor corresponds to the γ_l as presented in Section 3.7.

4.8. Material Factors

Eurocode standard [60] as presented in Table 4.8 is selected as it provides guidance for structures manufactured by both filament winding and pultrusion, compared to other codes like DNV-GL [11].

Table 4.8: Eurocode Material Factors

Material Factors	Value
Material Failure	2.25
Local Buckling	2.50
Global Buckling	2.25

The material factor, similar to a safety factor, provides a margin of tolerance between the design stress and the material's ultimate strength, ensuring structural reliability under various loading conditions. It could be defined as:

$$\sigma_d = \frac{\sigma_u}{\gamma_m} \tag{4.4}$$

where σ_d is the allowable maximum stress for the design, σ_u is the material ultimate strength and γ_m is the material factor. γ_m here could be considered as the partial safety factor γ_s as discussed in the Section 3.7.

4.9. Extreme Responses Estimation

In this study, the Gumbel distribution is adopted to predict the extreme values of stress responses, based on the selected extreme DLC output data, which are DLC 6.1 and 6.3 in this project as they are expected to give the most extreme stress responses. Under each selected case, the short-term simulation is repeated multiple times with different realizations of wind and wave seeds to capture variability.

For each case, the maximum stress values are collected from all simulation seeds by `MExtremes` and are used to fit a Gumbel distribution. The fitted distribution is then used to estimate the extreme response at a target non-exceedance probability, which is selected as the 90% percentile in this project.

The cumulative distribution function (CDF) of the Gumbel distribution is given as:

$$F_x(x) = \exp\left(-\exp\left(\frac{x-\mu}{\beta}\right)\right) \tag{4.5}$$

where $F_x(x)$ is the cumulative probability, and μ and β are the location and scale parameters of the distribution. These parameters are estimated using least-squares fitting in a probability plot. To facilitate linear fitting, the CDF is transformed into the following linear form:

$$-\ln\left(-\ln(F_x(x))\right) = \frac{x}{\beta} - \frac{\mu}{\beta} \tag{4.6}$$

This approach enables efficient prediction of the maximum stress response over longer periods based on short-term simulation results.

4.10. Structural Analysis

In this study, buckling and yielding are considered the primary failure modes of interest, rather than fatigue. This choice is supported by findings from previous studies, such as [11] and [61], which indicate that accumulated fatigue damage in composite materials used for tower or substructure is generally

not significant. Therefore, buckling and yielding are implemented as constraints in the optimization workflow, while fatigue load analysis is conducted only after an optimized structural solution is obtained.

In this study, the tower is discretized into 10 nodes, including the tower base node. The substructure is discretized into 20 nodes, together with a single interface node that coincides with the tower base. The external loads acting on these nodes are extracted from the DLC simulations and stored in .out files. These files are subsequently used for post-processing with tools such as MExtremes and MLife, as well as for stress and fatigue calculations using equations introduced in Section 3.7.

4.10.1. Yielding

Yielding failure is evaluated for both the filament-wound layer and the pultruded panel. To identify the most critical load conditions, MExtremes is used to extract the maximum loading values across all stochastic seeds for a given DLC. These peak loadings serve as the input for subsequent stress analysis and failure evaluation of the composite structure.

For the filament-wound layer, the first-ply failure approach is adopted to conservatively evaluate material yielding. This method assumes that the laminate has failed once the failure criterion is exceeded in any individual ply, without considering the progressive accumulation of damage throughout the laminate.

The Tsai–Wu failure criterion [62] is considered an appropriate method for capturing the interaction of multi-axial stress states in the filament wound layer. In contrast, the maximum stress criterion is applied to account for ply failure resulting from dominant uniaxial stress components. The failure index U_{FW} is expressed as a quadratic function of the in-plane stress components in the local ply coordinate system:

$$U_{\text{FW}} = F_1\sigma_x + F_2\sigma_y + F_6\sigma_{xy} + F_{11}\sigma_x^2 + F_{22}\sigma_y^2 + F_{66}\sigma_{xy}^2 + 2F_{12}\sigma_x\sigma_y \tag{4.7}$$

The coefficients F_i are calculated based on the material strength limits in tension, compression, and shear:

$$\begin{aligned} F_1 &= \frac{1}{X_t - X_c}, \quad F_2 = \frac{1}{Y_t - Y_c}, \quad F_6 = 0, \\ F_{11} &= \frac{1}{X_t X_c}, \quad F_{22} = \frac{1}{Y_t Y_c}, \quad F_{66} = \frac{1}{S_{xy}^2}, \quad F_{12} = \frac{-1}{2\sqrt{X_t X_c Y_t Y_c}} \end{aligned} \tag{4.8}$$

Here, σ_x, σ_y, and σ_{xy} represent the in-plane normal and shear stresses within a ply, while X_t and X_c represent the allowable tensile and compressive strengths in the fiber (ply x) direction, respectively; Y_t and Y_c denote the corresponding strengths in the transverse (ply y) direction; and S_{xy} refers to the maximum allowable in-plane shear strength. These strength parameters are used to evaluate the failure index, and the laminate is considered to have failed when $U_{\text{FW}} \geq 1$.

Since the Tsai–Wu failure criterion is defined in the local coordinate system of each ply, it is necessary to transform the global stress components obtained from OpenFAST into the ply-aligned directions before evaluating failure. In this study, the global normal stress σ and shear stress τ are transformed into the local ply coordinate system using standard 2D stress transformation relations based on the ply orientation angle θ.

The transformed stresses σ_x, σ_y, and σ_{xy} in the local coordinate system are calculated as follows:

$$\sigma_x = \sigma\cos^2\theta + \tau\sin\theta\cos\theta \tag{4.9}$$

$$\sigma_y = \sigma\sin^2\theta - \tau\sin\theta\cos\theta \tag{4.10}$$

$$\sigma_{xy} = (\sigma - \tau)\sin\theta\cos\theta + \tau(\cos^2\theta - \sin^2\theta) \tag{4.11}$$

Here, θ is the ply angle measured from the global axis, which is taken as 45° in this study. The transformed stresses are then substituted into the Tsai–Wu failure index U_{FW} expression.

For the pultruded panel, material failure is evaluated using a maximum stress criterion. This approach assumes that failure occurs when the applied stress in the ply exceeds the corresponding allowable strength, either in tension or compression. The failure index is defined as:

$$U_{\text{material}} = \frac{\sigma}{X} \tag{4.12}$$

where σ denotes the applied stress in the principal material direction, and X represents the corresponding ply strength, defined as the maximum allowable stress under the same loading mode.

4.10.2. Buckling

In this project, it is anticipated that structural failure will most likely be governed by buckling. The critical buckling stress is assumed to be primarily resisted by the inner structural layer, which consists of pultruded composite panels. According to the formulations presented in [27], the critical buckling stresses of pultruded panel sections under axial compression and in-plane shear can be calculated using Equations (4.13) and (4.14), corresponding to the loading scenarios illustrated in Figure 4.16 and Figure 4.17, respectively.

$$\sigma_{\text{Cr-Buckle}} = \frac{1}{6} \cdot \frac{E}{1-\nu^2} \left[\sqrt{12(1-\nu^2)} \left(\frac{t}{r}\right)^2 + \left(\frac{\pi t}{b}\right)^4 + \left(\frac{\pi t}{b}\right)^2 \right] \tag{4.13}$$

$$\tau_{\text{Cr-Buckle}} = 0.1E\frac{t}{r} + 5E\left(\frac{t}{b}\right)^2 \tag{4.14}$$

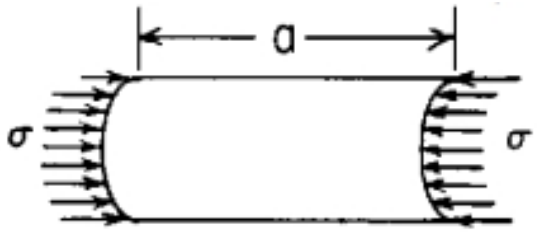

Figure 4.16: Curved panel under uniform compression on curved edge

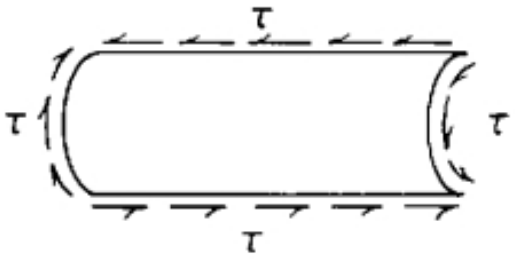

Figure 4.17: Curved panel under uniform shear on all edge

where ν is Poisson's ratio, b is the width of panel measured on arc, E is the modulus of elasticity, r is the radius of curvature. To evaluate the combined effects of axial and shear loading, the buckling utilization factor is defined as:

$$U_{\text{Buckle}} = \left(\frac{\sigma_{\text{xxBuckle}}}{\sigma_{\text{crBuckle}}}\right) + \left(\frac{\tau_{\text{xyBuckle}}}{\tau_{\text{crBuckle}}}\right)^2 \tag{4.15}$$

where U_{Buckle} represents the utilization ratio. A value of U_{Buckle}<1 indicates that the structure remains within its buckling limits under the applied combined loading.

With the geometries and material properties defined previously, $\sigma_{\text{cr-Buckle}}$ and $\tau_{\text{cr-Buckle}}$ are calculated as 72.88 Mpa and 92.11 Mpa.

4.10.3. Fatigue

In this study, the structural fatigue failure is evaluated using MLife, based on the methodology presented in Section 3.7. A conservative assumption is made that the applied loading and thus the resulting fatigue damage is dominated by a single principal direction. Given the anticipated low fatigue sensitivity of the

structure, the cumulative damage contributions from other wind and wave directions are considered negligible, provided that the damage from the dominant direction is sufficiently low.

The Wöhler exponent m is set to 10 in this study, which is commonly adopted in fatigue analyses of composite wind turbine blades based on empirical observations in the literature.

For each type of loading, the ultimate load L_{Ult} for a thin-walled circular cross-section can be estimated using the following equations according:

$$\text{Transverse shear:} \quad L_{\text{Ult}} = \tau_{\text{yield}} \cdot \frac{A}{2} \tag{4.16}$$

$$\text{Axial loading:} \quad L_{\text{Ult}} = \sigma_{\text{yield}} \cdot A \tag{4.17}$$

$$\text{Pure bending:} \quad L_{\text{Ult}} = \sigma_{\text{yield}} \cdot \frac{I}{y} \tag{4.18}$$

$$\text{Torsion:} \quad L_{\text{Ult}} = \tau_{\text{yield}} \cdot \frac{J}{r} \tag{4.19}$$

where:

- D_o: outer diameter
- D_i: inner diameter
- $r = y = \frac{D_o}{2}$: maximum radius
- $A = \frac{\pi}{4}(D_o^2 - D_i^2)$: cross-sectional area
- $I = \frac{\pi}{64}(D_o^4 - D_i^4)$: area moment of inertia
- $J = 2I = \frac{\pi}{32}(D_o^4 - D_i^4)$: polar moment of inertia

Because the loads near the interface between the substructure and the tower are significantly higher than those at other locations, fatigue failure is more likely to occur at the first few nodes adjacent to this connection. Therefore, fatigue damage is specifically evaluated for the three nodes near the water free surface.

The resulting fatigue damage D is interpreted as the fatigue utilization factor U_{F}. If the value of $U = U_{\text{F}}$ exceeds 1.0, the structure is considered to have failed the fatigue check at that location.

4.11. Optimization Workflow

Similar to many other FOWT optimization studies, this project aims to identify the optimal set of geometric parameters that minimize the structural cost, subject to ULS constraints. FLS analysis is performed after the optimal design is obtained, as fatigue was previously discussed not to be the governing design constraint for composite structures in this context.

The design variables $\vec{x}$ are selected as the geometric parameters, including the diameters and thicknesses of both structural layers. This choice is motivated by the fact that these parameters directly influence the effective stiffness and sectional inertia of the structure, which in turn govern its dynamic response and internal stress distribution. In addition, these geometric properties also have a direct impact on the structural cost, as they determine the overall material volume.

Based on the previous key assumptions and the expectation that the critical load occurs at the tower base, with equal thicknesses for both the spar and the tower, the selected design variables and their corresponding lower and upper bounds are summarized in Table 4.9. These bounds are established according to practical manufacturing constraints and physical configurations.

Table 4.9: Design variables $\vec{x}$ and their bounds

Variable	Lower Bound	Upper Bound
Tower Base Outer Diameter (D_{Twrbase}) [m]	10.0	18.60
Pultruded wall thickness (t_{p}) [m]	0.04	0.10
Filament wound thickness (t_{f}) [m]	0.04	0.15

The objective function $f(\vec{x})$ is defined as the total cost of the structure, which is approximated by the sum of the material costs of each composite layer. It is expressed as:

$$f(\vec{x}) = \text{Cost} = m_f P_f + m_p P_p \tag{4.20}$$

where m_f and P_f denote the mass and unit cost per kilogram of the filament-wound layer, respectively, while m_p and P_p represent the mass and unit cost per kilogram of the pultruded panel layer. The unit prices of both materials are taken from Reference [11], which employed these two composite manufacturing techniques in the structural optimization of a tower for the IEA 15 MW wind turbine. The resulting unit costs are:

$$P_f = 6.17\,€/\text{kg} \tag{4.21}$$

$$P_p = 4.00\,€/\text{kg} \tag{4.22}$$

In terms of constraints, in addition to the ULS checks that include yielding and buckling criteria, dynamic considerations are also incorporated. Specifically, the first natural frequency of the tower must be kept outside the excitation frequency ranges associated with the rotor's 1P and 3P frequencies to avoid resonance. Since the preliminary design adopts a soft–stiff configuration, the tower frequency is constrained to lie above the 1P frequency and below the 3P frequency.

As this project primarily focuses on structural strength assessment, and a fixed set of initial loadings is reused throughout the optimization process, it is challenging to impose displacement-based constraints. Accurately estimating displacements would require running full simulations, and design parameters such as geometric dimensions do not influence displacements as directly as they affect structural strength. Consequently, platform motions are not explicitly included as optimization constraints. However, the maximum platform motions obtained from the extreme environmental condition simulations (DLC6.1 and DLC6.3) with a simulation time of 6000 s are documented in order to qualitatively evaluate the platform's dynamic response to these conditions. The platform motion is constrained by the following commonly adopted limits:

- Maximum surge displacement [15]: 30 m
- Maximum heave displacement [20]: 0.1 × water depth (20 m in this study)
- Maximum pitch angle [20]: 15°

These constraints help check the dynamic stability of the initial design.

The design constraints applied in the optimization iterations can be summarized by the following set of equations:

$$\begin{aligned} U_{\text{Panel}} &= \max(U_{\text{Buckle}}, U_{\text{Material}}) \leq \frac{1}{\gamma_m \gamma_l} \\ U_{\text{FW}} &\leq \frac{1}{\gamma_m \gamma_l} \\ f_{\text{tower}} &\in [f_{\text{1P,max}},\ f_{\text{3P,min}}] \end{aligned} \tag{4.23}$$

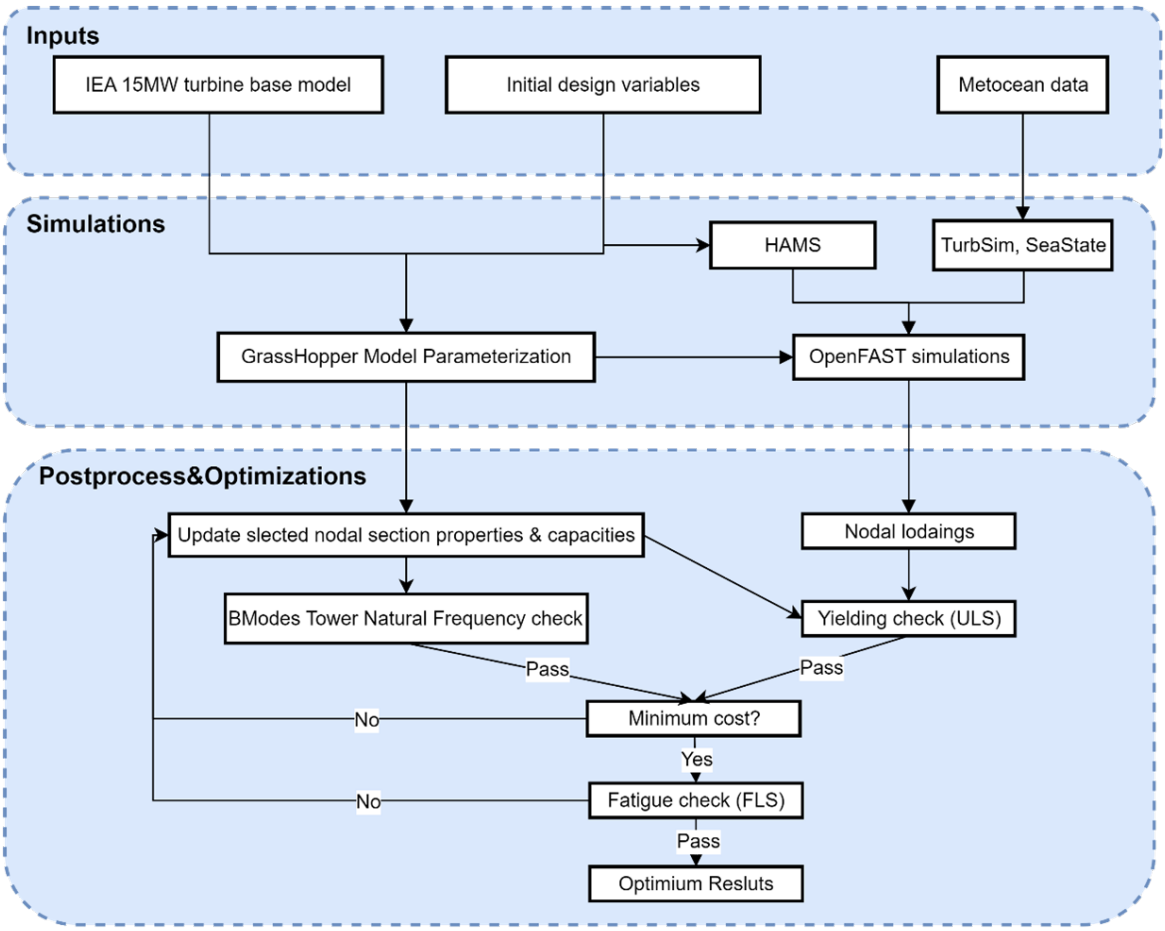

Figure 4.18: Optimization Workflow Overview

Although gradient-based algorithms are typically preferred for their rapid convergence characteristics, they proved ineffective in this study. This limitation primarily arises from inaccuracies in the analytical gradient formulations, which likely hindered convergence to a true optimum. For non-gradient-based approaches, such as Genetic Algorithms and Constrained Optimization BY Linear Approximations (COBYLA), three key shortcomings were identified: (1) significantly slower convergence rates, (2) an inherent tendency to converge to local optima rather than the global optimum, and (3) high sensitivity to the initial design variables, where different initial values can lead to convergence toward different local optima.

Consequently, a design space exploration approach was adopted for design variable optimization. This method systematically evaluates multiple input parameter sets to identify the optimal solution. The optimization process was implemented within the OpenMDAO framework. Figure 4.18 provides a comprehensive overview of the workflow, highlighting the iterative evaluation process and convergence criteria.

5

Results and Discussion

5.1. Preliminary Design

5.1.1. Static Equilibrium

Static equilibrium simulations were conducted to determine the static offsets in all DoFs. These results are used to evaluate the static balance of the system and to ensure that the offsets remain within acceptable limits, thereby avoiding potential numerical instabilities in subsequent DLC simulations. The outcomes of the static equilibrium tests are illustrated in Figure 5.1, and the corresponding offset values are summarized in Table 5.1.

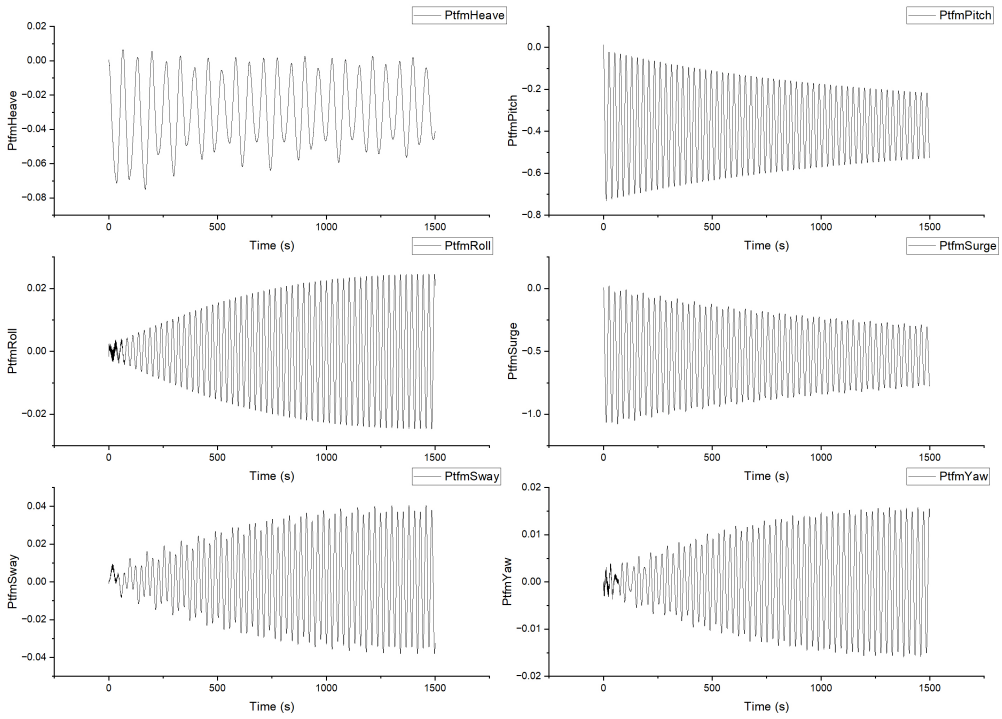

Figure 5.1: Static Equilibrium Tests

While the static offsets in most degrees of freedom are negligible, a moderate offset of approximately

0.5 m is observed in the surge direction which is considered due to the pitch offset, and the heave offset is around -0.03m. These offsets are considered normal and acceptable when compared with other spar buoy designs such as WindCrete [15].

Table 5.1: Static offsets of all DoFs from equilibrium simulation

Degree of Freedom (DoF)	Mean Offset
PtfmHeave (m)	-0.02969
PtfmPitch (°)	-0.3722
PtfmRoll (°)	3.19322E-5
PtfmSurge (m)	-0.5362
PtfmSway (m)	0.00133
PtfmYaw (°)	1.02655E-5

5.1.2. Structural loadings

The simulated structural loadings obtained from the preliminary design are reused in each iteration of the optimization process to reduce computational cost, as running a full time-domain simulation at every iteration would be prohibitively expensive.

For the flexible spar design model, both the substructure and the tower are discretized into 10 elements, resulting in 11 nodes for the spar substructure and 10 nodes for the tower. For the rigid spar model, only the tower is divided into 10 nodes. For the ULS yielding check, the maximum values from the nodal loading time series under DLC 6.1 and DLC 6.3 are extracted and used. The corresponding maximum loading distributions along both the substructure and the tower are presented in Appendix G.

Compared to DLC 6.1, under zero yaw angle and zero wave–wind misalignment, DLC 6.1 generally produces larger loadings, except for the vertical force F_z. This trend is expected, as DLC 6.1 represents more severe wind and wave conditions. However, at a yaw angle of $20°$, DLC 6.3 exhibits larger axial force F_y and in-plane bending moment M_{xy}. For the vertical axial force F_z, the results from both DLCs are nearly identical, which is reasonable because the weight distribution is the same in both cases, leading to identical internal structural loading.

For the tower, all force and moment components exhibit physically reasonable distributions along the height. The axial forces F_x and F_y show a consistent decrease from the bottom to the top, reflecting the cumulative reduction in structural load with height. The vertical force F_z also decreases with elevation, following a nonlinear pattern due to the combination of gravitational and aerodynamic forces. The bending moment M_{xy} decreases toward the top, consistent with the reduced moment arm and applied load. The torsional moment M_z remains nearly constant along the tower height, indicating minimal torsional deformation under the considered conditions.

These loading patterns validate the choice of DLC 6.1 and DLC 6.3 for the ULS yielding check, as they represent the most critical and representative loading scenarios for both the tower and the substructure.

5.1.3. Dynamical Stability Assessment

To assess the dynamic stability of the initial design, the maximum platform motion statistics were summarized. Additionally, the structural natural frequencies were computed through free decay tests and BModes simulations to verify and avoid potential resonances with turbine operational frequencies and environmental excitations.

Table 5.2 summarizes the maximum platform displacements across all six degrees of freedom (DoFs), obtained from statistical analysis of six simulation seeds for each case. The results demonstrate that DLC6.1 produces more significant heave and pitch responses compared to DLC6.3, which can be attributed to the more severe environmental conditions (50-year extreme events) considered in DLC6.1.

For the critical DoFs (surge, heave, and pitch), the maximum observed displacements remain below the established constraints (30 m surge, 20 m heave, and 15° pitch) in both extreme DLCs. While the maximum surge displacement of 25.07 m approaches the 30 m limit, this could be mitigated through optimized mooring system design.

Table 5.2: Platform motion values under DLC6.1 and DLC6.3

DLC	Case	Heave [m]	Pitch [°]	Roll [°]	Surge [m]	Sway [m]	Yaw [°]
DLC6.1	yaw = 0°, mis = 0°	13.34	4.41	1.00	25.07	1.94	2.26
DLC6.1	yaw = 0°, mis = 30°	13.02	3.83	1.67	22.43	10.94	4.80
DLC6.1	yaw = 8°, mis = 0°	13.55	4.33	3.56	24.94	8.01	8.57
DLC6.1	yaw = 8°, mis = 30°	13.02	3.74	3.24	22.18	9.39	10.13
DLC6.3	yaw = 0°, mis = 0°	2.96	2.23	0.63	13.25	1.19	0.94
DLC6.3	yaw = 0°, mis = 30°	2.83	2.00	1.17	11.59	7.08	2.22
DLC6.3	yaw = 20°, mis = 0°	2.62	2.34	3.98	13.42	9.13	6.73
DLC6.3	yaw = 20°, mis = 30°	2.41	2.23	3.78	11.71	9.57	7.38

Based on the initial design inputs, the natural frequencies of the system are computed using BModes. The resulting modal frequencies are summarized in Table 5.3. To validate these results, corresponding free-decay simulations are conducted, and the outcomes are presented in Figure 5.2 for comparison.

Table 5.3: Natural Frequencies and Corresponding Periods

DOF (Mode)	BModes, f (Hz)	BModes, T (s)	Decay Tests, f (Hz)	Decay Tests, T (s)
Heave	0.034388	29.08	0.02898	34.51
Surge	0.012242	81.67	0.013148	76.06
Pitch	0.022639	44.17	0.02045	48.91
Yaw	0.08111	12.33	0.08899	11.24
Tower S–S	0.200968	4.98	0.2000	5.00
Tower F–A	0.202616	4.94	0.2222	4.50

The results confirm that the first bending frequency of the tower falls within the previously defined soft–stiff range. Furthermore, the natural periods of the primary platform motions—including heave, surge, and pitch—are all greater than 20 s, which exceeds the wave peak period. In contrast, the yaw motion exhibits a natural period of approximately 12.5 s, which is shorter than the extreme wave peak period. This frequency separation helps to prevent resonance excitation of the platform by wave loading.

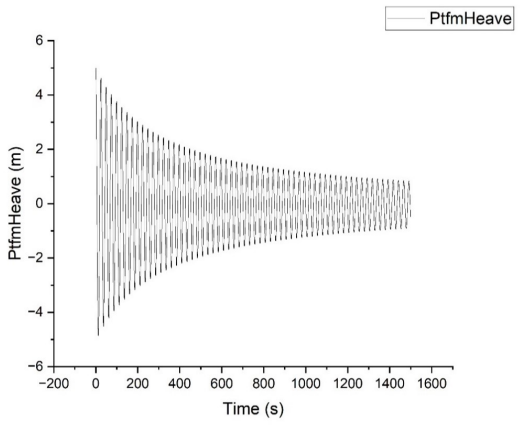

(a) Heave Decay

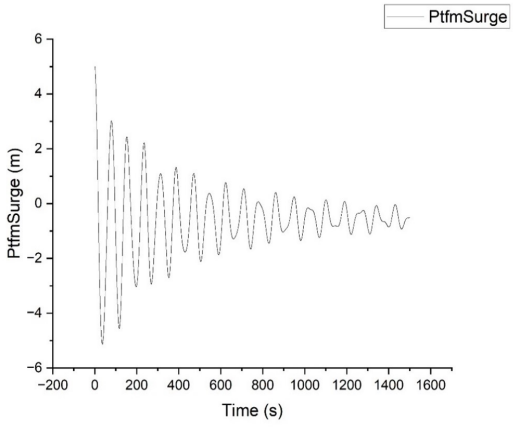

(b) Surge Decay

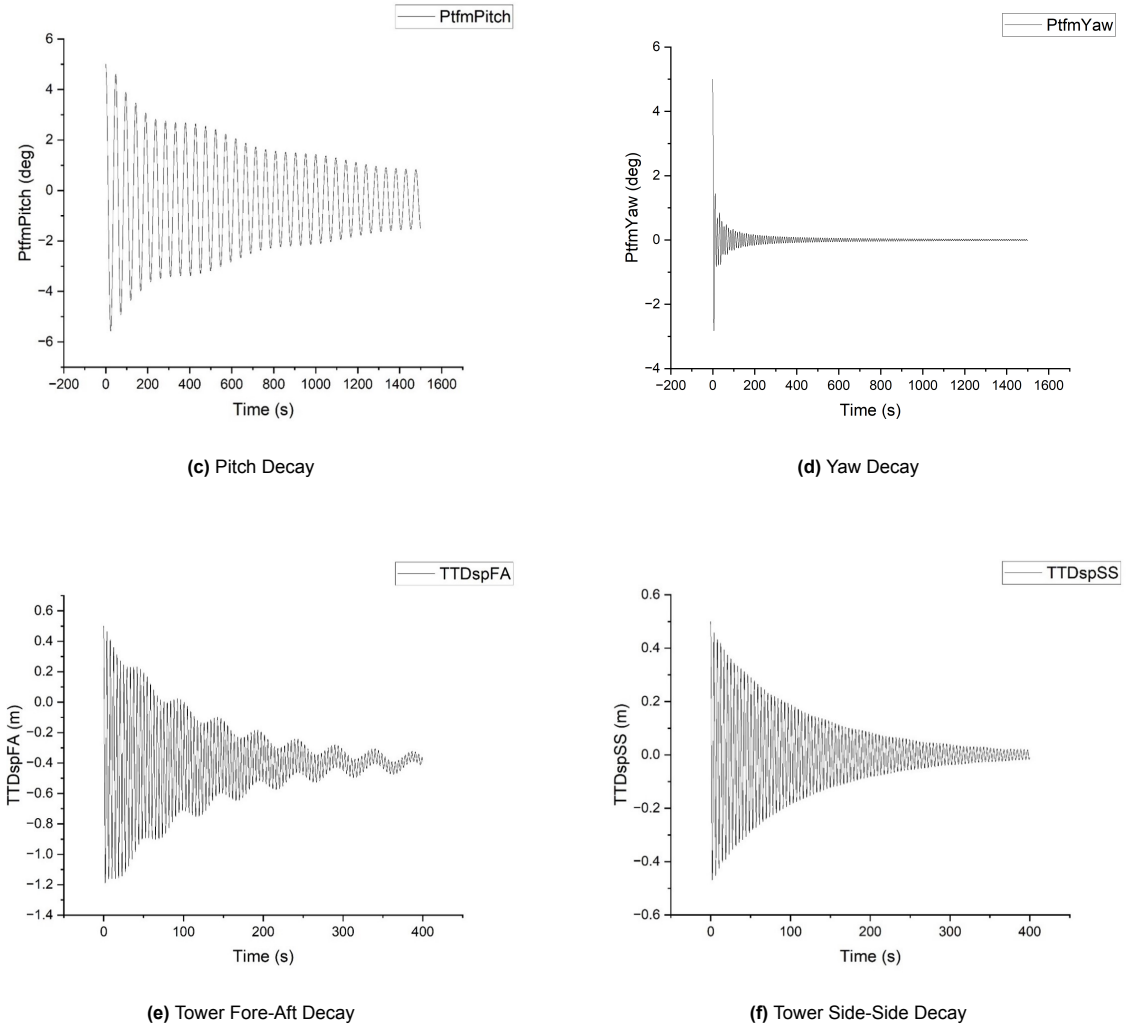

(c) Pitch Decay

(d) Yaw Decay

(e) Tower Fore-Aft Decay

(f) Tower Side-Side Decay

Figure 5.2: Decay test results for different rigid-body degrees of freedom

Based on the above maximum platform motion data and structural motion frequency checks, the dynamic stability of the initial design is considered acceptable.

5.1.4. Structural strength assessment

The initial design parameters have been verified against both static and dynamic stability criteria. In this step, the initial geometries are evaluated with respect to their material resistance under extreme loading conditions.

Using the structural loadings obtained from the extreme design load cases, the yielding and buckling failure indices U, multiplied by the material factor γ_m and the load factor γ_l, are computed for each structural component. The resulting values for the three failure indices, distributed along the corresponding nodes, are presented in the following figures in Figure 5.6.

From the plots, it is observed that both yielding and buckling are most likely to occur at the tower base node, which exhibits the highest values of U_{FW} for the filament-wound layer and $U_{Material}$ for the pultruded panel. This node corresponds to the interface between the substructure and the tower, located at the water surface (z=0m), where wave forces predominantly act. Furthermore, the failure indices from DLC 6.3 are larger than those from DLC 6.1, which can be attributed to the larger in-plane bending moment in DLC 6.3, as this parameter governs the stress calculation.

For the pultruded panel, both $U_{Material}\gamma_m\gamma_l$ and $U_{Buckle}\gamma_m\gamma_l$ have maximum values smaller than 1, indicating that the geometry satisfies the pultruded panel strength requirements. In contrast, for the

filament-wound layer, the Tsai–Wu failure index $U_{\mathrm{FW}}\gamma_{\mathrm{m}}\gamma_{\mathrm{l}}$ exceeds 1 for both DLC 6.1 and DLC 6.3, indicating that this layer must be strengthened to withstand the extreme loading conditions.

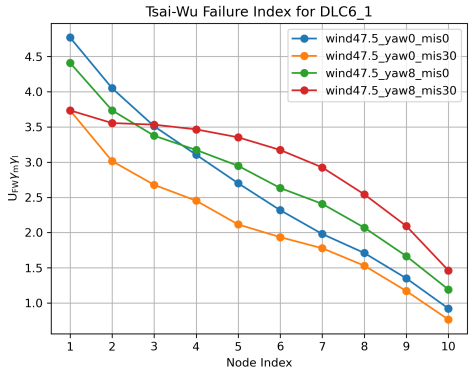

(a) DLC6.1 Rigid Spar Model U_{FW}

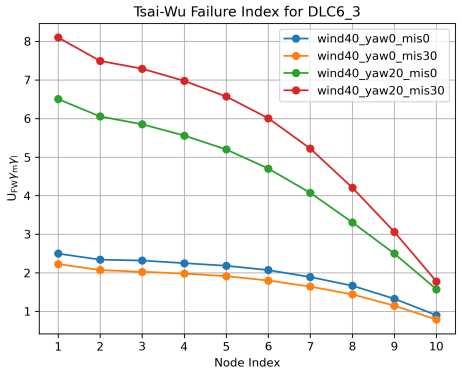

(b) DLC6.3 Rigid Spar Model U_{FW}

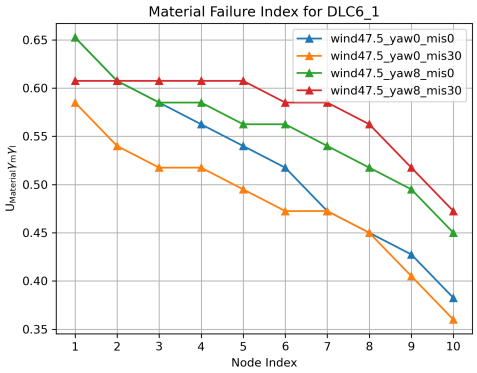

(c) DLC6.1 Rigid Spar Model U_{Material}

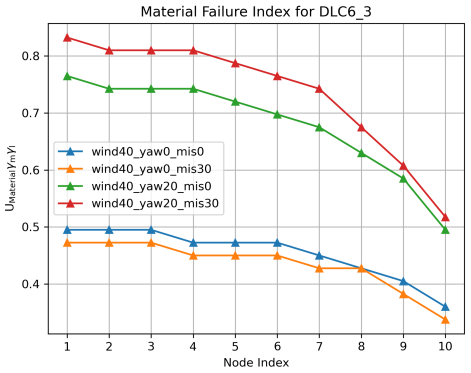

(d) DLC6.3 Rigid Spar Model U_{Material}

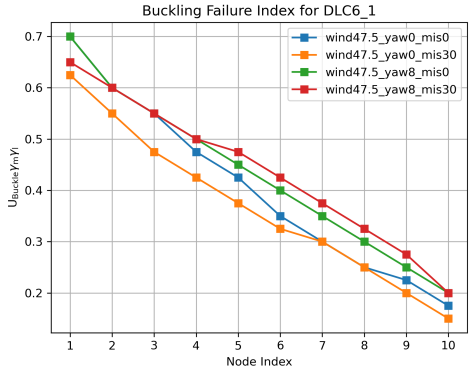

(a) DLC6.1 Rigid Spar Model U_{Buckle}

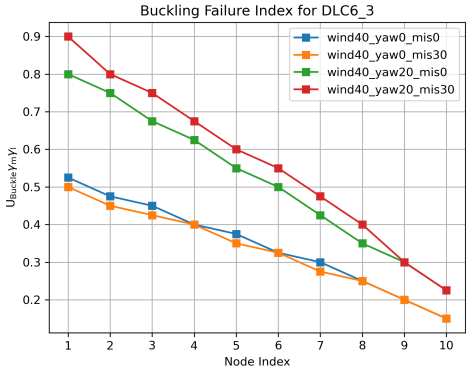

(b) DLC6.3 Rigid Spar Model U_{Buckle}

Figure 5.4: Failure index distributions for the initial design under DLC6.1 and DLC6.3

To further optimize the design, the initial configuration of the filament wound must be improved to satisfy the structural constraints, followed by an update of the input geometries. Based on the observations, only the filament wound layer require reinforcement. With the material selections remain unchanged, to enhance the structural capacity the outer diameter or the layer thickness needs to be increased.

When modifying the geometries to satisfy the structural checks, it is noted that the previously defined constraints must still be applied, including maintaining the tower frequency within the soft–stiff range

and adhering to manufacturing limits. Additionally, the diameter was kept unchanged, as variations in diameter are expected to influence the loadings more significantly than changes in thickness, while only the loading outputs from the initial design are available for the structural strength checks.

After several iterations of manually tuning the geometries in Grasshopper and verifying them against the yielding and buckling criteria, the filament-wound thickness was increased from 0.05 m to 0.12 m, while all other geometrical parameters remained the same. This adjustment led to a substantial reduction in U_{FW}, and the updated failure index results are presented as follows:

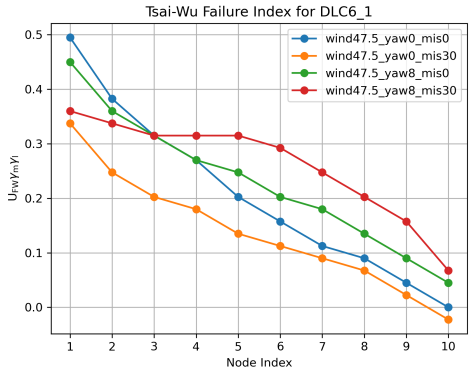

(a) DLC6.1 Rigid Spar Model U_{FW}

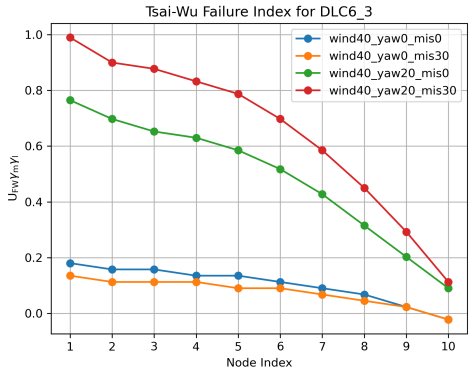

(b) DLC6.3 Rigid Spar Model U_{FW}

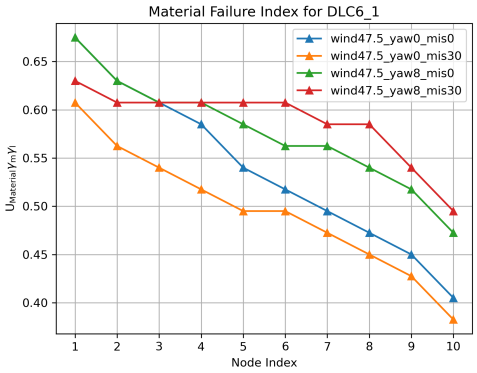

(c) DLC6.1 Rigid Spar Model U_{Material}

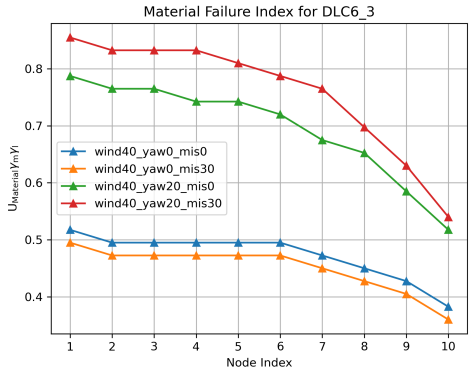

(d) DLC6.3 Rigid Spar Model U_{Material}

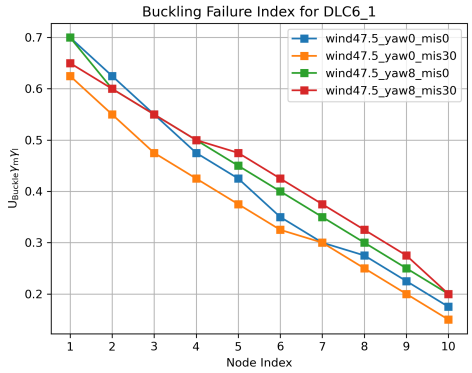

(a) DLC6.1 Rigid Spar Model U_{Buckle}

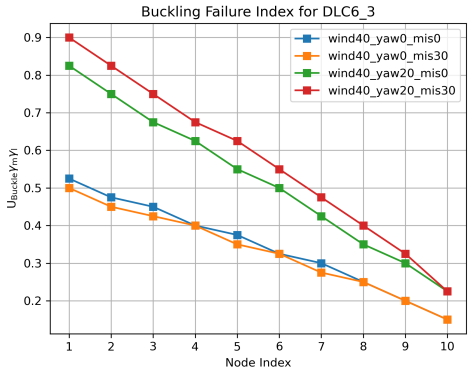

(b) DLC6.3 Rigid Spar Model U_{Buckle}

Figure 5.6: Failure index distributions for the initial design under DLC6.1 and DLC6.3

For the filament-wound Tsai–Wu failure index, the critical loading condition occurs at the tower base

under DLC6.3. After increasing the filament-wound thickness, the maximum value of $U_{\text{FW}\gamma_m\gamma_l}$ is approximately 0.99, which pushes the design to the limit of the imposed constraint. The updated tower first bending frequency is found to be about 0.22 Hz, which still satisfies the soft-stiff frequency range.

With all the above checks completed and the filament wound thickness improved, the set of geometric parameters is now ready for the optimization process.

5.2. Optimized Design

A total of 10,000 random samples of the selected geometric parameters, generated within the predefined design limits, were assessed during the optimization process. The corresponding outputs and constraints of each sample of geometries are evaluated. The best-performing sample was identified as the optimal design. In reporting the results, the tower base diameter is presented with two decimal places, whereas the thicknesses of both composite layers are given with three decimal places.

The input design variables, along with the resulting CAPEX and constraint values for both the improved initial design and the optimized design, are summarized in Table 5.4 and Table 5.5.

Table 5.4: Selected geometric design variables for the two designs.

Design	$D_{\text{tower,base}}$ [m]	$t_{p,\text{spar}}$ [m]	$t_{f,\text{spar}}$ [m]	$t_{p,\text{tower}}$ [m]	$t_{f,\text{tower}}$ [m]
Improved Initial Design	13.00	0.080	0.120	0.080	0.120
Optimized Design	15.06	0.075	0.089	0.075	0.089

Table 5.5: Objective function (CAPEX) and output constraints for the two designs.

Design	$f_{\text{s-s}}$ [Hz]	$f_{\text{f-a}}$ [Hz]	$U_{\text{FW,max}}$	$U_{\text{buckle,max}}$	$U_{\text{material,max}}$	CAPEX [€]
Improved Initial Design	0.222	0.221	0.99	0.90	0.855	2.723×10^7
Optimized Design	0.248	0.248	0.99	0.95	0.675	2.267×10^7

In terms of the input variables, the optimized design features an increased tower base diameter, while the thickness of both composite layers is reduced. This reduction in thickness decreases the overall stiffness of the structure; therefore, the stiffness must be compensated by a larger cross-sectional area and inertia to satisfy the strength requirements. The thickness of the pultruded panel remains relatively high and close to the upper limit, which is attributed to its higher stiffness compared to the filament-wound layer. Consequently, the pultruded panel layer plays a key role in retaining structural stiffness and preventing buckling.

Regarding the output objective variable (CAPEX) and the constraint variables, the optimized design is approximately 5 million € cheaper than the improved initial design. However, the constraints on both the natural frequency and the yielding failure index are very close to their respective upper limits, indicating that the design space for a soft–stiff configuration in this study is quite narrow. Because the thickness is assumed to be uniform along both the spar and the tower, the thickness in sections of the tower above the base could be reduced while still meeting the strength requirements, as the loadings in these regions are lower. Such a varied-thickness design is commonly adopted in other tower configurations.

Apart from the frequency constraints, the filament-wound yielding failure index emerges as the critical parameter among the three failure indices. This is primarily due to the relatively low modulus of elasticity of the filament-wound material. Employing stronger materials, such as carbon fiber, could significantly improve this performance, albeit at the expense of higher material costs.

The optimized set of geometric parameters was subsequently re-evaluated for hydrostatic stability using Eq. 3.12, and the design was verified to satisfy the stability requirement. The calculated masses of the tower and the spar are 1.41×10^6 kg and 2.78×10^6 kg, respectively, with a required ballast mass of 3.51×10^7 kg to ensure stability.

5.3. Fatigue Failure Check

The FLS analysis was conducted for three tower nodes around the tower base the tower base, node 1 to node 3. Since the bending moments M_{xt} and M_{yt} dominate the stress response and the maximum loadings occur near the tower base, these three locations were selected for evaluation. The life time fatigue damage D_{tot} and corresponding ultimate loading of three bending moments at these three nodes are presented in Table 5.6, Table 5.7 and Table 5.6

The results show that the total lifetime damage values D_{tot} are significantly below 1, indicating that the tower structure meets the fatigue life requirements with a substantial safety margin. These findings are consistent with the expectations for the composite 5 MW offshore wind turbine tower design reported in [11], which yielded fatigue damage values smaller than 10^{-5}.

Table 5.6: Fatigue lifetime damage results at Tower node 1 for various S/N curves.

	M_x	M_y	M_z
L_{Ult}	2.68×10^{7}	2.68×10^{7}	4.89×10^{6}
D_{tot}	4.12×10^{-19}	2.19×10^{-14}	5.73×10^{-17}

Table 5.7: Fatigue lifetime damage results at Tower node 11 for various S/N curves.

	M_x	M_y	M_z
L_{Ult}	2.54×10^{7}	2.54×10^{7}	4.64×10^{6}
D_{tot}	1.29×10^{-19}	9.99×10^{-15}	9.60×10^{-17}

Table 5.8: Fatigue lifetime damage results at Tower node 21 for various S/N curves.

	M_x	M_y	M_z
L_{Ult}	2.41×10^{7}	2.41×10^{7}	4.41×10^{6}
D_{tot}	4.83×10^{-20}	5.13×10^{-15}	1.63×10^{-16}

Furthermore, these results confirm that, compared with yielding and buckling, fatigue failure is far less critical for composite structures, owing to the inherently high fatigue strength of composite materials.

5.4. Comparison to steel design

To answer the second research question, the optimized CAPEX result is compared to published estimates for steel spar buoy FOWT designs supporting 15 MW class turbines. Rather than repeat the entire workflow by replacing the composite material with steel and re-running the optimization, the manufacturing CAPEX of the steel tower and spar is estimated from literature sources.

The steel tower manufacturing cost is reported to be approximately 1.6 to 1.7 million € for a 15 MW turbine [63], while the fabrication cost of the steel spar hull is on the order of 1.0-1.5 million € per MW of turbine capacity [64, 65]. This leads to an estimated spar CAPEX of about 15-22.5 million € for a 15 MW unit. Combining the tower and spar costs yields a total manufacturing CAPEX of roughly 16.6-24.2 million € for a steel spar-buoy design, excluding mooring and installation costs. Compared to the optimized composite design obtained in this study (22.67 million €), the lower bound of the estimated steel design CAPEX is much lower than the composite result, while the upper bound is marginally higher.

Several existing 15 MW class steel designs provide useful benchmarks for structural mass and price comparison when excluding ballast. For example, the optimized steel spar design by [66] for the IEA 15 MW reference turbine features an approximately 110 m long cylindrical hull with an 18 m base diameter and 6 cm thick steel walls, requiring about 3.4 thousand tonnes of structural steel for the spar

alone. Together with a conventional steel tower (10 m base diameter, about 860 tonnes), the total steel structural mass amounts to roughly 4.3 to 4.5 thousand tonnes. Similarly, [67] present a steel semi-submersible design for the same IEA 15MW turbine. The hull steel mass is 3914 tonnes, and the steel tower has a mass of 1263 tonnes.

In this study, the optimized design requires a smaller mass for the spar (approximately 2780 tonnes) compared with a steel counterpart, while the tower mass is larger (approximately 1410 tonnes) compared with steel tower mass. One key reason is that, in this study, the tower base height is set to 0 m, reflecting the monolithic design in which the tower and spar are rigidly connected. In contrast, most other steel designs for 15 MW turbines adopt a tower base height of about 15 m in typical offshore wind turbine configurations.

Additionally, as discussed previously, the thickness is kept constant along the structure in the present design, whereas most conventional designs adopt a tapered thickness profile that decreases from the critical loading location (tower base) toward other sections (e.g., tower top). If a variable-thickness approach were implemented for this composite design, the thickness in sections subjected to lower loadings could be reduced, thereby decreasing the overall mass and CAPEX.

However, designing a variable-thickness structure would require the use of a flexible spar model to assess each section along the spar with its corresponding thickness. As mentioned previously, simulations of the flexible spar model are significantly more time-consuming than those of the rigid spar model. Furthermore, additional verification would be necessary to compare the results of the flexible spar model against those of the rigid spar model to ensure consistency, which lies beyond the scope of this project.

5.5. Further Research

In this study, a preliminary design framework was developed to identify a feasible composite spar type FOWT capable of supporting a 15 MW turbine. Although the results indicate that the CAPEX of the optimized design is comparable to that of a steel-based counterpart, this work remains at the preliminary stage, and several avenues for further research and improvement are identified:

- Instead of employing a uniform thickness for both composite layers along the entire structure, a variable-thickness configuration could be implemented to reduce CAPEX, as discussed previously. This approach would introduce additional design variables and require investigation of constraints such as allowable thickness gradient, considering that current composite manufacturing processes typically produce components with uniform thickness.
- A significant limitation of this project is that the structural loadings used for all geometry sets in the optimization were fixed, being derived from the initial design simulations. This simplification, adopted due to the high computational cost of time-domain simulations for each iteration, introduces uncertainty into the optimization results. As identified in the literature review, many optimization studies utilize frequency-domain simulations to accelerate load estimation. Alternatively, surrogate modeling could be employed to approximate simulation outputs, substantially reducing the number of full time-domain simulations required.
- To enable variable-thickness optimization, a flexible spar model must be developed and validated against the rigid spar model. This would require additional simulation time and model verification.
- Due to time constraints, only three DLCs were simulated. A more comprehensive set of DLCs should be considered to fully evaluate the design's robustness under various operating and environmental conditions.
- In the final stage of the project, the Tsai–Wu failure index U_{FW} was identified as the governing failure criterion. To prevent filament-wound layer yielding, its thickness was significantly increased. Exploring alternative composite materials with higher elastic modulus for the filament-wound layer may yield improved results.
- The optimization results revealed that the design space under soft–stiff frequency constraints is relatively narrow. Alternative design strategies could be investigated, such as the double-wall pultruded panel configuration described in [11], where two pultruded panel walls are connected via an internal web. This design increases stiffness, enables the tower to operate in the stiff–stiff

range, and allows each wall to have a smaller thickness, avoiding the upper-limit constraint seen in this single-wall design.

- As the present work focused on coupled fluid–structure responses, the mooring and control systems were adopted directly from the WindCrete reference design, which has a similar size and identical turbine rating. Future research could integrate these systems into the optimization framework for a more holistic design process.

6

Conclusion

In this project, a preliminary design process for a monolithic composite spar-buoy type floating wind turbine platform is presented. Due to the limited availability of existing designs for composite floating wind platforms, the materials and configurations were initially selected based on literature from similar structures, while the geometries were first estimated using the WindCrete design as a reference.

After verifying the initially estimated geometries against hydrostatic stability and tower frequency constraints, the model was parametrized in Grasshopper and integrated into a workflow framework built in Python. This framework connects simulation tools including OpenFAST, BModes, and HAMS, post-processing tools such as MExtremes and MLife, and the optimization driver OpenMDAO. The framework enables automatic updates of OpenFAST input files and BModes frequency analysis files when geometries are modified in Grasshopper, providing flexibility for the subsequent platform dynamic stability and structural strength checks based on DLC time-domain simulations.

As flexible spar model simulations were found to be computationally expensive, and given that extreme sectional load distribution results from [57] indicate the tower base as the critical loading location, the spar's structural influence was considered secondary. Therefore, a rigid spar model was adopted to analyze loading at the tower sections, particularly at the tower base.

To cover yielding, buckling, and fatigue failure checks, DLC6.1, DLC6.3, and DLC1.2 from the IEC 61400-3 guidelines were simulated. For the extreme environmental conditions in DLC6.1 and DLC6.3, the initially estimated geometries produced maximum platform motions within constraints. However, the filament wound layer was found to be insufficiently strong to withstand extreme loadings, leading to a potential yielding failure, whereas the pultruded panel layer showed adequate strength to prevent both yielding and buckling. Increasing the filament-wound layer thickness from 0.05 m to 0.12 m reduced the yielding index U_{FW} to below 1. As the diameter remained unchanged, load variations were expected to be minimal. The improved initial design was therefore considered to satisfy all constraints.

With the improved initial design established, confirming that a soft–stiff tower design is feasible and that alternative geometries may be possible, an optimization with design space exploration using 10,000 samples was conducted. The goal was to identify geometries with the lowest CAPEX while satisfying structural performance, hydrodynamic stability, and manufacturing constraints. The resulting optimized design featured reduced thicknesses and a larger diameter, achieving a slightly lower CAPEX. This step addressed the first research question, with the optimized CAPEX of 22.67 million € then used to answer the second research question: comparison with steel designs.

From the literature review, the CAPEX for the steel spar and tower of a 15 MW FOWT is expected to range from 16.6 to 24.2 million €. The optimized composite design in this study (22.67 million €) is close to the upper bound of this range. However, it is expected that the CAPEX of the composite design could be further reduced if a tapered thickness distribution were adopted, with higher thickness in high-loading regions and lower thickness in low-loading regions. Nevertheless, 22.67 million € is still considered economically feasible, as it remains within the steel cost range.

References

[1] DNV Energy Transition Outlook. “A global and regional forecast to 2050”. In: *DNV: Høvik, Norway* (2023).

[2] DNV. *Energy Transition Outlook 2024*. Tech. rep. Accessed: 2024-11-07. Oslo, Norway: DNV, 2024. URL: https://www.dnv.com/focus-areas/floating-offshore-wind/.

[3] Tyler Stehly, Patrick Duffy, and Daniel Mulas Hernando. *2022 Cost of Wind Energy Review*. American English. Other. 2023. DOI: 10.2172/2278805.

[4] CorPower Ocean AB. *CorPower Wave Energy Converter: High-Efficiency Wave Power Technology*. https://www.corpowerocean.com/. Accessed: 2024-06-16. 2020.

[5] A. Doe and Y. Zhang. “Advances in Composite Materials for Offshore Applications”. In: *Ships and Offshore Structures* 20.4 (2025). Accessed: 2025-08-12, pp. 456–470. DOI: 10.1080/17445302.2025.2455987. URL: https://www.tandfonline.com/doi/full/10.1080/17445302.2025.2455987.

[6] International Electrotechnical Commission. *IEC 61400-3: Wind Turbines - Part 3: Design Requirements for Offshore Wind Turbines*. Edition 1.0. Geneva, Switzerland, 2009.

[7] Bhagwan D. Agarwal, Lawrence J. Broutman, and K. Chandrashekhara. *Analysis and Performance of Fiber Composites*. 4th. Accessed: 2025-08-12. John Wiley & Sons, 2017. ISBN: 978-1-118-93952-0. URL: https://www.wiley.com/en-us/Analysis+and+Performance+of+Fiber+Composites%2C+4th+Edition-p-9781118939520.

[8] C. Soutis. “Fibre reinforced composites in aircraft construction”. In: *Progress in Aerospace Sciences* 41.2 (2005). Accessed: 2025-08-12, pp. 143–151. DOI: 10.1016/j.paerosci.2005.02.004. URL: https://doi.org/10.1016/j.paerosci.2005.02.004.

[9] Mathijs Peeters et al. “The Concept of Segmented Wind Turbine Blades: A Review”. In: *Energies* 10 (July 2017), p. 1112. DOI: 10.3390/en10081112.

[10] Loc B Nguyen. “A multi-attribute decision process for structural material assessment and selection of light-weight, high-performance naval ships”. PhD thesis. The George Washington University, 2008.

[11] Kieran O’Leary, Vikram Pakrashi, and Denis Kelliher. “Optimization of composite material tower for offshore wind turbine structures”. In: *Renewable Energy* 140 (2019), pp. 928–942. ISSN: 0960-1481. DOI: https://doi.org/10.1016/j.renene.2019.03.101. URL: https://www.sciencedirect.com/science/article/pii/S0960148119304136.

[12] Tjeerd van der Zee, Marten Jan de Ruiter, and Ivo Wieling. “The C-Tower project – A composite tower for offshore wind turbines”. In: *Energy Procedia* 137 (2017). 14th Deep Sea Offshore Wind R&D Conference, EERA DeepWind’2017, pp. 401–405. ISSN: 1876-6102. DOI: https://doi.org/10.1016/j.egypro.2017.10.364. URL: https://www.sciencedirect.com/science/article/pii/S1876610217353419.

[13] InnoEnergy. *Windcrete - Online Marketplace for Energy Innovations*. Accessed: 2025-02-16. 2025. URL: https://www.innoenergy.com/discover-innovative-solutions/online-marketplace-for-energy-innovations/windcrete/.

[14] Equinor ASA. *Hywind Scotland: The World’s First Floating Offshore Wind Farm in the North Sea*. https://www.equinor.com/what-we-do/floating-wind/hywind-scotland. Accessed: 2024-06-16. 2017.

[15] M. Y. Mahfouz et al. “Response of the International Energy Agency (IEA) Wind 15 MW WindCrete and Activefloat floating wind turbines to wind and second-order waves”. In: *Wind Energy Science* 6.3 (2021), pp. 867–883. DOI: 10.5194/wes-6-867-2021. URL: https://wes.copernicus.org/articles/6/867/2021/.

[16] Andrew C. Young et al. “Methodology for optimizing composite towers for use on floating wind turbines”. In: *Journal of Renewable and Sustainable Energy* 9.3 (May 2017), p. 033305. ISSN: 1941-7012. DOI: 10.1063/1.4984259. eprint: https://pubs.aip.org/aip/jrse/article-pdf/doi/10.1063/1.4984259/14010688/033305_1_online.pdf. URL: https://doi.org/10.1063/1.4984259.

[17] Victoria Sykes, Maurizio Collu, and Andrea Coraddu. “A review and analysis of optimisation techniques applied to floating offshore wind platforms”. In: *Ocean Engineering* 285 (2023), p. 115247. ISSN: 0029-8018. DOI: 10.1016/j.oceaneng.2023.115247. URL: https://doi.org/10.1016/j.oceaneng.2023.115247.

[18] Katherine L Dykes et al. *Wind turbine optimization with WISDEM*. Tech. rep. National Renewable Energy Lab.(NREL), Golden, CO (United States), 2018.

[19] Justin S. Gray et al. “OpenMDAO: An open-source framework for multidisciplinary design, analysis, and optimization”. In: *Structural and Multidisciplinary Optimization* 59.4 (Apr. 2019), pp. 1075–1104. DOI: 10.1007/s00158-019-02211-z.

[20] John Marius Hegseth, Erin E. Bachynski, and Joaquim R.R.A. Martins. “Integrated design optimization of spar floating wind turbines”. In: *Marine Structures* 72 (2020), p. 102771. ISSN: 0951-8339. DOI: https://doi.org/10.1016/j.marstruc.2020.102771. URL: https://www.sciencedirect.com/science/article/pii/S0951833920300654.

[21] Kalimeris Theodoros. “Floating wind turbine optimization via surrogate modelling”. MA thesis. NTNU, 2023.

[22] John Marius Hegseth, Erin E Bachynski, and Joaquim RRA Martins. “Integrated design optimization of spar floating wind turbines”. In: *Marine Structures* 72 (2020), p. 102771.

[23] Mareike Leimeister, Athanasios Kolios, and Maurizio Collu. “Critical review of floating support structures for offshore wind farm deployment”. In: *Journal of physics: Conference series*. Vol. 1104. 1. IOP Publishing. 2018, p. 012007.

[24] Tonio Sant and Kurt Cuschieri. “Comparing Three Aerodynamic Models for Predicting The Thrust and Power Characteristics of Yawed Floating Wind Turbine Rotors”. In: *Journal of Solar Energy Engineering* 138 (Feb. 2016). DOI: 10.1115/1.4032684.

[25] Hans Frederik Greve Lehmann and Mai Dolang Kristiansen. “Design and optimization model of floating offshore wind platforms”. In: (2023).

[26] Simon Lefebvre and Maurizio Collu. “Preliminary design of a floating support structure for a 5MW offshore wind turbine”. In: *Ocean Engineering* 40 (2012), pp. 15–26. ISSN: 0029-8018. DOI: https://doi.org/10.1016/j.oceaneng.2011.12.009. URL: https://www.sciencedirect.com/science/article/pii/S0029801811002769.

[27] Warren Clarence Young, Richard Gordon Budynas, Ali M Sadegh, et al. *Roark’s formulas for stress and strain*. Vol. 7. McGraw-hill New York, 2002.

[28] Jelle ter Harmsel. “Relevant Mechanical Characterization Methods of Hybrid Composites Joints -A Review”. In: Nov. 2023.

[29] TF Composite. *What is Pultrusion?* Accessed: 2025-02-16. 2025. URL: https://www.tfcomposite.com/what-is-pultrusion.

[30] Nada Aldoumani et al. “Optimisation of the filament winding approach using a newly developed in-house uncertainty model”. In: *Eng* 1.2 (2020), p. 8.

[31] Laszlo Arany et al. “Closed form solution of Eigen frequency of monopile supported offshore wind turbines in deeper waters incorporating stiffness of substructure and SSI”. In: *Soil Dynamics and Earthquake Engineering* 83 (Feb. 2016). DOI: 10.1016/j.soildyn.2015.12.011.

[32] Zhaolong Yu and Jørgen Amdahl. “A Rayleigh-Ritz solution for high order natural frequencies and eigenmodes of monopile supported offshore wind turbines considering tapered towers and soil pile interactions”. In: *Marine Structures* 92 (2023), p. 103482. ISSN: 0951-8339. DOI: https://doi.org/10.1016/j.marstruc.2023.103482. URL: https://www.sciencedirect.com/science/article/pii/S0951833923001156.

[33] Gunjit Bir. *User's Guide to BModes (Software for Computing Rotating Beam Coupled Modes)*. Tech. rep. NREL/TP-500-39133. Prepared under Task No. WER6.2302. Golden, CO, United States: National Renewable Energy Laboratory (NREL), Dec. 2006. URL: https://www.nrel.gov/docs/fy07osti/39133.pdf.

[34] Odd Faltinsen. *Sea loads on ships and offshore structures*. Vol. 1. Cambridge university press, 1993.

[35] Vaibhav Raghavan et al. "HAMS-MREL, a new open source multiple body solver for marine renewable energies: Model description, application and validation". In: *Renewable Energy* 237 (2024), p. 121577. ISSN: 0960-1481. DOI: https://doi.org/10.1016/j.renene.2024.121577. URL: https://www.sciencedirect.com/science/article/pii/S0960148124016458.

[36] WAMIT, Inc. *WAMIT User Manual*. Accessed: 2025-02-16. 2025. URL: https://www.wamit.com/manual.htm.

[37] Garbis H Keulegan, Lloyd H Carpenter, et al. "Forces on cylinders and plates in an oscillating fluid". In: *Journal of research of the National Bureau of Standards* 60.5 (1958), pp. 423–440.

[38] R. C. McCamy and R. A. Fuchs. "Wave Forces on Pile: A Diffraction Theory". In: *U.S. Army Corps of Engineers, Coastal Engineering Research Center, Technical Memo* 69 (1954). Available from the U.S. Army Coastal Engineering Research Center.

[39] Jan Van Der Tempel. "Design of support structures for offshore wind turbines". In: (2006).

[40] Waves Research Group. *Ocean Wave Spectra - JONSWAP Wave Spectrum*. Accessed: 2024-12-14. 2024. URL: https://wikiwaves.org/Ocean-Wave_Spectra.

[41] W.E. Cummins. *The Impulse Response Function and Ship Motions*. Tech. rep. DTMB Report 1661. David Taylor Model Basin, 1962.

[42] T.F. Ogilvie. "First- and second-order forces on a cylinder in a fluid stream". In: *Proceedings of the Symposium on Naval Hydrodynamics*. Washington, DC, USA: National Academy of Sciences – National Research Council, 1964, pp. 495–517.

[43] American Institute of Steel Construction. *Load and Resistance Factor Design Manual of Steel Construction*. 3rd. AISC LRFD Specification for Structural Steel Buildings. Chicago, IL: American Institute of Steel Construction, 2010.

[44] American Institute of Steel Construction. *Steel Construction Manual*. 8th Edition, 2nd Revised Printing. Figure recreated by the author based on Table C.1.8.1. Chicago, IL: American Institute of Steel Construction, 1987.

[45] National Renewable Energy Laboratory (NREL). *MLife User's Guide*. Part of the OpenFAST suite. National Renewable Energy Laboratory (NREL). 2020. URL: https://openfast.readthedocs.io/.

[46] Giorgio Triulzi. *Engineering Design Optimisation*. Cambridge University Press, 2015. ISBN: 9781108833417.

[47] Bernard Le Méhauté. *An introduction to hydrodynamics and water waves*. Springer Science & Business Media, 2013.

[48] Evan Gaertner et al. "Definition of the IEA 15-megawatt offshore reference wind turbine". In: (2020).

[49] National Renewable Energy Laboratory (NREL). *OpenFAST Documentation*. https://openfast.readthedocs.io/. Accessed: 2024-06-17. 2024.

[50] Qi Pan and Po Wen Cheng. "Cost-based mooring designs and a parametric study of bridles for a 15 MW spar-type floating offshore wind turbine". In: *Journal of Physics: Conference Series* 2265 (May 2022), p. 042013. DOI: 10.1088/1742-6596/2265/4/042013.

[51] Jason Mark Jonkman. *Dynamics modeling and loads analysis of an offshore floating wind turbine*. University of Colorado at Boulder, 2007.

[52] John L Clarke. *Structural design of polymer composites: Eurocomp design code and background document*. CRC Press, 2003.

[53] Nada Aldoumani et al. "Optimisation of the filament winding approach using a newly developed in-house uncertainty model". In: *Eng* 1.2 (2020), p. 8.

[54] A.R. Bunsell and B. Harris. “Hybrid composites based on glass fibre reinforced epoxy resin: Mechanical properties and performance”. In: *Composites Science and Technology* 34.2 (1989). Glass fibre reinforced epoxy composite properties, pp. 183–210. DOI: 10.1016/0266-3538(89)90017-1.

[55] B. J. Jonkman and J. M. Buhl Jr. *TurbSim User’s Guide: Version 2.0*. NREL/TP-500-41136. Golden, CO, USA, 2007. URL: https://www.nrel.gov/docs/fy08osti/41136.pdf.

[56] Jason Jonkman et al. *Implementation of Substructure Flexibility and Member-Level Load Capabilities for Floating Offshore Wind Turbines in OpenFAST*. Tech. rep. NREL/TP-5000-75062. Golden, CO, USA: National Renewable Energy Laboratory (NREL), 2020. URL: https://www.nrel.gov/docs/fy20osti/75062.pdf.

[57] Carlos Eduardo Silva de Souza and Erin E. Bachynski-Polić. “Design, structural modeling, control, and performance of 20 MW spar floating wind turbines”. In: *Marine Structures* 84 (2022), p. 103182. ISSN: 0951-8339. DOI: https://doi.org/10.1016/j.marstruc.2022.103182. URL: https://www.sciencedirect.com/science/article/pii/S0951833922000259.

[58] NREL. *HydroDyn User’s Guide and Theory Manual*. https://openfast.readthedocs.io/en/main/source/user/hydrodyn/input_files.html. Accessed: 2025-06-25. 2024.

[59] Matthew Barone et al. *Extreme Event Statistics for Wind Turbines: MExtremes User’s Guide*. Tech. rep. NREL/TP-5000-65435. Golden, CO, USA: National Renewable Energy Laboratory (NREL), 2016. URL: https://www.nrel.gov/docs/fy16osti/65435.pdf.

[60] L. Ascione et al. *Prospect for New Guidance in the Design of FRP*. Technical Report. European Commission, 2016. URL: https://ec.europa.eu/jrc/en/publication/eur-scientific-and-technical-research-reports/prospect-new-guidance-design-frp.

[61] Claes-Göran Gustafson and Andreas Echtermeyer. “Long-term properties of carbon fibre composite tethers”. In: *International journal of fatigue* 28.10 (2006), pp. 1353–1362.

[62] Stephen W. Tsai and Edward M. Wu. “A General Theory of Strength for Anisotropic Materials”. In: *Journal of Composite Materials* 5.1 (1971), pp. 58–80. DOI: 10.1177/002199837100500106. eprint: https://doi.org/10.1177/002199837100500106. URL: https://doi.org/10.1177/002199837100500106.

[63] BVG Associates. *Guide to Offshore Wind Components and Supply Chain Costs*. Tech. rep. Industry cost guide for offshore wind turbine components. Reports tower manufacturing cost for 15 MW offshore turbines at approximately £1.4 million. BVG Associates, 2025.

[64] Alessandro Ghigo, Giovanni Bracco, and Giacomo Mattiazzo. “Optimization of spar floating substructures for offshore wind turbines”. In: *Ocean Engineering* 202 (2020), p. 107211. DOI: 10.1016/j.oceaneng.2020.107211.

[65] Cinzia Maienza, Theofanis Soukissian, and Konstantinos Topouzelis. “A methodology for life cycle cost modelling of floating offshore wind farms”. In: *Renewable Energy* 162 (2020), pp. 1762–1776. DOI: 10.1016/j.renene.2020.08.052.

[66] Nicolò Pollini et al. “Gradient-based optimization of a 15 MW wind turbine spar floater”. In: *Journal of Physics: Conference Series*. Vol. 2018. 2021, p. 012032. DOI: 10.1088/1742-6596/2018/1/012032.

[67] Allen Christopher et al. “Definition of the UMaine VolturnUS-S reference platform developed for the IEA wind 15-Megawatt offshore reference wind turbine”. In: *National Renewable Energy Lab (NREL)* (2020).

A

Generalized Mass and Stiffness Matrix

$$\overline{\mathbf{M}} = \rho_T A_{tb} L_T \begin{pmatrix} \frac{1}{3c_0}+\frac{1}{4c_1} & \frac{1}{4c_0}+\frac{1}{5c_1} & \frac{1}{5c_0}+\frac{1}{6c_1} & \frac{1}{6c_0}+\frac{1}{7c_1} & \frac{1}{7c_0}+\frac{1}{8c_1} & \frac{1}{8c_0}+\frac{1}{9c_1} \\ \frac{1}{4c_0}+\frac{1}{5c_1} & \frac{1}{5c_0}+\frac{1}{6c_1} & \frac{1}{6c_0}+\frac{1}{7c_1} & \frac{1}{7c_0}+\frac{1}{8c_1} & \frac{1}{8c_0}+\frac{1}{9c_1} & \frac{1}{9c_0}+\frac{1}{10c_1} \\ \frac{1}{5c_0}+\frac{1}{6c_1} & \frac{1}{6c_0}+\frac{1}{7c_1} & \frac{1}{7c_0}+\frac{1}{8c_1} & \frac{1}{8c_0}+\frac{1}{9c_1} & \frac{1}{9c_0}+\frac{1}{10c_1} & \frac{1}{10c_0}+\frac{1}{11c_1} \\ \frac{1}{6c_0}+\frac{1}{7c_1} & \frac{1}{7c_0}+\frac{1}{8c_1} & \frac{1}{8c_0}+\frac{1}{9c_1} & \frac{1}{9c_0}+\frac{1}{10c_1} & \frac{1}{10c_0}+\frac{1}{11c_1} & \frac{1}{11c_0}+\frac{1}{12c_1} \\ \frac{1}{7c_0}+\frac{1}{8c_1} & \frac{1}{8c_0}+\frac{1}{9c_1} & \frac{1}{9c_0}+\frac{1}{10c_1} & \frac{1}{10c_0}+\frac{1}{11c_1} & \frac{1}{11c_0}+\frac{1}{12c_1} & \frac{1}{12c_0}+\frac{1}{13c_1} \\ \frac{1}{8c_0}+\frac{1}{9c_1} & \frac{1}{9c_0}+\frac{1}{10c_1} & \frac{1}{10c_0}+\frac{1}{11c_1} & \frac{1}{11c_0}+\frac{1}{12c_1} & \frac{1}{12c_0}+\frac{1}{13c_1} & \frac{1}{13c_0}+\frac{1}{14c_1} \end{pmatrix}$$

$$+m_{RNA} \begin{pmatrix} 1 & 1 & 1 & 1 & 1 & 1 \\ 1 & 1 & 1 & 1 & 1 & 1 \\ 1 & 1 & 1 & 1 & 1 & 1 \\ 1 & 1 & 1 & 1 & 1 & 1 \\ 1 & 1 & 1 & 1 & 1 & 1 \\ 1 & 1 & 1 & 1 & 1 & 1 \end{pmatrix}$$

$$+\frac{J_{RNA}}{L_T^2} \begin{pmatrix} 1 & 2 & 3 & 4 & 5 & 6 \\ 2 & 4 & 6 & 8 & 10 & 12 \\ 3 & 6 & 9 & 12 & 15 & 18 \\ 4 & 8 & 12 & 16 & 20 & 24 \\ 5 & 10 & 15 & 20 & 25 & 30 \\ 6 & 12 & 18 & 24 & 30 & 36 \end{pmatrix}$$

$$\overline{\mathbf{K}} = \frac{E_T I_{Tb}}{L_T^3} \begin{bmatrix} 0 & 0 & 0 & 0 & 0 & 0 \\ 0 & (4b_0+2b_1+b_2\cdot\frac{4}{3}) & (6b_0+4b_1+3b_2) & (8b_0+6b_1+\frac{24}{5}b_2) & (10b_0+8b_1+\frac{40}{6}b_2) & (12b_0+10b_1+\frac{60}{7}b_2) \\ 0 & (6b_0+4b_1+3b_2) & (12b_0+9b_1+\frac{36}{5}b_2) & (18b_0+\frac{72}{5}b_1+12b_2) & (24b_0+20b_1+\frac{120}{7}b_2) & \dots \\ 0 & (8b_0+6b_1+\frac{24}{5}b_2) & (18b_0+\frac{72}{5}b_1+12b_2) & (144/5b_0+24b_1+\frac{144}{7}b_2) & \dots & \dots \\ 0 & \dots & \dots & \dots & \dots & \dots \\ 0 & \dots & \dots & \dots & \dots & \dots \end{bmatrix}$$

$$+\frac{k_{\text{rot}}}{L_T^2} \begin{bmatrix} 1 & 0 & 0 & 0 & 0 & 0 \\ 0 & 0 & 0 & 0 & 0 & 0 \\ 0 & 0 & 0 & 0 & 0 & 0 \\ 0 & 0 & 0 & 0 & 0 & 0 \\ 0 & 0 & 0 & 0 & 0 & 0 \\ 0 & 0 & 0 & 0 & 0 & 0 \end{bmatrix}$$

where k_{rot} is the rotational stiffness at the tower base.

B

Rayleigh-Ritz modal analysis code

```
import numpy as np
from scipy.linalg import eigh # For eigenvalue problem
import matplotlib.pyplot as plt


# Given parameters
rho_T = 1964.307692 # Tower material density [kg/m^3]
Atb = 5.256198669 # Tower base cross-sectional area [m^2]
LT = 145          # Tower length [m]
mRNA = 1.02E+06   # RNA mass [kg]
mT = 1.12E+06     # Tower mass [kg]
JRNA = 3.52E+08   # RNA rotational inertia [kg·m^2]
k_rot = 5.28E+10  # Rotational stiffness [Nm/rad]
ET = 3.138E+10     # Young's modulus [Pa]
ITb = 217.6773 # Moment of inertia at tower bottom cross-section [m^4]
b0, b1, b2 = 0.9945, -1.4396, 0.5719
c0, c1 = 1, -0.5051

# 1. Construct the mass matrix M
alpha = mRNA / (rho_T * Atb * LT)
beta = JRNA / (rho_T * Atb * LT**3)

# Mass matrix components
mass_matrix1 = np.zeros((6, 6))
for i in range(6):
    for j in range(6):
        stiffness_term = 1 / (i + j + 3) * c0 + 1 / (i + j + 4) * c1
        mass_matrix1[i, j] = stiffness_term

identity_matrix = np.ones((6, 6))
coeff_matrix = np.array(
    [[1, 2, 3, 4, 5, 6],
     [2, 4, 6, 8, 10, 12],
     [3, 6, 9, 12, 15, 18],
     [4, 8, 12, 16, 20, 24],
     [5, 10, 15, 20, 25, 30],
     [6, 12, 18, 24, 30, 36]]
)

mass_matrix2 = mass_matrix1 + (alpha * identity_matrix + beta * coeff_matrix)
mass_matrix_scaled = rho_T * Atb * LT * mass_matrix2 # Scale with material and geometric properties

# 2. Construct the stiffness matrix K
stiffness_matrix = ET * ITb / (LT**3) * np.array(
    [[0, 0,               0,                  0,                    0,                    0],
     [0, 4*b0+2*b1+b2*4/3, 6*b0+4*b1+3*b2,     8*b0+6*b1+24/5*b2,    10*b0+8*b1+40/6*b2,   12*b0+10*b1
          +60/7*b2],
     [0, 6*b0+4*b1+3*b2,   12*b0+9*b1+36/5*b2, 18*b0+72/5*b1+12*b2, 24*b0+20*b1+120/7*b2, 30*b0+180/7*b1
          +180/8*b2],
```

```
    [0, 8*b0+6*b1+24/5*b2, 18*b0+72/5*b1+12*b2, 144/5*b0+24*b1+144/7*b2, 240/6*b0+240/7*b1+30*b2, 360/7*b0+360/8*b1+40*b2],
    [0, 10*b0+8*b1+40/6*b2, 24*b0+20*b1+120/7*b2, 240/6*b0+240/7*b1+30*b2, 400/7*b0+50*b1+400/9*b2, 600/8*b0+600/9*b1+60*b2],
    [0, 12*b0+10*b1+60/7*b2, 30*b0+180/7*b1+180/8*b2, 360/7*b0+360/8*b1+40*b2, 600/8*b0+600/9*b1+60*b2, 900/9*b0+90*b1+900/11*b2]]
)

# Add rotational stiffness at the base
rotational_stiffness = np.zeros((6, 6))
rotational_stiffness[0, 0] = ET * ITb / (LT**3) * k_rot * LT / (ET * ITb)
stiffness_matrix += rotational_stiffness

# 3. Modal analysis: Solve eigenvalue problem
eigenvalues, eigenvectors = eigh(stiffness_matrix, mass_matrix_scaled)

# Calculate natural frequencies (rad/s to Hz)
natural_frequencies = np.sqrt(eigenvalues) / (2 * np.pi)
print('natural_frequencies [Hz]:', natural_frequencies)

# Plot mode shapes
z_positions = np.linspace(0, 1, 1000) # Assuming uniform tower discretization
S_W1 = np.zeros(1000)
S_W2 = np.zeros(1000)
S_W3 = np.zeros(1000)
for i in range(1000):
    zi = z_positions[i]
    for j in range(6):
        S_W1[i] = S_W1[i] + eigenvectors[j, 0] * zi ** (j)
        S_W2[i] = S_W2[i] + eigenvectors[j, 1] * zi ** (j)
        S_W3[i] = S_W3[i] + eigenvectors[j, 2] * zi ** (j)

plt.figure(figsize=(8, 6))
plt.plot(S_W1/max(abs(S_W1)), z_positions, label="Mode 1") #
plt.plot(S_W2/max(abs(S_W2)), z_positions, label="Mode 2") #
plt.plot(S_W3/max(abs(S_W3)), z_positions, label="Mode 3") #

plt.title("Mode Shapes in the Same Plot")
plt.xlabel("Normalized Amplitude")
plt.ylabel("Normalized Height (Z/Lt)")

plt.legend()

plt.grid()

plt.show()
```

C

BModes Input Files

C.1. BModes main input file

```
====================== BModes v1.03 Main Input File ==================
Modes of a 145m tower with tip mass

--------- General parameters ------------------------------------------------------------------------
False    Echo      - Echo input file contents to *.echo file if true.
2        beam_type - 1: blade, 2: tower (-)
0.       romg      - rotor speed (rpm), automatically set to zero for tower modal analysis
1.0      romg_mult - rotor speed muliplicative factor (-)
145.0          radius    - rotor tip radius measured along coned blade axis OR tower height (m)
0.0            hub_rad   - hub radius measured along coned blade axis OR tower rigid-base height (m)
0.       precone   - built-in precone angle (deg), automatically set to zero for a tower
0.       bl_thp    - blade pitch setting (deg), automatically set to zero for a tower
2        hub_conn  - hub-to-blade connection [1: cantilevered; 2: connected to a substructure (monopile/
     floater)]
12       modepr    - number of modes to be printed (-)
t        TabDelim  - (true: tab-delimited output tables; false: space-delimited tables)
f        mid_node_tw - (true: output twist at mid-node of elements; false: no mid-node outputs)

--------- Blade-tip or tower-top mass properties -----------------------------------------
950057.799 tip_mass - blade-tip or tower-top mass (see users' manual) (kg)
-7.1687  cm_loc    - tip-mass c.m. offset from the tower axis measured along the tower-tip x reference
     axis (m)
4.584963 cm_axial - tip-mass c.m. offset tower tip measures axially along the z axis (m)
3.7173e+08 ixx_tip  - blade lag or tower s-s mass moment of inertia about the tip-section x reference axis
      (kg-m^2)
2.6268e+08 iyy_tip  - blade flap or tower f-a mass moment of inertia about the tip-section y reference
     axis (kg-m^2)
3.5877e+08 izz_tip  - torsion mass moment of inertia about the tip-section z reference axis (kg-m^2)
0.       ixy_tip   - cross product of inertia about x and y reference axes(kg-m^2)
1.6418e+07 izx_tip   - cross product of inertia about z and x reference axes(kg-m^2)
0.       iyz_tip   - cross product of inertia about y and z reference axes(kg-m^2)

--------- Distributed-property identifiers -----------------------------------------------------
1        id_mat   - material_type [1: isotropic; non-isotropic composites option not yet available]
'D:\Thesis\Optimization_Project\openFAST\BModes_jj\IEA15_CSpar_Bmodes_tower_secs.dat' sec_props_file -
     name of beam section properties file (-)

Property scaling factors.............................
1.0      sec_mass_mult - mass density multiplier (-)
1.0      flp_iner_mult - blade flap or tower f-a inertia multiplier (-)
1.0      lag_iner_mult - blade lag or tower s-s inertia multiplier (-)
1.0      flp_stff_mult - blade flap or tower f-a bending stiffness multiplier (-)
1.0      edge_stff_mult - blade lag or tower s-s bending stiffness multiplier (-)
1.0      tor_stff_mult - torsion stiffness multiplier (-)
1.0      axial_stff_mult - axial stiffness multiplier (-)
1.0      cg_offst_mult - cg offset multiplier (-)
1.0      sc_offst_mult - shear center multiplier (-)
```

```
1.0     tc_offst_mult - tension center multiplier (-)

--------- Finite element discretization ----------------------------------------------------
20      nselt  - no of blade or tower elements (-)
Distance of element boundary nodes from blade or flexible-tower root (normalized wrt blade or tower
     length), el_loc()
0.00   0.05   0.10   0.15   0.20   0.25   0.30   0.35   0.40   0.45   0.50   0.55   0.60   0.65   0.70
     0.75   0.80   0.85   0.90   0.95   1.00

--------- Properties of additional tower support subsystem (read only if beam_type is 2) ------------
1        tow_support - aditional tower support [0: no additional support; 1: floating-platform or
     monopile with or without tension wires] (-)
-0.0          draft - depth of tower base from the ground or the MSL (mean sea level) (m)
-117.85517653842312 cm_pform - distance of platform c.m. below the MSL (m)
38133767.29552025 mass_pform - platform mass (kg)
Platform mass inertia 3X3 matrix (i_matrix_pform):
    5.49E+11 0        0
    0         5.49E+11 0
    0        0         1.70E+09
0 ref_msl - distance of platform reference point below the MSL (m)
Platform-reference-point-referred hydrodynamic 6X6 matrix (hydro_M):
4.021020E+07  1.725940E+00  -5.690996E-01 2.476085E+02 -2.928415E+09 -1.423690E-07
9.447746E+00  4.021020E+07  -1.949496E+00 2.928415E+09 -5.481634E+02 4.626359E-07
1.417601E-02  7.312334E-01  1.750224E+06  -1.250984E+01 -2.981952E+01 2.752406E-08
6.838149E+02  2.928528E+09  -2.266386E+02 2.807380E+11 -5.003068E+04 3.952652E-05
-2.928528E+09 -3.356354E+01 7.720035E+01 -1.631447E+04 2.807380E+11 -1.428908E-06
3.073035E-06  -2.693109E-06 -1.185944E-07 2.056762E-04 2.783905E-05 1.954176E-06
Platform-reference-point-referred hydrodynamic 6X6 stiffness matrix (hydro_K):
0.00   0.00   0.00   0.00   0.00   0.00
0.00   0.00   0.00   0.00   0.00   0.00
0.00   0.00   1333295.85  0.00  0.00  0.00
0.00   0.00   0.00   11597274437.39  0.00  0.00
0.00   0.00   0.00   0.00   11597274437.39  0.00
0.00   0.00   0.00   0.00   0.00   0.00
Mooring-system 6X6 stiffness matrix (mooring_K):
5.44E+05  2.81E+00  -6.99E-01 2.47E+02  -4.85E+07 6.74E-01
2.17E-02  5.44E+05  1.14E-01  4.85E+07  -1.52E+00 -5.54E+01
4.27E-01  7.32E-01  1.07E+05  6.34E+01  -3.02E+01 -1.79E+00
-1.75E-01 4.86E+07  1.01E-01  4.78E+10  1.12E+01  6.78E+03
-4.86E+07 3.23E-01  -6.22E+01 2.88E+01  4.78E+10  1.39E+00
5.80E-01  -5.24E+01 -1.92E+00 -5.36E+03 -5.30E+01 5.64E+08

Distributed (hydrodynamic) added-mass per unit length along a flexible portion of the tower length:
0 n_secs_m_distr - number of sections at which added mass per unit length is specified (-)
0. 0. : z_distr_m - [row array of size n_added_m_pts; section locations wrt the flexible tower base over
     which distributed mass is specified] (m)
0. 0. : distr_m - [row array of size n_added_m_pts; added distributed masses per unit length] (kg/m)

Distributed elastic stiffness per unit length along a flexible portion of the tower length:
0 n_secs_k_distr - number of points at which distributed stiffness per unit length is specified (-)
0. 0. : z_distr_k - [row array of size n_added_m_pts; section locations wrt the flexible tower base over
     which distributed stiffness is specified] (m)
0. 0. : distr_k - [row array of size n_added_m_pts; distributed stiffness per unit length] (N/m^2)

Tension wires data
0 n_attachments - no of wire-attachment locations on tower [0: no tension wires] (-)
3 3 n_wires - no of wires attached at each location (must be 3 or higher) (-)
6 9 node_attach - node numbers of attacments location (node number must be more than 1 and less than
     nselt+2) (-)
0.e0 0.e0 wire_stfness - wire spring constant in each set (see users manual) (N/m)
0. 0. th_wire - angle of tension wires (wrt the horizontal ground plane) at each attachment point (deg)
```

C.2. BModes tower sectional properties

D

HAMS Mesh Convergence Study

D.1. Single body

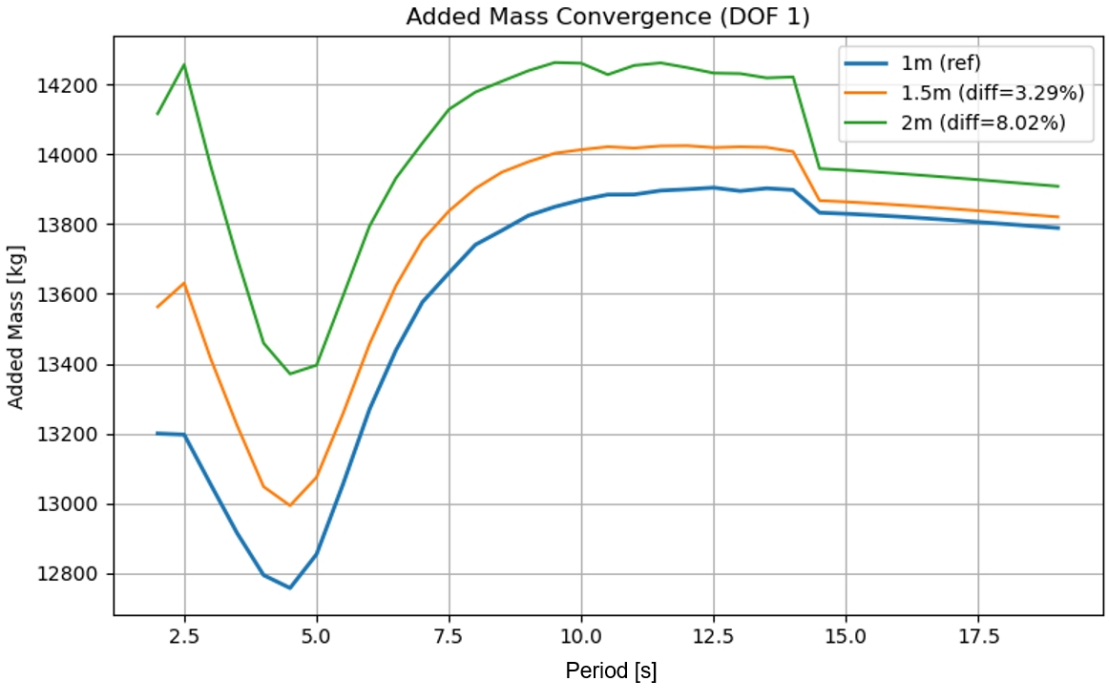

Figure D.1: HAMS surge added mass results of 3 mesh sizes

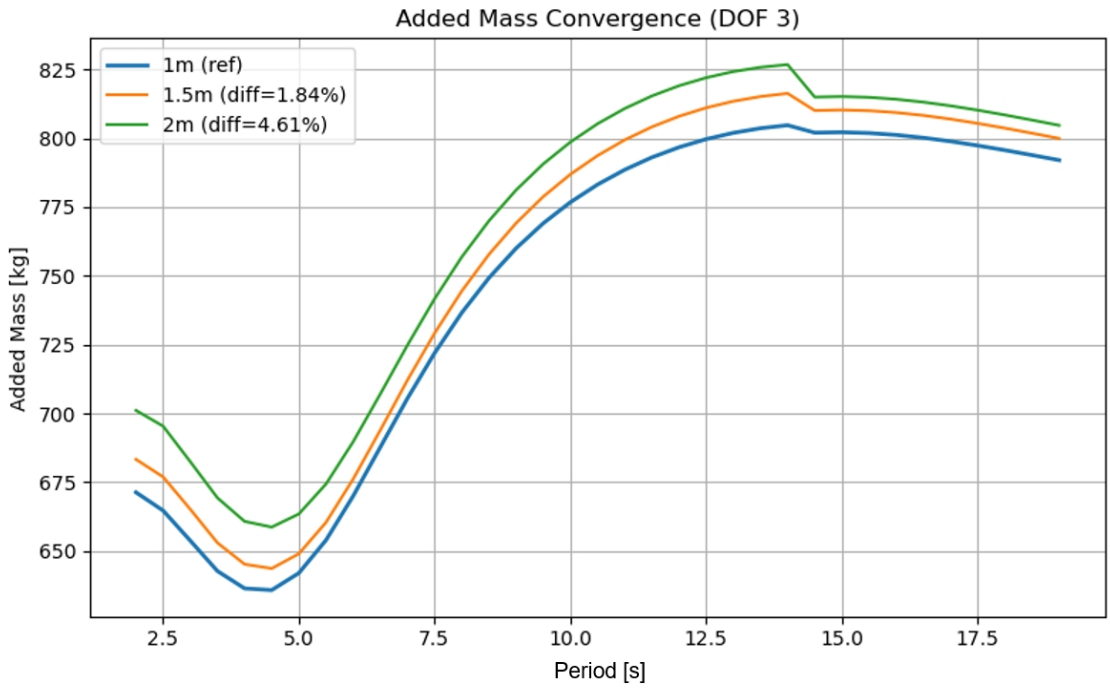

Figure D.2: HAMS heave added mass results of 3 mesh sizes

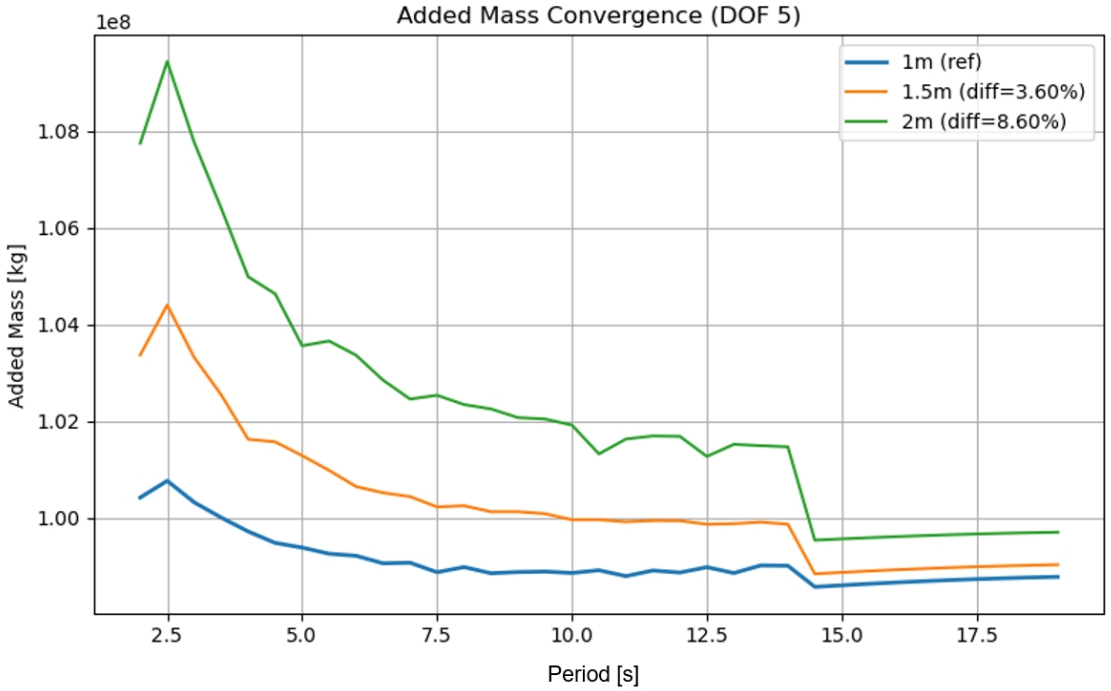

Figure D.3: HAMS pitch added mass results of 3 mesh sizes

E

Grasshopper modularization

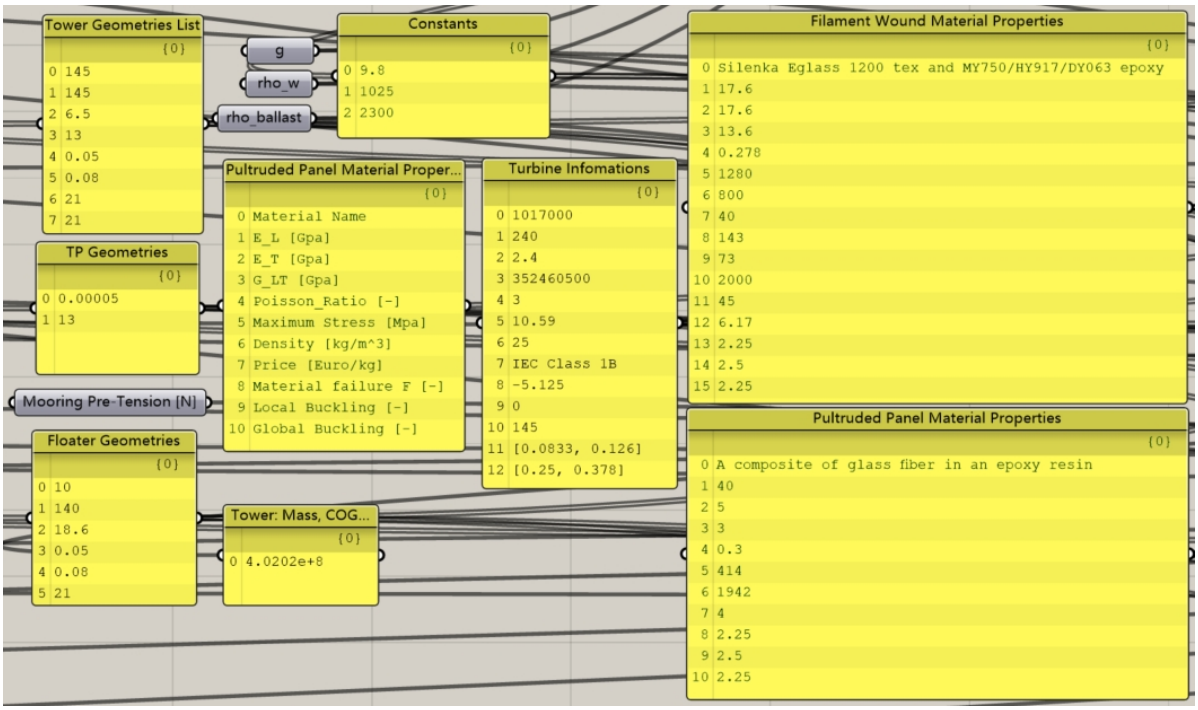

Figure E.1: Constants definition in Grasshopper

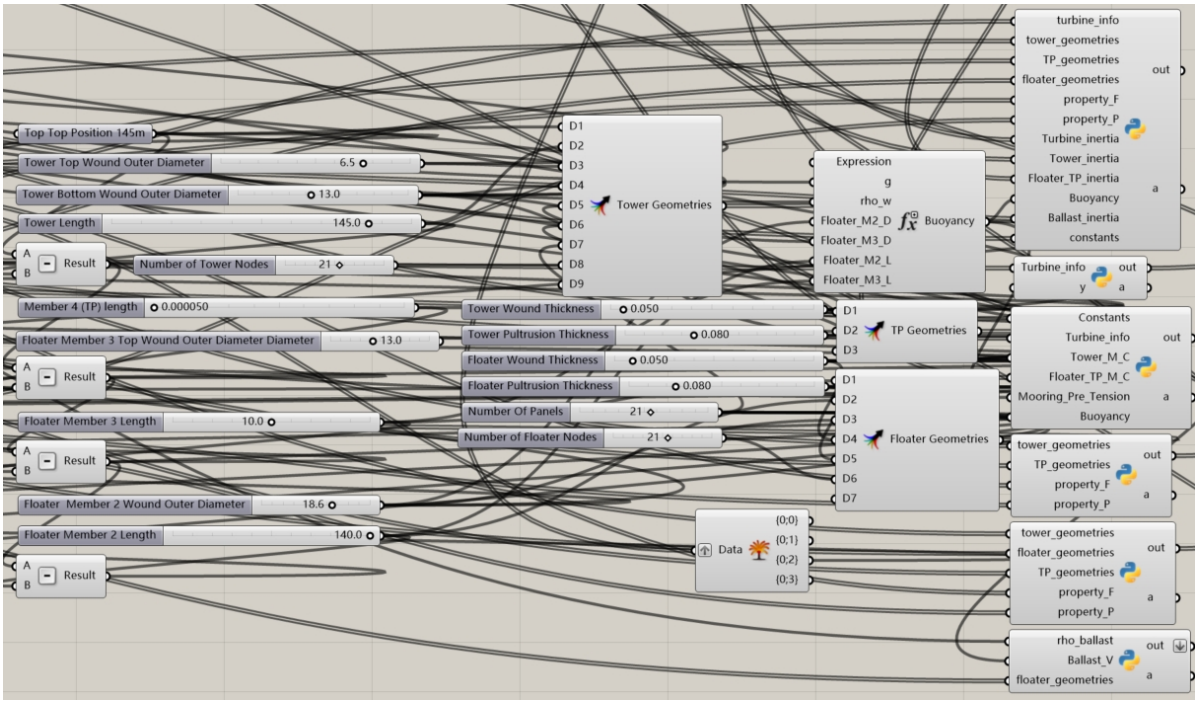

Figure E.2: Design variables definition interface in Grasshopper

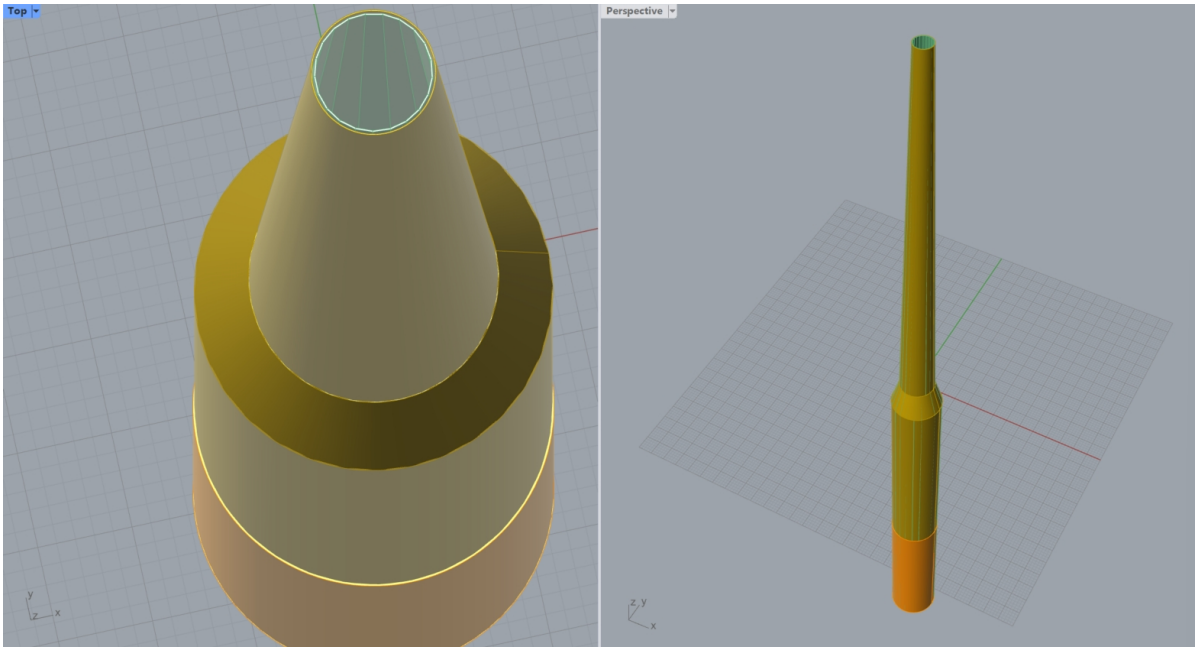

Figure E.3: Design visualization

F

OpenFAST input files template

```
------- CSpar INPUT FILE ------------------------------------------
IEA 15 MW Baseline Wind Turbine with CSpar tower-spar floater foundation
---------------------- SIMULATION CONTROL --------------------------------------
True                Echo      - Echo input data to <RootName>.ech (flag)
"FATAL"             AbortLevel - Error level when simulation should abort (string) {"WARNING", "SEVERE", "FATAL"}
6000          TMax      - Total run time (s)
0.0125        DT        - Recommended module time step (s)
2                   InterpOrder - Interpolation order for input/output time history (-) {1=linear, 2=quadratic}
1                   NumCrctn  - Number of correction iterations (-) {0=explicit calculation, i.e., no corrections}
1.0                 DT_UJac   - Time between calls to get Jacobians (s)
4.0E7               UJacSclFact - Scaling factor used in Jacobians (-)
---------------------- FEATURE SWITCHES AND FLAGS ------------------------------
        1   CompElast     - Compute structural dynamics (switch) {1=ElastoDyn; 2=ElastoDyn + BeamDyn for blades}
        1   CompInflow    - Compute inflow wind velocities (switch) {0=still air; 1=InflowWind; 2=external from OpenFOAM}
        2   CompAero      - Compute aerodynamic loads (switch) {0=None; 1=AeroDyn v14; 2=AeroDyn v15}
        1   CompServo     - Compute control and electrical-drive dynamics (switch) {0=None; 1=ServoDyn}
        1   CompSeaSt     - Compute sea state information (switch) {0=None; 1=SeaState}
        1   CompHydro     - Compute hydrodynamic loads (switch) {0=None; 1=HydroDyn}
        0              CompSub      - Compute sub-structural dynamics (switch) {0=None; 1=SubDyn; 2=External Platform MCKF}
        3   CompMooring   - Compute mooring system (switch) {0=None; 1=MAP++; 2=FEAMooring; 3=MoorDyn; 4=OrcaFlex}
        0   CompIce       - Compute ice loads (switch) {0=None; 1=IceFloe; 2=IceDyn}
        0   MHK           - MHK turbine type (switch) {0=Not an MHK turbine; 1=Fixed MHK turbine; 2=Floating MHK turbine}
---------------------- ENVIRONMENTAL CONDITIONS --------------------------------
       9.8  Gravity       - Gravitational acceleration (m/s^2)
     1.225  AirDens       - Air density (kg/m^3)
      1025  WtrDens       - Water density (kg/m^3)
  1.464E-05 KinVisc       - Kinematic viscosity of working fluid (m^2/s)
       335  SpdSound      - Speed of sound in working fluid (m/s)
    103500  Patm          - Atmospheric pressure (Pa) [used only for an MHK turbine cavitation check]
      1700  Pvap          - Vapour pressure of working fluid (Pa) [used only for an MHK turbine cavitation check]
       200  WtrDpth       - Water depth (m)
         0  MSL2SWL       - Offset between still-water level and mean sea level (m) [positive upward]
---------------------- INPUT FILES ---------------------------------------------
"IEA15_CSpar_ElastoDyn.dat" EDFile      - Name of file containing ElastoDyn input parameters (quoted string)
"D:/Thesis/Optimization_Project/openFAST/openfast/IEA-15-240-RWT/IEA-15-240-RWT_BeamDyn.dat" BDBldFile(1)      - Name of file containing BeamDyn input parameters for blade 1 (quoted string)
"D:/Thesis/Optimization_Project/openFAST/openfast/IEA-15-240-RWT/IEA-15-240-RWT_BeamDyn.dat" BDBldFile(2)      - Name of file containing BeamDyn input parameters for blade 2 (quoted string)
```

```
"D:/Thesis/Optimization_Project/openFAST/openfast/IEA-15-240-RWT/IEA-15-240-RWT_BeamDyn.dat" BDBldFile(3)
     - Name of file containing BeamDyn input parameters for blade 3 (quoted string)
"IEA15_CSpar_InflowFile.dat" InflowFile  - Name of file containing inflow wind input parameters (quoted
    string)
"D:/Thesis/Optimization_Project/openFAST/openfast/IEA15_CSpar_AeroDyn.dat" AeroFile - Name of file
    containing aerodynamic input parameters (quoted string)
"IEA15_CSpar_ServoDyn.dat" ServoFile   - Name of file containing control and electrical-drive input
    parameters (quoted string)
"IEA15_CSpar_SeaState.dat" SeaStFile   - Name of file containing sea state input parameters (quoted
    string)
"D:/Thesis/Optimization_Project/openFAST/openfast/IEA15_CSpar_HydroDyn.dat" HydroFile - Name of file
    containing hydrodynamic input parameters (quoted string)
"D:/Thesis/Optimization_Project/openFAST/openfast/IEA15_CSpar_SubDyn.dat" SubFile - Name of file
    containing sub-structural input parameters (quoted string)
"D:/Thesis/Optimization_Project/openFAST/openfast/IEA15_CSpar_MoorDyn.dat" MooringFile - Name of file
    containing mooring system input parameters (quoted string)
"unused"    IceFile       - Name of file containing ice input parameters (quoted string)
---------------------- OUTPUT --------------------------------------------------
True                SumPrint  - Print summary data to "<RootName>.sum" (flag)
10.0                SttsTime  - Amount of time between screen status messages (s)
99999.0             ChkptTime - Amount of time between creating checkpoint files for potential restart (s)

0.1            DT_Out    - Time step for tabular output (s) (or "default")
0.0                 TStart    - Time to begin tabular output (s)
1                   OutFileFmt - Format for tabular (time-marching) output file (switch) {1: text file [<
    RootName>.out], 2: binary file [<RootName>.outb], 3: both}
True                TabDelim  - Use tab delimiters in text tabular output file? (flag) {uses spaces if
    false}
"ES10.3E2"          OutFmt    - Format used for text tabular output, excluding the time channel.
    Resulting field should be 10 characters. (quoted string)
---------------------- LINEARIZATION -------------------------------------------
False       Linearize     - Linearization analysis (flag)
False       CalcSteady    - Calculate a steady-state periodic operating point before linearization? [
    unused if Linearize=False] (flag)
         3  TrimCase      - Controller parameter to be trimmed {1:yaw; 2:torque; 3:pitch} [used only if
              CalcSteady=True] (-)
     0.001  TrimTol       - Tolerance for the rotational speed convergence [used only if CalcSteady=True]
          (-)
      0.01  TrimGain      - Proportional gain for the rotational speed error (>0) [used only if CalcSteady
           =True] (rad/(rad/s) for yaw or pitch; Nm/(rad/s) for torque)
         0  Twr_Kdmp      - Damping factor for the tower [used only if CalcSteady=True] (N/(m/s))
         0  Bld_Kdmp      - Damping factor for the blades [used only if CalcSteady=True] (N/(m/s))
         2  NLinTimes     - Number of times to linearize (-) [>=1] [unused if Linearize=False]
        30,       60   LinTimes      - List of times at which to linearize (s) [1 to NLinTimes] [used only
              when Linearize=True and CalcSteady=False]
         1  LinInputs     - Inputs included in linearization (switch) {0=none; 1=standard; 2=all module
              inputs (debug)} [unused if Linearize=False]
         1  LinOutputs    - Outputs included in linearization (switch) {0=none; 1=from OutList(s); 2=all
              module outputs (debug)} [unused if Linearize=False]
False       LinOutJac     - Include full Jacobians in linearization output (for debug) (flag) [unused if
    Linearize=False; used only if LinInputs=LinOutputs=2]
False       LinOutMod     - Write module-level linearization output files in addition to output for full
    system? (flag) [unused if Linearize=False]
---------------------- VISUALIZATION -------------------------------------------
         0  WrVTK         - VTK visualization data output: (switch) {0=none; 1=initialization data only;
              2=animation; 3=mode shapes}
         2  VTK_type      - Type of VTK visualization data: (switch) {1=surfaces; 2=basic meshes (lines/
              points); 3=all meshes (debug)} [unused if WrVTK=0]
false       VTK_fields    - Write mesh fields to VTK data files? (flag) {true/false} [unused if WrVTK=0]
        15  VTK_fps       - Frame rate for VTK output (frames per second){will use closest integer
             multiple of DT} [used only if WrVTK=2 or WrVTK=3]
```

F.0.1. ElastoDyn file

```
------- ELASTODYN v1.03.* INPUT FILE ------------------------------------------
IEA 15 MW offshore reference model on CSpar floating platform ElastoDyn input properties
---------------------- SIMULATION CONTROL --------------------------------------
False       Echo      - Echo input data to "<RootName>.ech" (flag)
         3  Method    - Integration method: {1: RK4, 2: AB4, or 3: ABM4} (-)
"default"   DT        - Integration time step (s)
```

```
---------------------- DEGREES OF FREEDOM --------------------------------------
True           FlapDOF1  - First flapwise blade mode DOF (flag)
True           FlapDOF2  - Second flapwise blade mode DOF (flag)
True           EdgeDOF   - First edgewise blade mode DOF (flag)
False          TeetDOF   - Rotor-teeter DOF (flag) [unused for 3 blades]
False          DrTrDOF   - Drivetrain rotational-flexibility DOF (flag)
False          GenDOF    - Generator DOF (flag) #     PARKEDFALSE
True           YawDOF    - Yaw DOF (flag)
True           TwFADOF1  - First fore-aft tower bending-mode DOF (flag)
True           TwFADOF2  - Second fore-aft tower bending-mode DOF (flag)
True           TwSSDOF1  - First side-to-side tower bending-mode DOF (flag)
True           TwSSDOF2  - Second side-to-side tower bending-mode DOF (flag)
True           PtfmSgDOF - Platform horizontal surge translation DOF (flag)
True           PtfmSwDOF - Platform horizontal sway translation DOF (flag)
True           PtfmHvDOF - Platform vertical heave translation DOF (flag)
True           PtfmRDOF  - Platform roll tilt rotation DOF (flag)
True           PtfmPDOF  - Platform pitch tilt rotation DOF (flag)
True           PtfmYDOF  - Platform yaw rotation DOF (flag)
---------------------- INITIAL CONDITIONS --------------------------------------
         0   OoPDefl    - Initial out-of-plane blade-tip displacement (meters)
         0   IPDefl     - Initial in-plane blade-tip deflection (meters)
         90  BlPitch(1) - Blade 1 initial pitch (degrees) #     PARKED90°
         90  BlPitch(2) - Blade 2 initial pitch (degrees) #     PARKED90°
         90  BlPitch(3) - Blade 3 initial pitch (degrees) #     PARKED90° [unused for 2 blades]
         0   TeetDefl   - Initial or fixed teeter angle (degrees) [unused for 3 blades]
         0   Azimuth    - Initial azimuth angle for blade 1 (degrees)
         0                     RotSpeed          - Initial or fixed rotor speed (rpm) #       RPM,
                ParkIdilingOexpected (mean) value conditioned the mean wind speed your are simulating
         0                     NacYaw            - Initial or fixed nacelle-yaw angle (degrees) # Yaw
               errorServoDynYawNeut
         0   TTDspFA    - Initial fore-aft tower-top displacement (meters)
         0   TTDspSS    - Initial side-to-side tower-top displacement (meters)
         0   PtfmSurge -    static  offsetInitial or fixed horizontal surge translational displacement of
              platform (meters)
         0   PtfmSway  -    static  offsetInitial or fixed horizontal sway translational displacement of
              platform (meters)
         0   PtfmHeave -    static  offsetInitial or fixed vertical heave translational displacement of
              platform (meters)
         0   PtfmRoll  -    static  offsetInitial or fixed roll tilt rotational displacement of platform (
              degrees)
         0   PtfmPitch -    static  offsetInitial or fixed pitch tilt rotational displacement of platform
              (degrees)
         0   PtfmYaw   -    static  offsetInitial or fixed yaw rotational displacement of platform (
              degrees)
---------------------- TURBINE CONFIGURATION ------------------------------------
         3   NumBl      - Number of blades (-)
    120.97   TipRad     - The distance from the rotor apex to the blade tip (meters)
      3.97   HubRad     - The distance from the rotor apex to the blade root (meters)
        -4   PreCone(1) - Blade 1 cone angle (degrees)
        -4   PreCone(2) - Blade 2 cone angle (degrees)
        -4   PreCone(3) - Blade 3 cone angle (degrees) [unused for 2 blades]
         0   HubCM      - Distance from rotor apex to hub mass [positive downwind] (meters)
         0   UndSling   - Undersling length [distance from teeter pin to the rotor apex] (meters) [unused
              for 3 blades]
         0   Delta3     - Delta-3 angle for teetering rotors (degrees) [unused for 3 blades]
         0   AzimB1Up   - Azimuth value to use for I/O when blade 1 points up (degrees)
   -12.098   OverHang   - Distance from yaw axis to rotor apex [3 blades] or teeter pin [2 blades] (meters)
       0.0   ShftGagL   - Distance from rotor apex [3 blades] or teeter pin [2 blades] to shaft strain
             gages [positive for upwind rotors] (meters)
      -6.0   ShftTilt   - Rotor shaft tilt angle (degrees)
    -5.125   NacCMxn    - Downwind distance from the tower-top to the nacelle CM (meters)
       0.0   NacCMyn    - Lateral distance from the tower-top to the nacelle CM (meters)
     4.315   NacCMzn    - Vertical distance from the tower-top to the nacelle CM (meters)
       0.0   NcIMUxn    - Downwind distance from the tower-top to the nacelle IMU (meters)
       0.0   NcIMUyn    - Lateral distance from the tower-top to the nacelle IMU (meters)
       0.0   NcIMUzn    - Vertical distance from the tower-top to the nacelle IMU (meters)
    4.3495   Twr2Shft   - Vertical distance from the tower-top to the rotor shaft (meters)
       145.0          TowerHt    - Height of tower above ground level [onshore] or MSL [offshore] (meters)
       0              TowerBsHt  - Height of tower base above ground level [onshore] or MSL [offshore] (
             meters)
```

```
        0.0           PtfmCMxt  - Downwind distance from the ground level [onshore] or MSL [offshore] to the platform CM (meters)
        0.0           PtfmCMyt  - Lateral distance from the ground level [onshore] or MSL [offshore] to the platform CM (meters)
        -117.8547553061533 PtfmCMzt - Vertical distance from the ground level [onshore] or MSL [offshore] to the platform CM (meters)
        0  PtfmRefzt - Vertical distance from the ground level [onshore] or MSL [offshore] to the platform reference point (meters)
---------------------- MASS AND INERTIA ----------------------------------------
        0  TipMass(1) - Tip-brake mass, blade 1 (kg)
        0  TipMass(2) - Tip-brake mass, blade 2 (kg)
        0  TipMass(3) - Tip-brake mass, blade 3 (kg) [unused for 2 blades]
190000.           HubMass   - Hub mass (kg)
1373471.226       HubIner   - Hub inertia about rotor axis [3 blades] or teeter axis [2 blades] (kg m^2)

3222631.          GenIner   - Generator inertia about HSS (kg m^2)
530887.918        NacMass   - Nacelle mass (kg)
18886965.482      NacYIner  - Nacelle inertia about yaw axis (kg m^2)
100000.           YawBrMass - Yaw bearing mass (kg)
   38134364.02924424 PtfmMass - Platform mass (kg)
   548720926814.21783 PtfmRIner - Platform inertia for roll tilt rotation about the platform CM (kg m^2)
   548720926814.21783 PtfmPIner - Platform inertia for pitch tilt rotation about the platform CM (kg m^2)
   1701087033.100567 PtfmYIner - Platform inertia for yaw rotation about the platform CM (kg m^2)
   0.0           PtfmXYIner - Platform xy moment of inertia about the platform CM (=-int(xydm)) (kg m^2)
   -0.0          PtfmYZIner - Platform yz moment of inertia about the platform CM (=-int(yzdm)) (kg m^2)
   -0.0          PtfmXZIner - Platform xz moment of inertia about the platform CM (=-int(xzdm)) (kg m^2)
---------------------- BLADE ---------------------------------------------------
       50  BldNodes  - Number of blade nodes (per blade) used for analysis (-)
"D:/Thesis/Optimization_Project/openFAST/openfast/IEA-15-240-RWT/IEA-15-240-RWT_ElastoDyn_blade.dat"    BldFile1 - Name of file containing properties for blade 1 (quoted string)
"D:/Thesis/Optimization_Project/openFAST/openfast/IEA-15-240-RWT/IEA-15-240-RWT_ElastoDyn_blade.dat"    BldFile2 - Name of file containing properties for blade 2 (quoted string)
"D:/Thesis/Optimization_Project/openFAST/openfast/IEA-15-240-RWT/IEA-15-240-RWT_ElastoDyn_blade.dat"    BldFile3 - Name of file containing properties for blade 3 (quoted string) [unused for 2 blades]
---------------------- ROTOR-TEETER --------------------------------------------
        0  TeetMod   - Rotor-teeter spring/damper model {0: none, 1: standard, 2: user-defined from routine UserTeet} (switch) [unused for 3 blades]
        0  TeetDmpP  - Rotor-teeter damper position (degrees) [used only for 2 blades and when TeetMod=1]
        0  TeetDmp   - Rotor-teeter damping constant (N-m/(rad/s)) [used only for 2 blades and when TeetMod=1]
        0  TeetCDmp  - Rotor-teeter rate-independent Coulomb-damping moment (N-m) [used only for 2 blades and when TeetMod=1]
        0  TeetSStP  - Rotor-teeter soft-stop position (degrees) [used only for 2 blades and when TeetMod=1]
        0  TeetHStP  - Rotor-teeter hard-stop position (degrees) [used only for 2 blades and when TeetMod=1]
        0  TeetSSSp  - Rotor-teeter soft-stop linear-spring constant (N-m/rad) [used only for 2 blades and when TeetMod=1]
        0  TeetHSSp  - Rotor-teeter hard-stop linear-spring constant (N-m/rad) [used only for 2 blades and when TeetMod=1]
---------------------- YAW-FRICTION --------------------------------------------
        0  YawFrctMod - Yaw-friction model {0: none, 1: friction independent of yaw-bearing force and bending moment, 2: friction with Coulomb terms depending on yaw-bearing force and bending moment, 3: user defined model} (switch)
      300  M_CSmax   - Maximum static Coulomb friction torque (N-m) [M_CSmax when YawFrctMod=1; |Fz|*M_CSmax when YawFrctMod=2 and Fz<0]
        0  M_FCSmax  - Maximum static Coulomb friction torque proportional to yaw bearing shear force (N-m) [sqrt(Fx^2+Fy^2)*M_FCSmax; only used when YawFrctMod=2]
        0  M_MCSmax  - Maximum static Coulomb friction torque proportional to yaw bearing bending moment (N-m) [sqrt(Mx^2+My^2)*M_MCSmax; only used when YawFrctMod=2]
       40  M_CD      - Dynamic Coulomb friction moment (N-m) [M_CD when YawFrctMod=1; |Fz|*M_CD when YawFrctMod=2 and Fz<0]
        0  M_FCD     - Dynamic Coulomb friction moment proportional to yaw bearing shear force (N-m) [sqrt(Fx^2+Fy^2)*M_FCD; only used when YawFrctMod=2]
        0  M_MCD     - Dynamic Coulomb friction moment proportional to yaw bearing bending moment (N-m) [sqrt(Mx^2+My^2)*M_MCD; only used when YawFrctMod=2]
        0  sig_v     - Linear viscous friction coefficient (N-m/(rad/s))
        0  sig_v2    - Quadratic viscous friction coefficient (N-m/(rad/s)^2)
        0  OmgCut    - Yaw angular velocity cutoff below which viscous friction is linearized (rad/s)
---------------------- DRIVETRAIN ----------------------------------------------
```

```
100.0              GBoxEff    - Gearbox efficiency (%)
1.0                GBRatio    - Gearbox ratio (-)
8.235E+11          DTTorSpr   - Drivetrain torsional spring (N-m/rad)
6215000.0          DTTorDmp   - Drivetrain torsional damper (N-m/(rad/s))
---------------------- FURLING -----------------------------------------------
False       Furling   - Read in additional model properties for furling turbine (flag) [must currently be
     FALSE)
"unused"    FurlFile  - Name of file containing furling properties (quoted string) [unused when Furling=
    False]
---------------------- TOWER -------------------------------------------------
       20            TwrNodes  - Number of tower nodes used for analysis (-)
"D:\Thesis\Optimization_Project\openFAST\openfast\IEA15_CSpar_ElastoDyn_Tower.dat" TwrFile - Name of file
     containing tower properties (quoted string)
---------------------- OUTPUT ------------------------------------------------
True       SumPrint  - Print summary data to "<RootName>.sum" (flag)
        1  OutFile   - Switch to determine where output will be placed: {1: in module output file only;
             2: in glue code output file only; 3: both} (currently unused)
True       TabDelim  - Use tab delimiters in text tabular output file? (flag) (currently unused)
"ES10.3E2" OutFmt    - Format used for text tabular output (except time). Resulting field should be 10
    characters. (quoted string) (currently unused)
        0  TStart    - Time to begin tabular output (s) (currently unused)
        1  DecFact   - Decimation factor for tabular output {1: output every time step} (-) (currently
             unused)
        9  NTwGages  - Number of tower nodes that have strain gages for output [0 to 9] (-)
        3, 5, 7, 9, 11, 13, 15, 17, 19 TwrGagNd - List of tower nodes that have strain gages [1 to
             TwrNodes] (-) [unused if NTwGages=0] TwrGagNd - List of tower nodes that have strain gages
             [1 to TwrNodes] (-) [unused if NTwGages=0] TwrGagNd - List of tower nodes that have strain
             gages [1 to TwrNodes] (-) [unused if NTwGages=0]
        3  NBlGages  - Number of blade nodes that have strain gages for output [0 to 9] (-)
        5,        9,       13   BldGagNd  - List of blade nodes that have strain gages [1 to BldNodes]
             (-) [unused if NBlGages=0] BldGagNd - List of blade nodes that have strain gages [1 to
             BldNodes] (-) [unused if NBlGages=0] BldGagNd - List of blade nodes that have strain gages
             [1 to BldNodes] (-) [unused if NBlGages=0]
           OutList          - The next line(s) contains a list of output parameters. See
                OutListParameters.xlsx for a listing of available output channels, (-)
"TTDspFA"             - Tower fore-aft  deflection
"TTDspSS"             - Tower side-to-side deflection
"TTDspTwst"           - Tower top twist
"TwrBsFxt"            - Fore-aft   shear force at the base of the tower (platform)
"TwrBsFyt"            - Side-to-side shear force at the base of the tower (platform)
"TwrBsFzt"            - Vertical       force at the base of the tower (platform)
"TwrBsMxt"            - Side-to-side bending moment at the base of the tower (platform)
"TwrBsMyt"            - Fore-aft   bending moment at the base of the tower (platform)
"TwrBsMzt"            - Yaw              moment at the base of the tower (platform)
"PtfmHeave"
"PtfmPitch"
"PtfmRoll"
"PtfmSurge"
"PtfmSway"
"PtfmYaw"
"YawPzn"
   "TwHt1MLxt"  - Local tower roll (or side-to-side) moment of tower gage 1
   "TwHt1MLyt"  - Local tower pitching (or fore-aft) moment of tower gage 1
   "TwHt1MLzt"  - Local tower yaw (or torsional) moment of tower gage 1
   "TwHt2MLxt"  - Local tower roll (or side-to-side) moment of tower gage 2
   "TwHt2MLyt"  - Local tower pitching (or fore-aft) moment of tower gage 2
   "TwHt2MLzt"  - Local tower yaw (or torsional) moment of tower gage 2
   "TwHt3MLxt"  - Local tower roll (or side-to-side) moment of tower gage 3
   "TwHt3MLyt"  - Local tower pitching (or fore-aft) moment of tower gage 3
   "TwHt3MLzt"  - Local tower yaw (or torsional) moment of tower gage 3
   "TwHt4MLxt"  - Local tower roll (or side-to-side) moment of tower gage 4
   "TwHt4MLyt"  - Local tower pitching (or fore-aft) moment of tower gage 4
   "TwHt4MLzt"  - Local tower yaw (or torsional) moment of tower gage 4
   "TwHt5MLxt"  - Local tower roll (or side-to-side) moment of tower gage 5
   "TwHt5MLyt"  - Local tower pitching (or fore-aft) moment of tower gage 5
   "TwHt5MLzt"  - Local tower yaw (or torsional) moment of tower gage 5
   "TwHt6MLxt"  - Local tower roll (or side-to-side) moment of tower gage 6
   "TwHt6MLyt"  - Local tower pitching (or fore-aft) moment of tower gage 6
   "TwHt6MLzt"  - Local tower yaw (or torsional) moment of tower gage 6
   "TwHt7MLxt"  - Local tower roll (or side-to-side) moment of tower gage 7
   "TwHt7MLyt"  - Local tower pitching (or fore-aft) moment of tower gage 7
```

```
   "TwHt7MLzt"  - Local tower yaw (or torsional) moment of tower gage 7
   "TwHt8MLxt"  - Local tower roll (or side-to-side) moment of tower gage 8
   "TwHt8MLyt"  - Local tower pitching (or fore-aft) moment of tower gage 8
   "TwHt8MLzt"  - Local tower yaw (or torsional) moment of tower gage 8
   "TwHt9MLxt"  - Local tower roll (or side-to-side) moment of tower gage 9
   "TwHt9MLyt"  - Local tower pitching (or fore-aft) moment of tower gage 9
   "TwHt9MLzt"  - Local tower yaw (or torsional) moment of tower gage 9
   "TwHt1FLxt"  - Local tower roll (or side-to-side) force of tower gage 1
   "TwHt1FLyt"  - Local tower pitching (or fore-aft) force of tower gage 1
   "TwHt1FLzt"  - Local tower yaw (or torsional) force of tower gage 1
   "TwHt2FLxt"  - Local tower roll (or side-to-side) force of tower gage 2
   "TwHt2FLyt"  - Local tower pitching (or fore-aft) force of tower gage 2
   "TwHt2FLzt"  - Local tower yaw (or torsional) force of tower gage 2
   "TwHt3FLxt"  - Local tower roll (or side-to-side) force of tower gage 3
   "TwHt3FLyt"  - Local tower pitching (or fore-aft) force of tower gage 3
   "TwHt3FLzt"  - Local tower yaw (or torsional) force of tower gage 3
   "TwHt4FLxt"  - Local tower roll (or side-to-side) force of tower gage 4
   "TwHt4FLyt"  - Local tower pitching (or fore-aft) force of tower gage 4
   "TwHt4FLzt"  - Local tower yaw (or torsional) force of tower gage 4
   "TwHt5FLxt"  - Local tower roll (or side-to-side) force of tower gage 5
   "TwHt5FLyt"  - Local tower pitching (or fore-aft) force of tower gage 5
   "TwHt5FLzt"  - Local tower yaw (or torsional) force of tower gage 5
   "TwHt6FLxt"  - Local tower roll (or side-to-side) force of tower gage 6
   "TwHt6FLyt"  - Local tower pitching (or fore-aft) force of tower gage 6
   "TwHt6FLzt"  - Local tower yaw (or torsional) force of tower gage 6
   "TwHt7FLxt"  - Local tower roll (or side-to-side) force of tower gage 7
   "TwHt7FLyt"  - Local tower pitching (or fore-aft) force of tower gage 7
   "TwHt7FLzt"  - Local tower yaw (or torsional) force of tower gage 7
   "TwHt8FLxt"  - Local tower roll (or side-to-side) force of tower gage 8
   "TwHt8FLyt"  - Local tower pitching (or fore-aft) force of tower gage 8
   "TwHt8FLzt"  - Local tower yaw (or torsional) force of tower gage 8
   "TwHt9FLxt"  - Local tower roll (or side-to-side) force of tower gage 9
   "TwHt9FLyt"  - Local tower pitching (or fore-aft) force of tower gage 9
   "TwHt9FLzt"  - Local tower yaw (or torsional) force of tower gage 9
END of input file (the word "END" must appear in the first 3 columns of this last OutList line)
---------------------------------------------------------------------------------------
```

F.0.2. ElastoDyn_Tower file

```
------- ELASTODYN V1.00.* TOWER INPUT FILE ------------------------------------
IEA 15 MW offshore reference model on UMaine VolturnUS-S semi-submersible floating platform
---------------------- TOWER PARAMETERS ----------------------------------------
21                  NTwInpSt  - Number of input stations to specify tower geometry
1.0                 TwrFADmp(1) - Tower 1st fore-aft mode structural damping ratio (%)
1.0                 TwrFADmp(2) - Tower 2nd fore-aft mode structural damping ratio (%)
1.0                 TwrSSDmp(1) - Tower 1st side-to-side mode structural damping ratio (%)
1.0                 TwrSSDmp(2) - Tower 2nd side-to-side mode structural damping ratio (%)
---------------------- TOWER ADJUSTMUNT FACTORS --------------------------------
1.0                 FAStTunr(1) - Tower fore-aft modal stiffness tuner, 1st mode (-)
1.0                 FAStTunr(2) - Tower fore-aft modal stiffness tuner, 2nd mode (-)
1.0                 SSStTunr(1) - Tower side-to-side stiffness tuner, 1st mode (-)
1.0                 SSStTunr(2) - Tower side-to-side stiffness tuner, 2nd mode (-)
1.0                 AdjTwMa   - Factor to adjust tower mass density (-)
1.0                 AdjFASt   - Factor to adjust tower fore-aft stiffness (-)
1.0                 AdjSSSt   - Factor to adjust tower side-to-side stiffness (-)
---------------------- DISTRIBUTED TOWER PROPERTIES ----------------------------
  HtFract     TMassDen       TwFAStif     TwSSStif
   (-)         (kg/m)         (Nm^2)       (Nm^2)
    0.000    10325.520 3.39835E+12 3.39835E+12
    0.050    10064.793 3.14694E+12 3.14694E+12
    0.100    9804.066  2.90825E+12 2.90825E+12
    0.150    9543.339  2.68194E+12 2.68194E+12
    0.200    9282.612  2.46769E+12 2.46769E+12
    0.250    9021.885  2.26517E+12 2.26517E+12
    0.300    8761.158  2.07404E+12 2.07404E+12
    0.350    8500.431  1.89398E+12 1.89398E+12
    0.400    8239.704  1.72465E+12 1.72465E+12
    0.450    7978.977  1.56573E+12 1.56573E+12
    0.500    7718.250  1.41688E+12 1.41688E+12
    0.550    7457.523  1.27778E+12 1.27778E+12
```

```
   0.600    7196.796 1.14810E+12 1.14810E+12
   0.650    6936.069 1.02750E+12 1.02750E+12
   0.700    6675.342 9.15663E+11 9.15663E+11
   0.750    6414.614 8.12248E+11 8.12248E+11
   0.800    6153.887 7.16928E+11 7.16928E+11
   0.850    5893.160 6.29374E+11 6.29374E+11
   0.900    5632.433 5.49256E+11 5.49256E+11
   0.950    5371.706 4.76244E+11 4.76244E+11
   1.000    5110.979 4.10007E+11 4.10007E+11
---------------------- TOWER FORE-AFT MODE SHAPES ------------------------------
0.636         TwFAM1Sh(2) - Mode 1, coefficient of x^2 term
1.281         TwFAM1Sh(3) -    , coefficient of x^3 term
-1.916         TwFAM1Sh(4) -    , coefficient of x^4 term
1.592         TwFAM1Sh(5) -    , coefficient of x^5 term
-0.593         TwFAM1Sh(6) -    , coefficient of x^6 term
61.337         TwFAM2Sh(2) - Mode 2, coefficient of x^2 term
-15.943         TwFAM2Sh(3) -    , coefficient of x^3 term
-40.913         TwFAM2Sh(4) -    , coefficient of x^4 term
-43.500         TwFAM2Sh(5) -    , coefficient of x^5 term
40.018         TwFAM2Sh(6) -    , coefficient of x^6 term
---------------------- TOWER SIDE-TO-SIDE MODE SHAPES --------------------------
0.643         TwSSM1Sh(2) - Mode 1, coefficient of x^2 term
1.267         TwSSM1Sh(3) -    , coefficient of x^3 term
-1.893         TwSSM1Sh(4) -    , coefficient of x^4 term
1.569         TwSSM1Sh(5) -    , coefficient of x^5 term
-0.587         TwSSM1Sh(6) -    , coefficient of x^6 term
41.689         TwSSM2Sh(2) - Mode 2, coefficient of x^2 term
-12.661         TwSSM2Sh(3) -    , coefficient of x^3 term
-24.222         TwSSM2Sh(4) -    , coefficient of x^4 term
-34.273         TwSSM2Sh(5) -    , coefficient of x^5 term
30.467         TwSSM2Sh(6) -    , coefficient of x^6 term
```

F.0.3. HydroDyn file

```
------- HydroDyn v2.03.* Input File ------------------------------------------
IEA 15 MW offshore reference model on CSpar floating platform HydroDyn input properties
False          Echo         - Echo the input file data (flag)
---------------------- FLOATING PLATFORM ------------------------------------- [unused with WaveMod=6]
           1             PotMod       - Potential-flow model {0: none=no potential flow, 1: frequency-to-time-domain transforms based on WAMIT output, 2: fluid-impulse theory (FIT)} (switch)
           1   ExctnMod     - Wave-excitation model {0: no wave-excitation calculation, 1: DFT, 2: state-space} (switch) [only used when PotMod=1; STATE-SPACE REQUIRES *.ssexctn INPUT FILE]
           0   ExctnDisp    - Method of computing Wave Excitation {0: use undisplaced position, 1: use displaced position, 2: use low-pass filtered displaced position) [only used when PotMod=1 and ExctnMod>0 and SeaState's WaveMod>0]} (switch)
          10   ExctnCutOff  - Cutoff (corner) frequency of the low-pass time-filtered displaced position (Hz) [>0.0] [used only when PotMod=1, ExctnMod>0, and ExctnDisp=2]) [only used when PotMod=1 and ExctnMod>0 and SeaState's WaveMod>0]} (switch)
           0   PtfmYMod     - Model for large platform yaw offset {0: Static reference yaw offset based on PtfmRefY, 1: dynamic reference yaw offset based on low-pass filtering the PRP yaw motion with cutoff frequency PtfmYCutOff} (switch)
           0   PtfmRefY     - Constant (if PtfmYMod=0) or initial (if PtfmYMod=1) platform reference yaw offset (deg)
        0.01   PtfmYCutOff  - Cutoff frequency for the low-pass filtering of PRP yaw motion when PtfmYMod=1 [unused when PtfmYMod=0] (Hz)
          36   NExctnHdg    - Number of evenly distributed platform yaw/heading angles over the range of [-180, 180) deg for which the wave excitation shall be computed [only used when PtfmYMod=1] (-)
           1   RdtnMod      - Radiation memory-effect model {0: no memory-effect calculation, 1: convolution, 2: state-space} (switch) [only used when PotMod=1; STATE-SPACE REQUIRES *.ss INPUT FILE]
          60   RdtnTMax     - Analysis time for wave radiation kernel calculations (sec) [only used when PotMod=1 and RdtnMod>0; determines RdtnDOmega=Pi/RdtnTMax in the cosine transform; MAKE SURE THIS IS LONG ENOUGH FOR THE RADIATION IMPULSE RESPONSE FUNCTIONS TO DECAY TO NEAR-ZERO FOR THE GIVEN PLATFORM!]
    "default" RdtnDT       - Time step for wave radiation kernel calculations (sec) [only used when PotMod=1 and ExctnMod>0 or RdtnMod>0; DT<=RdtnDT<=0.1 recommended; determines RdtnOmegaMax=Pi/RdtnDT in the cosine transform]
           1             NBody        - Number of WAMIT bodies to be used (-) [>=1; only used when PotMod=1. If NBodyMod=1, the WAMIT data contains a vector of size 6*NBody x 1 and matrices of
```

```
                size 6*NBody x 6*NBody; if NBodyMod>1, there are NBody sets of WAMIT data each with a
                vector of size 6 x 1 and matrices of size 6 x 6]
17            1   NBodyMod     - Body coupling model {1: include coupling terms between each body and NBody
                in HydroDyn equals NBODY in WAMIT, 2: neglect coupling terms between each body and NBODY
                =1 with XBODY=0 in WAMIT, 3: Neglect coupling terms between each body and NBODY=1 with
                XBODY=/0 in WAMIT} (switch) [only used when PotMod=1]
18 'D:\Thesis\Optimization_Project\openFAST\openfast\IEA-15-240-RWT\HydroData\Single_Body\cspar' PotFile -
     Root name of potential-flow model data; WAMIT output files containing the linear, nondimensionalized,
      hydrostatic restoring matrix (.hst), frequency-dependent hydrodynamic added mass matrix and damping
      matrix (.1), and frequency- and direction-dependent wave excitation force vector per unit wave
     amplitude (.3) (quoted string) [1 to NBody if NBodyMod>1] [MAKE SURE THE FREQUENCIES INHERENT IN
     THESE WAMIT FILES SPAN THE PHYSICALLY-SIGNIFICANT RANGE OF FREQUENCIES FOR THE GIVEN PLATFORM; THEY
     MUST CONTAIN THE ZERO- AND INFINITE-FREQUENCY LIMITS!]
19            1   WAMITULEN    - Characteristic body length scale used to redimensionalize WAMIT output (
                meters) [1 to NBody if NBodyMod>1] [only used when PotMod=1]
20          0.0   PtfmRefxt    - The xt offset of the body reference point(s) from (0,0,0) (meters) [1 to
                NBody] [only used when PotMod=1]
21          0.0   PtfmRefyt    - The yt offset of the body reference point(s) from (0,0,0) (meters) [1 to
                NBody] [only used when PotMod=1]
22          0.0   PtfmRefzt    - The zt offset of the body reference point(s) from (0,0,0) (meters) [1 to
                NBody] [only used when PotMod=1. If NBodyMod=2,PtfmRefzt=0.0]
23          0.0   PtfmRefztRot - The rotation about zt of the body reference frame(s) from xt/yt (degrees) [1
                 to NBody] [only used when PotMod=1]
24       40021.48185236621 PtfmVol0  - Displaced volume of water when the body is in its undisplaced
               position (m^3) [1 to NBody] [only used when PotMod=1; USE THE SAME VALUE COMPUTED BY WAMIT AS
               OUTPUT IN THE .OUT FILE!]
25          0.0   PtfmCOBxt    - The xt offset of the center of buoyancy (COB) from (0,0) (meters) [1 to
                NBody] [only used when PotMod=1]
26          0.0   PtfmCOByt    - The yt offset of the center of buoyancy (COB) from (0,0) (meters) [1 to
                NBody] [only used when PotMod=1]
27 ---------------------- 2ND-ORDER FLOATING PLATFORM FORCES ---------------------- [unused with WaveMod=0
     or 6, or PotMod=0 or 2]
28            0   MnDrift      - Mean-drift 2nd-order forces computed                         {0: None; [7,
                  8, 9, 10, 11, or 12]: WAMIT file to use} [Only one of MnDrift, NewmanApp, or DiffQTF can
                 be non-zero. If NBody>1, MnDrift /=8]
29            0   NewmanApp    - Mean- and slow-drift 2nd-order forces computed with Newman's approximation
                 {0: None; [7, 8, 9, 10, 11, or 12]: WAMIT file to use} [Only one of MnDrift, NewmanApp,
                 or DiffQTF can be non-zero. If NBody>1, NewmanApp/=8. Used only when WaveDirMod=0]
30            0   DiffQTF      - Full difference-frequency 2nd-order forces computed with full QTF {0: None;
                 [10, 11, or 12]: WAMIT file to use} [Only one of MnDrift, NewmanApp, or DiffQTF can be
                 non-zero]
31            0   SumQTF       - Full summation -frequency 2nd-order forces computed with full QTF {0: None;
                 [10, 11, or 12]: WAMIT file to use}
32 ---------------------- PLATFORM ADDITIONAL STIFFNESS AND DAMPING --------------
33     0.000
34     0.000
35     0.000
36     0.000
37     0.000
38     0.000
39     0.000     0.000     0.000     0.000     0.000     0.000
40     0.000     0.000     0.000     0.000     0.000     0.000
41     0.000     0.000     0.000     0.000     0.000     0.000
42     0.000     0.000     0.000     0.000     0.000     0.000
43     0.000     0.000     0.000     0.000     0.000     0.000
44     0.000     0.000     0.000     0.000     0.000     0.000
45     0.000     0.000     0.000     0.000     0.000     0.000
46     0.000     0.000     0.000     0.000     0.000     0.000
47     0.000     0.000     0.000     0.000     0.000     0.000
48     0.000     0.000     0.000     0.000     0.000     0.000
49     0.000     0.000     0.000     0.000     0.000     0.000
50     0.000     0.000     0.000     0.000     0.000     0.000
51     0.000     0.000     0.000     0.000     0.000     0.000
52     0.000     0.000     0.000     0.000     0.000     0.000
53     0.000     0.000     0.000     0.000     0.000     0.000
54     0.000     0.000     0.000     0.000     0.000     0.000
55     0.000     0.000     0.000     0.000     0.000     0.000
56     0.000     0.000     0.000     0.000     0.000     0.000
57 ---------------------- STRIP THEORY OPTIONS ----------------------------------
58            0   WaveDisp     - Method of computing Wave Kinematics {0: use undisplaced position, 1: use
                 displaced position) } (switch)
```

```
           1   AMMod        - Method of computing distributed added-mass force. (0: Only and always on
                nodes below SWL at the undisplaced position. 2: Up to the instantaneous free surface) [
                overwrite to 0 when WaveMod = 0 or 6 or when WaveStMod = 0 in SeaState]
---------------------- AXIAL COEFFICIENTS -------------------------------------
           2   NAxCoef      - Number of axial coefficients (-)
AxCoefID AxCd   AxCa    AxCp
  (-)   (-)     (-)     (-)
   1    0.00    0.00    0.00
   2    0.2     0.00    0.00
---------------------- MEMBER JOINTS ------------------------------------------ !!!
           3             NJoints      - Number of joints (-) [must be exactly 0 or at least 2]
JointID  Jointxi   Jointyi   Jointzi JointAxID JointOvrlp [JointOvrlp= 0: do nothing at joint, 1:
     eliminate overlaps by calculating super member]
  (-)    (m)       (m)       (m)       (-)      (switch)
   1        0.000    0.000    -150.000 2.000    0.000
   2        0.000    0.000    -10.000  1.000    0.000
   3        0.000    0.000    0.010    1.000    0.000
---------------------- MEMBER CROSS-SECTION PROPERTIES -------------------------
           2             NPropSetsCyl    - Number of member property sets (-)
PropSetID  PropD       PropThck
  (-)       (m)          (m)
   1        18.600    0.130
   2        13.000    0.130
---------------- RECTANGULAR MEMBER CROSS-SECTION PROPERTIES --------------------
           0  NPropSetsRec  - Number of rectangular member property sets (-)
MPropSetID PropA     PropB   PropThck
  (-)       (m)       (m)      (m)
-------- SIMPLE CYLINDRICAL-MEMBER HYDRODYNAMIC COEFFICIENTS (model 1) ---------
SimplCd  SimplCdMG  SimplCa  SimplCaMG  SimplCp  SimplCpMG SimplAxCd SimplAxCdMG SimplAxCa SimplAxCaMG
     SimplAxCp SimplAxCpMG SimplCb SimplCbMG
  (-)       (-)       (-)       (-)       (-)       (-)       (-)       (-)       (-)       (-)
       (-)       (-)          (-)       (-)
  0.7      0.00      0.00       0.00       0.00      0.00      0.00      0.00      0.00      0.00
       0.00      0.00         1.00      1.00
-------- SIMPLE RECTANGULAR-MEMBER HYDRODYNAMIC COEFFICIENTS (model 1) ---------
SimplCdA  SimplCdAMG  SimplCdB  SimplCdBMG  SimplCaA  SimplCaAMG  SimplCaB  SimplCaBMG  SimplCp
     SimplCpMG SimplAxCd SimplAxCdMG SimplAxCa SimplAxCaMG SimplAxCp SimplAxCpMG SimplCb SimplCbMG
  (-)       (-)         (-)       (-)         (-)       (-)         (-)       (-)         (-)       (-)
             (-)       (-)       (-)       (-)       (-)       (-)       (-)     (-)
  0.0       0.0         0.0       0.0         0.0       0.0         0.0       0.0         0.0       0.0
             0.0       0.0       0.0       0.0       0.0       0.0       1.0     1.0
------ DEPTH-BASED CYLINDRICAL-MEMBER HYDRODYNAMIC COEFFICIENTS (model 2) -------
           0  NCoefDpthCyl  - Number of depth-dependent cylindrical member coefficients (-)
Dpth     DpthCd  DpthCdMG  DpthCa  DpthCaMG     DpthCp  DpthCpMG  DpthAxCd  DpthAxCdMG  DpthAxCa  DpthAxCaMG
     DpthAxCp  DpthAxCpMG DpthCb  DpthCbMG
(m)      (-)     (-)       (-)     (-)          (-)     (-)       (-)       (-)         (-)       (-)
     (-)       (-)         (-)     (-)
------ DEPTH-BASED RECTANGULAR-MEMBER HYDRODYNAMIC COEFFICIENTS (model 2) -------
           0  NCoefDpthRec  - Number of depth-dependent rectangular member coefficients (-)
Dpth   DpthCdA  DpthCdAMG  DpthCdB  DpthCdBMG DpthCaA  DpthCaAMG DpthCaB  DpthCaBMG   DpthCp  DpthCpMG
     DpthAxCd  DpthAxCdMG DpthAxCa  DpthAxCaMG DpthAxCp  DpthAxCpMG DpthCb  DpthCbMG
(m)      (-)       (-)         (-)       (-)       (-)       (-)       (-)       (-)         (-)       (-)      (-)
            (-)         (-)       (-)       (-)       (-)       (-)       (-)     (-)
------ MEMBER-BASED CYLINDRICAL-MEMBER HYDRODYNAMIC COEFFICIENTS (model 3) ------
           0  NCoefMembersCyl - Number of member-based cylindrical member coefficients (-)
MemberID  MemberCd1   MemberCd2  MemberCdMG1 MemberCdMG2  MemberCa1   MemberCa2  MemberCaMG1 MemberCaMG2
     MemberCp1   MemberCp2  MemberCpMG1 MemberCpMG2 MemberAxCd1 MemberAxCd2 MemberAxCdMG1 MemberAxCdMG2
     MemberAxCa1 MemberAxCa2 MemberAxCaMG1 MemberAxCaMG2 MemberAxCp1 MemberAxCp2 MemberAxCpMG1
     MemberAxCpMG2 MemberCb1 MemberCb2 MemberCbMG1 MemberCbMG2
  (-)       (-)         (-)         (-)         (-)         (-)         (-)         (-)         (-)         (-)
               (-)         (-)         (-)         (-)         (-)         (-)         (-)         (-)         (-)
               (-)         (-)         (-)         (-)         (-)         (-)         (-)         (-)         (-)
                  (-)         (-)         (-)         (-)
------ MEMBER-BASED RECTANGULAR-MEMBER HYDRODYNAMIC COEFFICIENTS (model 3) ------
          0  NCoefMembersRec - Number of member-based rectangular member coefficients (-)
MemberID  MemberCdA1   MemberCdA2  MemberCdAMG1 MemberCdAMG2 MemberCdB1   MemberCdB2  MemberCdBMG1
     MemberCdBMG2 MemberCaA1   MemberCaA2  MemberCaAMG1 MemberCaAMG2 MemberCaB1   MemberCaB2  MemberCaBMG1
      MemberCaBMG2 MemberCp1   MemberCp2  MemberCpMG1 MemberCpMG2 MemberAxCd1 MemberAxCd2 MemberAxCdMG1
     MemberAxCdMG2 MemberAxCa1 MemberAxCa2 MemberAxCaMG1 MemberAxCaMG2 MemberAxCp1 MemberAxCp2
     MemberAxCpMG1 MemberAxCpMG2 MemberCb1 MemberCb2 MemberCbMG1 MemberCbMG2
```

```
  (-)       (-)          (-)          (-)          (-)          (-)          (-)          (-)          (-)
               (-)          (-)          (-)          (-)          (-)          (-)          (-)
      (-)          (-)          (-)          (-)          (-)          (-)          (-)          (-)          (-)
               (-)          (-)          (-)          (-)          (-)          (-)          (-)          (-)
              (-)          (-)          (-)          (-)
---------------------- MEMBERS -----------------------------------------------
          2             NMembers     - Number of members (-)
MemberID MJointID1 MJointID2 MPropSetID1 MPropSetID2 MSecGeom MSpinOrient MDivSize MCoefMod MHstLMod
    PropPot [MCoefMod=1: use simple coeff table, 2: use depth-based coeff table, 3: use member-based
    coeff table] [ PropPot/=0 if member is modeled with potential-flow theory] (-) (-) (-) (-) (-)   (m)
         (switch) (switch) (flag)
 (-)       (-)       (-)       (-)        (-)     (switch)     (deg)      (m)     (switch) (switch) (flag)
   1         1         2         1          1         1          0        1.000     1         1         True
   2         2         3         1          2         1          0        0.500     1         2         True
---------------------- FILLED MEMBERS ----------------------------------------
          0   NFillGroups   - Number of filled member groups (-) [If FillDens = DEFAULT, then FillDens =
                WtrDens; FillFSLoc is related to MSL2SWL]
FillNumM FillMList         FillFSLoc   FillDens
(-)     (-)                (m)         (kg/m^3)
---------------------- MARINE GROWTH -----------------------------------------
          0   NMGDepths     - Number of marine-growth depths specified (-)
MGDpth    MGThck      MGDens
(m)       (m)         (kg/m^3)
---------------------- MEMBER OUTPUT LIST ------------------------------------
          0   NMOutputs     - Number of member outputs (-) [must be <= 99]
MemberID NOutLoc  NodeLocs [NOutLoc < 10; node locations are normalized distance from the start of the
    member, and must be >=0 and <= 1] [unused if NMOutputs=0]
  (-)       (-)       (-)
---------------------- JOINT OUTPUT LIST -------------------------------------
          0   NJOutputs     - Number of joint outputs [Must be < 10]
   0          JOutLst      - List of JointIDs which are to be output (-)[unused if NJOutputs=0]
---------------------- OUTPUT ------------------------------------------------
True           HDSum         - Output a summary file [flag]
False          OutAll        - Output all user-specified member and joint loads (only at each member end,
    not interior locations) [flag]
          2   OutSwtch      - Output requested channels to: [1=Hydrodyn.out, 2=GlueCode.out, 3=both files]
"E15.7e2"     OutFmt        - Output format for numerical results (quoted string) [not checked for validity
    !]
"A11"          OutSFmt       - Output format for header strings (quoted string) [not checked for validity!]
---------------------- OUTPUT CHANNELS ---------------------------------------
"HydroFxi"            - Total integrated hydrodynamic load along the global x-direction from both
    potential flow and strip theory at (0,0,0)  (N)
"HydroFyi"            - Total integrated hydrodynamic load along the global y-direction from both
    potential flow and strip theory at (0,0,0)  (N)
"HydroFzi"            - Total integrated hydrodynamic load along the global z-direction from both
    potential flow and strip theory at (0,0,0)  (N)
"HydroMxi"            - Total integrated hydrodynamic moment about the global x-axis from both potential
    flow and strip theory at (0,0,0)  (N-m)
"HydroMyi"            - Total integrated hydrodynamic moment about the global y-axis from both potential
    flow and strip theory at (0,0,0)  (N-m)
"HydroMzi"            - Total integrated hydrodynamic moment about the global z-axis from both potential
    flow and strip theory at (0,0,0)  (N-m)
"B1AddFxi"
"B1AddFyi"
"B1AddFzi"
"B1WvsF1xi"
"B1WvsF1yi"
"B1WvsF1zi"
"B1WvsM1xi"
"B1WvsM1yi"
"B1WvsM1zi"
"B1WvsFxi"
"B1WvsFyi"
"B1WvsFzi"
"B1WvsMxi"
"B1WvsMyi"
"B1WvsMzi"
"B1HdSFxi"
"B1HdSFyi"
"B1HdSFzi"
"B1HdSMxi"
```

```
"B1HdSMyi"
"B1HdSMzi"
"B1RdtFxi"
"B1RdtFyi"
"B1RdtFzi"
"B1RdtMxi"
"B1RdtMyi"
"B1RdtMzi"




END of output channels and end of file. (the word "END" must appear in the first 3 columns of this line)
```

F.0.4. SeaState file

```
   ------- SeaState Input File ----------------------------------------------------
IEA 15 MW offshore reference model on CSpar floating platform SeaState input properties
False         Echo        - Echo the input file data (flag)
---------------------- ENVIRONMENTAL CONDITIONS -------------------------------
1025          WtrDens     - Water density (kg/m^3)
200           WtrDpth     - Water depth (meters) relative to MSL
0             MSL2SWL     - Offset between still-water level and mean sea level (meters) [positive upward; unused when WaveMod = 6; must be zero if PotMod=1 or 2]
---------------------- SPATIAL DISCRETIZATION ---------------------------------------------------
          30  X_HalfWidth -  Half-width of the domain in the X direction (m) [>0, NOTE: X[nX] = nX*dX, where nX = {-NX+1,-NX…+2,,NX-1} and dX = X_HalfWidth/(NX-1)]
          30  Y_HalfWidth -  Half-width of the domain in the Y direction (m) [>0, NOTE: Y[nY] = nY*dY, where nY = {-NY+1,-NY…+2,,NY-1} and dY = Y_HalfWidth/(NY-1)]
     DEFAULT  Z_Depth -      Depth of the domain the Z direction (m) relative to SWL [0 < Z_Depth <= WtrDpth+MSL2SWL; "default": Z_Depth = WtrDpth+MSL2SWL; Z[nZ] = ( COS( nZ*dthetaZ ) -1 )* Z_Depth, where nZ = …{0,1,NZ-1} and dthetaZ = pi/( 2*(NZ-1) )]
           2  NX -           Number of nodes in half of the X-direction domain (-) [>=2]
           2  NY -           Number of nodes in half of the Y-direction domain (-) [>=2]
          40  NZ -           Number of nodes in the Z direction (-) [>=2]
---------------------- WAVES --------------------------------------------------
           2  WaveMod      - Incident wave kinematics model {0: none=still water, 1: regular (periodic), 1P#: regular with user-specified phase, 2: JONSWAP/Pierson-Moskowitz spectrum (irregular), 3: White noise spectrum (irregular), 4: user-defined spectrum from routine UserWaveSpctrm (irregular), 5: Externally generated wave-elevation time series, 6: Externally generated full wave-kinematics time series, 7: wave frequency components [option 6 is invalid for PotMod/=0]} (switch)
           3  WaveStMod    - Model for stretching incident wave kinematics to instantaneous free surface {0: none=no stretching, 1: vertical stretching, 2: extrapolation stretching, 3: Wheeler stretching} (switch) [unused when WaveMod=0 or when PotMod/=0]
       10000  WaveTMax     - Analysis time for incident wave calculations (sec) [unused when WaveMod=0; determines WaveDOmega=2Pi/WaveTMax in the IFFT]
        0.25  WaveDT       - Time step for incident wave calculations (sec) [unused when WaveMod=0 or 7; 0.1<=WaveDT<=1.0 recommended; determines WaveOmegaMax=Pi/WaveDT in the IFFT]
        10.8          WaveHs       - [DLC6.1:13.8, DLC1.2:2] Significant wave height of incident waves (meters) [used only when WaveMod=1, 2, or 3]
        17.6          WaveTp       - [DLC6.1:19.1, DLC1.2:6] Peak-spectral period of incident waves (sec) [used only when WaveMod=1 or 2]
"DEFAULT"     WavePkShp    - Peak-shape parameter of incident wave spectrum (-) or DEFAULT (string) [used only when WaveMod=2; use 1.0 for Pierson-Moskowitz]
           0  WvLowCOff    - Low cut-off frequency or lower frequency limit of the wave spectrum beyond which the wave spectrum is zeroed (rad/s) [unused when WaveMod=0, 1, 6, or 7]
         500  WvHiCOff     - High cut-off frequency or upper frequency limit of the wave spectrum beyond which the wave spectrum is zeroed (rad/s) [unused when WaveMod=0, 1, 6, or 7]
           0                    WaveDir          - Wave Misalignment Incident wave propagation heading direction           (degrees) [unused when WaveMod=0, 6 or 7]
           0  WaveDirMod   - Directional spreading function {0: none, 1: COS2S}       (-)      [only used when WaveMod=2,3, or 4]
           1  WaveDirSpread - Wave direction spreading coefficient ( > 0 )            (-)      [only used when WaveMod=2,3, or 4 and WaveDirMod=1]
           1  WaveNDir     - Number of wave directions                                (-)      [only used when WaveMod=2,3, or 4 and WaveDirMod=1; odd number only]
          90  WaveDirRange - Range of wave directions (full range: WaveDir +/- 1/2*WaveDirRange) (degrees) [only used when WaveMod=2,3,or 4 and WaveDirMod=1]
```

```
           -1425596469          WaveSeed(1)       - First random seed of incident waves [-2147483648 to
                2147483647] (-) [unused when WaveMod=0, 5, or 6]
"RANLUX"      WaveSeed(2)  - Second random seed of incident waves [-2147483648 to 2147483647] for
    intrinsic pRNG, or an alternative pRNG: "RanLux" (-) [unused when WaveMod=0, 5, or 6]
TRUE          WaveNDAmp    - Flag for normally distributed amplitudes                 (flag)   [only used
     when WaveMod=2, 3, or 4]
""            WvKinFile    - Root name of externally generated wave data file(s) (quoted string) [used
    only when WaveMod=5, 6 or 7]
---------------------- 2ND-ORDER WAVES ---------------------------------------- [unused with WaveMod=0
    or 6]
FALSE         WvDiffQTF    - Full difference-frequency 2nd-order wave kinematics (flag)
FALSE         WvSumQTF     - Full summation-frequency 2nd-order wave kinematics (flag)
          0   WvLowCOffD   - Low frequency cutoff used in the difference-frequencies (rad/s) [Only used
                with a difference-frequency method]
        3.5   WvHiCOffD    - High frequency cutoff used in the difference-frequencies (rad/s) [Only used
               with a difference-frequency method]
        0.1   WvLowCOffS   - Low frequency cutoff used in the summation-frequencies (rad/s) [Only used
               with a summation-frequency method]
        3.5   WvHiCOffS    - High frequency cutoff used in the summation-frequencies (rad/s) [Only used
               with a summation-frequency method]
---------------------- CONSTRAINED WAVES -------------------------------------
          0   ConstWaveMod - Constrained wave model: 0=none; 1=Constrained wave with specified crest
                elevation, alpha; 2=Constrained wave with guaranteed peak-to-trough crest height, HCrest
                (flag)
          1   CrestHmax    - Crest height (2*alpha for ConstWaveMod=1 or HCrest for ConstWaveMod=2), must
                 be larger than WaveHs (m) [unused when ConstWaveMod=0]
         60   CrestTime    - Time at which the crest appears (s) [unused when ConstWaveMod=0]
          0   CrestXi      - X-position of the crest (m) [unused when ConstWaveMod=0]
          0   CrestYi      - Y-position of the crest (m) [unused when ConstWaveMod=0]
---------------------- CURRENT ------------------------------------------------ [unused with WaveMod=6]
          1   CurrMod      - Current profile model {0: none=no current, 1: standard, 2: user-defined from
                routine UserCurrent} (switch)
        1.4            CurrSSV0     - Sub-surface current velocity at still water level (m/s) [used only
               when CurrMod=1]
"DEFAULT"     CurrSSDir    - Sub-surface current heading direction (degrees) or DEFAULT (string) [used
    only when CurrMod=1]
         20   CurrNSRef    - Near-surface current reference depth     (meters) [used only when CurrMod=1]
          0   CurrNSV0     - Near-surface current velocity at still water level (m/s) [used only when
                CurrMod=1]
          0   CurrNSDir    - Near-surface current heading direction  (degrees) [used only when CurrMod=1]
          0   CurrDIV      - Depth-independent current velocity         (m/s) [used only when CurrMod=1]
          0   CurrDIDir    - Depth-independent current heading direction (degrees) [used only when
                CurrMod=1]
---------------------- MacCamy-Fuchs diffraction model -------------------------
          0   MCFD         - MacCamy-Fuchs member radius (ignored if radius <= 0) [must be 0 when WaveMod
                 0 or 6]
---------------------- OUTPUT --------------------------------------------------
False         SeaStSum     - Output a summary file [flag]
          2   OutSwtch     - Output requested channels to: [1=SeaState.out, 2=GlueCode.out, 3=both files]
"E15.7e2"     OutFmt       - Output format for numerical results (quoted string) [not checked for
    validity!]
"A11"         OutSFmt      - Output format for header strings (quoted string) [not checked for validity!]
          1   NWaveElev    - Number of points where the incident wave elevations can be computed (-) [
                maximum of 9 output locations]
          0   WaveElevxi   - List of xi-coordinates for points where the incident wave elevations can be
                output (meters) [NWaveElev points, separated by commas or white space; usused if
                NWaveElev = 0]
          0   WaveElevyi   - List of yi-coordinates for points where the incident wave elevations can be
                output (meters) [NWaveElev points, separated by commas or white space; usused if
                NWaveElev = 0]
          0   NWaveKin     - Number of points where the wave kinematics can be output (-) [maximum of 9
                output locations]
          0   WaveKinxi    - List of xi-coordinates for points where the wave kinematics can be output (
                meters) [NWaveKin points, separated by commas or white space; usused if NWaveKin = 0]
          0   WaveKinyi    - List of yi-coordinates for points where the wave kinematics can be output (
                meters) [NWaveKin points, separated by commas or white space; usused if NWaveKin = 0]
          0   WaveKinzi    - List of zi-coordinates for points where the wave kinematics can be output (
                meters) [NWaveKin points, separated by commas or white space; usused if NWaveKin = 0]
---------------------- OUTPUT CHANNELS -----------------------------------------
"Wave1Elev, Wave1Elv1"          - Wave elevation
END of output channels and end of file. (the word "END" must appear in the first 3 columns of this line)
```

F.0.5. Inflow File

```
1    ------- InflowWind v3.01.* INPUT FILE
         ------------------------------------------------------------------------
2  IEA 15 MW Offshore Reference Turbine
3  ---------------------------------------------------------------------------------------------------------------
4  False              Echo      - Echo input data to <RootName>.ech (flag)
5  3                  WindType  - switch for wind file type (1=steady; 2=uniform; 3=binary TurbSim FF; 4=
       binary Bladed-style FF; 5=HAWC format; 6=User defined; 7=native Bladed FF)
6  0.0                PropagationDir - Direction of wind propagation (meteoroligical rotation from aligned
       with X (positive rotates towards -Y) -- degrees)
7  0.0                VFlowAng  - Upflow angle (degrees) (not used for native Bladed format WindType=7)
8  False              VelInterpCubic - Use cubic interpolation for velocity in time (false=linear, true=
       cubic) [Used with WindType=2,3,4,5,7]
9  1                  NWindVel  - Number of points to output the wind velocity (0 to 9)
10 0.0                WindVxiList - List of coordinates in the inertial X direction (m)
11 0.0                WindVyiList - List of coordinates in the inertial Y direction (m)
12 145.0          WindVziList - List of coordinates in the inertial Z direction (m)
13 ================== Parameters for Steady Wind Conditions [used only for WindType = 1]
       =========================
14 10.0               HWindSpeed - Horizontal windspeed                    (m/s)
15 145.0          RefHt     - Reference height for horizontal wind speed (m)
16 0.12               PLexp     - Power law exponent                       (-)
17 ================== Parameters for Uniform wind file [used only for WindType = 2]
       ============================
18 "Wind/NoShr_9-14_Inc1_50s.wnd"          Filename_Uni - Filename of time series data for uniform wind
       field. (-)
19 145.0          RefHt_Uni - Reference height for horizontal wind speed       (m)
20 240.0              RefLength - Reference length for linear horizontal and vertical sheer (-)
21 ================== Parameters for Binary TurbSim Full-Field files [used only for WindType = 3]
       ==============
22 "D:\Thesis\Optimization_Project\openFAST\openfast\IEA-15-240-RWT\Wind/DLC6_3_Wind_40_Seed_1.bts"
       FileName_BTS - Name of the Full field wind file to use (.bts)
23 ================== Parameters for Binary Bladed-style Full-Field files [used only for WindType = 4]
       =========
24 "Wind/90m_12mps_twr"            FilenameRoot - Rootname of the full-field wind file to use (.wnd, .sum)
25 True               TowerFile - Have tower file (.twr) (flag)
26 ================== Parameters for HAWC-format binary files [Only used with WindType = 5]
       =====================
27 "none"             FileName_u - name of the file containing the u-component fluctuating wind (.bin)
28 "none"             FileName_v - name of the file containing the v-component fluctuating wind (.bin)
29 "none"             FileName_w - name of the file containing the w-component fluctuating wind (.bin)
30 64                 nx        - number of grids in the x direction (in the 3 files above) (-)
31 32                 ny        - number of grids in the y direction (in the 3 files above) (-)
32 32                 nz        - number of grids in the z direction (in the 3 files above) (-)
33 16.0               dx        - distance (in meters) between points in the x direction (m)
34 3.0                dy        - distance (in meters) between points in the y direction (m)
35 3.0                dz        - distance (in meters) between points in the z direction (m)
36 145.0              RefHt_Hawc - reference height; the height (in meters) of the vertical center of the
       grid (m)
37 ------------ Scaling parameters for turbulence ---------------------------------------------------------
38 2                  ScaleMethod - Turbulence scaling method [0 = none, 1 = direct scaling, 2 = calculate
       scaling factor based on a desired standard deviation]
39 1.0                SFx       - Turbulence scaling factor for the x direction (-) [ScaleMethod=1]
40 1.0                SFy       - Turbulence scaling factor for the y direction (-) [ScaleMethod=1]
41 1.0                SFz       - Turbulence scaling factor for the z direction (-) [ScaleMethod=1]
42 1.2                SigmaFx   - Turbulence standard deviation to calculate scaling from in x direction (m/
       s) [ScaleMethod=2]
43 0.8                SigmaFy   - Turbulence standard deviation to calculate scaling from in y direction (m/
       s) [ScaleMethod=2]
44 0.2                SigmaFz   - Turbulence standard deviation to calculate scaling from in z direction (m/
       s) [ScaleMethod=2]
45 ------------ Mean wind profile parameters (added to HAWC-format files) ---------------------------------
46 12.0               URef      - Mean u-component wind speed at the reference height (m/s)
47 2                  WindProfile - Wind profile type (0=constant;1=logarithmic,2=power law)
48 0.2                PLExp_Hawc - Power law exponent (-) (used for PL wind profile type only)
49 0.03               Z0        - Surface roughness length (m) (used for LG wind profile type only)
```

```
0                   XOffset    - Initial offset in +x direction (shift of wind box) (-)
================== LIDAR Parameters
     ================================================================================
0                   SensorType       - Switch for lidar configuration (0 = None, 1 = Single Point Beam(s),
      2 = Continuous, 3 = Pulsed)
0                   NumPulseGate     - Number of lidar measurement gates (used when SensorType = 3)
30                  PulseSpacing     - Distance between range gates (m) (used when SensorType = 3)
0                   NumBeam          - Number of lidar measurement beams (0-5)(used when SensorType = 1)
-200                FocalDistanceX   - Focal distance co-ordinates of the lidar beam in the x direction (
     relative to hub height) (only first coordinate used for SensorType 2 and 3) (m)
0                   FocalDistanceY   - Focal distance co-ordinates of the lidar beam in the y direction (
     relative to hub height) (only first coordinate used for SensorType 2 and 3) (m)
0                   FocalDistanceZ   - Focal distance co-ordinates of the lidar beam in the z direction (
     relative to hub height) (only first coordinate used for SensorType 2 and 3) (m)
0.0 0.0 0.0         RotorApexOffsetPos - Offset of the lidar from hub height (m)
17                  URefLid          - Reference average wind speed for the lidar[m/s]
0.25                MeasurementInterval - Time between each measurement [s]
False               LidRadialVel     - TRUE => return radial component, FALSE => return 'x' direction
     estimate
1                   ConsiderHubMotion - Flag whether to consider the hub motion's impact on Lidar
     measurements
====================== OUTPUT ==================================================
False               SumPrint  - Print summary data to <RootName>.IfW.sum (flag)
OutList    - The next line(s) contains a list of output parameters. See OutListParameters.xlsx for a
     listing of available output channels, (-)
Wind1VelX
Wind1VelY
Wind1VelZ
END of input file (the word "END" must appear in the first 3 columns of this last OutList line)
---------------------------------------------------------------------------------------
```

F.0.6. AeroDyn file

```
   ------- AERODYN v15.03.* INPUT FILE ------------------------------------------------
IEA 15 MW Offshore Reference Turbine
====== General Options ============================================================================
False               Echo       - Echo the input to "<rootname>.AD.ech"? (flag)
default             DTAero     - Time interval for aerodynamic calculations {or "default"} (s)
0                   Wake_Mod   -    ParkedIdilingOType of wake/induction model (switch) {0=none, 1=BEMT,
     2=DBEMT, 3=OLAF} [WakeMod cannot be 2 or 3 when linearizing]
1                   TwrPotent  - Type tower influence on wind based on potential flow around the tower (
     switch) {0=none, 1=baseline potential flow, 2=potential flow with Bak correction}
1                   TwrShadow  - Calculate tower influence on wind based on downstream tower shadow (
     switch) {0=none, 1=Powles model, 2=Eames model}
True                TwrAero    - Calculate tower aerodynamic loads? (flag)
False               CavitCheck - Perform cavitation check? (flag) [AFAeroMod must be 1 when CavitCheck=
     true]
False               Buoyancy   - Include buoyancy effects? (flag)
False               NacelleDrag - Include Nacelle Drag effects? (flag)
False               CompAA     - Flag to compute AeroAcoustics calculation [only used when WakeMod=1 or 2]
AeroAcousticsInput.dat AA_InputFile - AeroAcoustics input file [used only when CompAA=true]
====== Environmental Conditions ===================================================================
"default"           AirDens    - Air density (kg/m^3)
"default"           KinVisc    - Kinematic air viscosity (m^2/s)
"default"           SpdSound   - Speed of sound (m/s)
"default"           Patm       - Atmospheric pressure (Pa) [used only when CavitCheck=True]
"default"           Pvap       - Vapour pressure of fluid (Pa) [used only when CavitCheck=True]
====== Blade-Element/Momentum Theory Options ====================================================== [used
      only when WakeMod=1]
1                   BEM_Mod    - BEM model {1=legacy NoSweepPitchTwist, 2=polar} (switch) [used for all
     Wake_Mod to determine output coordinate system]
--- Skew correction
0                   Skew_Mod   -  Park2 Type of skewed-wake correction model (switch) {1=coupled, 0=
     uncoupled, -1=nonlinear} [unused when WakeMod=0 or 3]
False               SkewMomCorr - Turn the skew momentum correction on or off [used only when Skew_Mod=1]
default             SkewRedistr_Mod - Type of skewed-wake correction model (switch) {0=no redistribution,
     1=Glauert/Pitt/Peters, default=1} [used only when Skew_Mod=1]
"default"           SkewRedistrFactor - Constant used in Pitt/Peters skewed wake model {or "default" is
     15/32*pi} (-) [used only when Skew_Mod=1 and SkewRedistr_Mod=1]
--- BEM algorithm
```

```
True                TipLoss    - Use the Prandtl tip-loss model? (flag) [unused when WakeMod=0 or 3]
True                HubLoss    - Use the Prandtl hub-loss model? (flag) [unused when WakeMod=0 or 3]
True                TanInd     - Include tangential induction in BEMT calculations? (flag) [unused when
     WakeMod=0 or 3]
True                AIDrag     - Include the drag term in the axial-induction calculation? (flag) [unused
     when WakeMod=0 or 3]
True                TIDrag     - Include the drag term in the tangential-induction calculation? (flag) [
     unused when WakeMod=0,3 or TanInd=FALSE]
default             IndToler   - Convergence tolerance for BEMT nonlinear solve residual equation {or "
     default"} (-) [unused when WakeMod=0 or 3]
500                 MaxIter    - Maximum number of iteration steps (-) [unused when WakeMod=0]
--- Shear correction
False               SectAvg    - Use sector averaging (flag)
1                   SectAvgWeighting - Weighting function for sector average {1=Uniform, default=1} within
      a sector centered on the blade (switch) [used only when SectAvg=True]
default             SectAvgNPoints - Number of points per sectors (-) {default=5} [used only when SectAvg=
     True]
default             SectAvgPsiBwd - Backward azimuth relative to blade where the sector starts (<=0) {
     default=-60} (deg) [used only when SectAvg=True]
default             SectAvgPsiFwd - Forward azimuth relative to blade where the sector ends (>=0) {default
     =60} (deg) [used only when SectAvg=True]
--- Dynamic wake/inflow
2                   DBEMT_Mod - Type of dynamic BEMT (DBEMT) model {1=constant tau1, 2=time-dependent
     tau1} (-) [used only when WakeMod=2]
29.03               tau1_const - Time constant for DBEMT (s) [used only when WakeMod=2 and DBEMT_Mod=1]
====== OLAF -- cOnvecting LAgrangian Filaments (Free Vortex Wake) Theory Options ================== [used
      only when WakeMod=3]
../IEA-15-240-RWT-OLAF/IEA-15-240-RWT_OLAF.dat OLAFInputFileName - Input file for OLAF [used only when
     WakeMod=3]
====== Unsteady Airfoil Aerodynamics Options ====================================================
False               AoA34      -     TrueParkedIdilingAFAeroMOD =1UA_Mod =0AoA34= FalseSample the angle of
     attack (AoA) at the 3/4 chord or the AC point {default=True} [always used]
0                   UAMod      -   3  ParkedIdilingAFAeroMOD =1UA_Mod =0AoA34= FalseUnsteady Aero Model
     Switch (switch) {1=Baseline model (Original), 2=Gonzalez's variant (changes in Cn,Cc,Cm), 3=Minnema/
     Pierce variant (changes in Cc and Cm)} [used only when AFAeroMod=2]
True                FLookup    - Flag to indicate whether a lookup for f' will be calculated (TRUE) or
     whether best-fit exponential equations will be used (FALSE); if FALSE S1-S4 must be provided in
     airfoil input files (flag) [used only when AFAeroMod=2]
3            IntegrationMethod - Switch to indicate which integration method UA uses (1=RK4, 2=AB4, 3=
     ABM4, 4=BDF2)
0.1                 UAStartRad - Starting radius for dynamic stall (fraction of rotor radius) [used only
     when AFAeroMod=2]
1.0                 UAEndRad   - Ending radius for dynamic stall (fraction of rotor radius) [used only
     when AFAeroMod=2]
====== Airfoil Information ======================================================================
1                   AFTabMod   - Interpolation method for multiple airfoil tables {1=1D interpolation on
     AoA (first table only); 2=2D interpolation on AoA and Re; 3=2D interpolation on AoA and UserProp}
     (-)
1                   InCol_Alfa - The column in the airfoil tables that contains the angle of attack (-)
2                   InCol_Cl   - The column in the airfoil tables that contains the lift coefficient (-)
3                   InCol_Cd   - The column in the airfoil tables that contains the drag coefficient (-)
4                   InCol_Cm   - The column in the airfoil tables that contains the pitching-moment
     coefficient; use zero if there is no Cm column (-)
0                   InCol_Cpmin - The column in the airfoil tables that contains the Cpmin coefficient;
     use zero if there is no Cpmin column (-)
50                  NumAFfiles - Number of airfoil files used (-)
"IEA-15-240-RWT/Airfoils/IEA-15-240-RWT_AeroDyn15_Polar_00.dat" AFNames  - Airfoil file names (NumAFfiles
      lines) (quoted strings)
"IEA-15-240-RWT/Airfoils/IEA-15-240-RWT_AeroDyn15_Polar_01.dat"
"IEA-15-240-RWT/Airfoils/IEA-15-240-RWT_AeroDyn15_Polar_02.dat"
"IEA-15-240-RWT/Airfoils/IEA-15-240-RWT_AeroDyn15_Polar_03.dat"
"IEA-15-240-RWT/Airfoils/IEA-15-240-RWT_AeroDyn15_Polar_04.dat"
"IEA-15-240-RWT/Airfoils/IEA-15-240-RWT_AeroDyn15_Polar_05.dat"
"IEA-15-240-RWT/Airfoils/IEA-15-240-RWT_AeroDyn15_Polar_06.dat"
"IEA-15-240-RWT/Airfoils/IEA-15-240-RWT_AeroDyn15_Polar_07.dat"
"IEA-15-240-RWT/Airfoils/IEA-15-240-RWT_AeroDyn15_Polar_08.dat"
"IEA-15-240-RWT/Airfoils/IEA-15-240-RWT_AeroDyn15_Polar_09.dat"
"IEA-15-240-RWT/Airfoils/IEA-15-240-RWT_AeroDyn15_Polar_10.dat"
"IEA-15-240-RWT/Airfoils/IEA-15-240-RWT_AeroDyn15_Polar_11.dat"
"IEA-15-240-RWT/Airfoils/IEA-15-240-RWT_AeroDyn15_Polar_12.dat"
"IEA-15-240-RWT/Airfoils/IEA-15-240-RWT_AeroDyn15_Polar_13.dat"
```

```
"IEA-15-240-RWT/Airfoils/IEA-15-240-RWT_AeroDyn15_Polar_14.dat"
"IEA-15-240-RWT/Airfoils/IEA-15-240-RWT_AeroDyn15_Polar_15.dat"
"IEA-15-240-RWT/Airfoils/IEA-15-240-RWT_AeroDyn15_Polar_16.dat"
"IEA-15-240-RWT/Airfoils/IEA-15-240-RWT_AeroDyn15_Polar_17.dat"
"IEA-15-240-RWT/Airfoils/IEA-15-240-RWT_AeroDyn15_Polar_18.dat"
"IEA-15-240-RWT/Airfoils/IEA-15-240-RWT_AeroDyn15_Polar_19.dat"
"IEA-15-240-RWT/Airfoils/IEA-15-240-RWT_AeroDyn15_Polar_20.dat"
"IEA-15-240-RWT/Airfoils/IEA-15-240-RWT_AeroDyn15_Polar_21.dat"
"IEA-15-240-RWT/Airfoils/IEA-15-240-RWT_AeroDyn15_Polar_22.dat"
"IEA-15-240-RWT/Airfoils/IEA-15-240-RWT_AeroDyn15_Polar_23.dat"
"IEA-15-240-RWT/Airfoils/IEA-15-240-RWT_AeroDyn15_Polar_24.dat"
"IEA-15-240-RWT/Airfoils/IEA-15-240-RWT_AeroDyn15_Polar_25.dat"
"IEA-15-240-RWT/Airfoils/IEA-15-240-RWT_AeroDyn15_Polar_26.dat"
"IEA-15-240-RWT/Airfoils/IEA-15-240-RWT_AeroDyn15_Polar_27.dat"
"IEA-15-240-RWT/Airfoils/IEA-15-240-RWT_AeroDyn15_Polar_28.dat"
"IEA-15-240-RWT/Airfoils/IEA-15-240-RWT_AeroDyn15_Polar_29.dat"
"IEA-15-240-RWT/Airfoils/IEA-15-240-RWT_AeroDyn15_Polar_30.dat"
"IEA-15-240-RWT/Airfoils/IEA-15-240-RWT_AeroDyn15_Polar_31.dat"
"IEA-15-240-RWT/Airfoils/IEA-15-240-RWT_AeroDyn15_Polar_32.dat"
"IEA-15-240-RWT/Airfoils/IEA-15-240-RWT_AeroDyn15_Polar_33.dat"
"IEA-15-240-RWT/Airfoils/IEA-15-240-RWT_AeroDyn15_Polar_34.dat"
"IEA-15-240-RWT/Airfoils/IEA-15-240-RWT_AeroDyn15_Polar_35.dat"
"IEA-15-240-RWT/Airfoils/IEA-15-240-RWT_AeroDyn15_Polar_36.dat"
"IEA-15-240-RWT/Airfoils/IEA-15-240-RWT_AeroDyn15_Polar_37.dat"
"IEA-15-240-RWT/Airfoils/IEA-15-240-RWT_AeroDyn15_Polar_38.dat"
"IEA-15-240-RWT/Airfoils/IEA-15-240-RWT_AeroDyn15_Polar_39.dat"
"IEA-15-240-RWT/Airfoils/IEA-15-240-RWT_AeroDyn15_Polar_40.dat"
"IEA-15-240-RWT/Airfoils/IEA-15-240-RWT_AeroDyn15_Polar_41.dat"
"IEA-15-240-RWT/Airfoils/IEA-15-240-RWT_AeroDyn15_Polar_42.dat"
"IEA-15-240-RWT/Airfoils/IEA-15-240-RWT_AeroDyn15_Polar_43.dat"
"IEA-15-240-RWT/Airfoils/IEA-15-240-RWT_AeroDyn15_Polar_44.dat"
"IEA-15-240-RWT/Airfoils/IEA-15-240-RWT_AeroDyn15_Polar_45.dat"
"IEA-15-240-RWT/Airfoils/IEA-15-240-RWT_AeroDyn15_Polar_46.dat"
"IEA-15-240-RWT/Airfoils/IEA-15-240-RWT_AeroDyn15_Polar_47.dat"
"IEA-15-240-RWT/Airfoils/IEA-15-240-RWT_AeroDyn15_Polar_48.dat"
"IEA-15-240-RWT/Airfoils/IEA-15-240-RWT_AeroDyn15_Polar_49.dat"
====== Rotor/Blade Properties ===================================================================
True               UseBlCm    - Include aerodynamic pitching moment in calculations? (flag)
"IEA-15-240-RWT/IEA-15-240-RWT_AeroDyn15_blade.dat" ADBlFile(1) - Name of file containing distributed
    aerodynamic properties for Blade #1 (-)
"IEA-15-240-RWT/IEA-15-240-RWT_AeroDyn15_blade.dat" ADBlFile(2) - Name of file containing distributed
    aerodynamic properties for Blade #2 (-) [unused if NumBl < 2]
"IEA-15-240-RWT/IEA-15-240-RWT_AeroDyn15_blade.dat" ADBlFile(3) - Name of file containing distributed
    aerodynamic properties for Blade #3 (-) [unused if NumBl < 3]
====== Hub Properties ======================================================================== [
    used only when Buoyancy=True]
0.0  VolHub          - Hub volume (m^3)
0.0  HubCenBx        - Hub center of buoyancy x direction offset (m)
====== Nacelle Properties ==================================================================== [
    used only when Buoyancy=True]
0.0  VolNac          - Nacelle volume (m^3)
0,0,0 NacCenB        - Position of nacelle center of buoyancy from yaw bearing in nacelle coordinates (m)
0, 0, 0    NacArea      - Projected area of the nacelle in X, Y, Z in the nacelle coordinate system (m^2)
0, 0, 0  NacCd        - Drag coefficient for the nacelle areas defined above (-)
0, 0, 0       NacDragAC       - Position of aerodynamic center of nacelle drag in nacelle coordinates (m)
====== Tail fin Aerodynamics ====================================================================
False       TFinAero        - Calculate tail fin aerodynamics model (flag)
"unused"    TFinFile        - Input file for tail fin aerodynamics [used only when TFinAero=True]
====== Tower Influence and Aerodynamics ========================================================== [
    used only when TwrPotent/=0, TwrShadow/=0, or TwrAero=True]
17            NumTwrNds - Number of tower nodes used in the analysis (-) [used only when TwrPotent/=0,
    TwrShadow/=0, or TwrAero=True]
TwrElev      TwrDiam      TwrCd       TwrTI     TwrCb !TwrTI used only with TwrShadow=2, TwrCb used only
    with Buoyancy=True
(m)            (m)          (-)          (-)       (-)
   29.000    11.700    0.500     0.100     0
   36.250    11.375    0.500     0.100     0
   43.500    11.050    0.500     0.100     0
   50.750    10.725    0.500     0.100     0
   58.000    10.400    0.500     0.100     0
   65.250    10.075    0.500     0.100     0
```

```
   72.500   9.750    0.500    0.100    0
   79.750   9.425    0.500    0.100    0
   87.000   9.100    0.500    0.100    0
   94.250   8.775    0.500    0.100    0
   101.500  8.450    0.500    0.100    0
   108.750  8.125    0.500    0.100    0
   116.000  7.800    0.500    0.100    0
   123.250  7.475    0.500    0.100    0
   130.500  7.150    0.500    0.100    0
   137.750  6.825    0.500    0.100    0
   145.000  6.500    0.500    0.100    0
====== Outputs ==============================================================================
False              SumPrint  - Generate a summary file listing input options and interpolated properties to "<rootname>.AD.sum"? (flag)
9                  NBlOuts   - Number of blade node outputs [0 - 9] (-)
6, 11, 16, 21, 25, 30, 35, 40, 45 BlOutNd - Blade nodes whose values will be output (-)
0                  NTwOuts   - Number of tower node outputs [0 - 9] (-)
0                  TwOutNd   - Tower nodes whose values will be output (-)
                OutList          - The next line(s) contains a list of output parameters. See OutListParameters.xlsx for a listing of available output channels, (-)
"RtFldCp"
"RtFldCt"
"RtArea"
"RtSpeed"
"RtTSR"
END of input file (the word "END" must appear in the first 3 columns of this last OutList line)
====== Outputs for all blade stations (same ending as above for B1N1.... ========================== [optional section]
  1           BldNd_BladesOut  - Number of blades to output all node information at. Up to number of blades on turbine. (-)
  "All"       BldNd_BlOutNd    - Future feature will allow selecting a portion of the nodes to output. Not implemented yet. (-)
              OutList          - The next line(s) contains a list of output parameters. See OutListParameters.xlsx for a listing of available output channels, (-)
END (the word "END" must appear in the first 3 columns of this last OutList line in the optional nodal output section)
```

F.0.7. MoorDyn file

```
   ---------------------- MoorDyn Input File ------------------------------------
IEA 15 MW offshore reference model on CSpar floating platform MoorDyn v2 input properties
FALSE   Echo     - echo the input file data (flag)
---------------------- LINE TYPES -------------------------------------------
Name Diam MassDen EA     BA/-zeta EI   Cd=(Cdn)  Ca(=Can)  CdAx(=Cdt) CaAx(=Cat)
(-)  (m)  (kg/m)  (N)    (N-s/-)  (-)  (-)  (-)  (-)   (-)
CHAIN 0.16 561.252 2.304E+09 -1.0   0   2.0  1   0.8   0.0
---------------------- POINTS -----------------------------------
ID  Type     X      Y      Z      M    V    CdA  CA
(-) (-)     (m)    (m)    (m)    (kg) (m^3) (m^2) (-)
1   fixed  -600      0       -200    0    0    0   0
2   Free   -47.665   0       -114.23 0    0    0   0
3   fixed  300        -519.6152 -200   0   0   0   0
4   Free   23.8325 -41.2791 -114.23 0 0   0   0
5   fixed  300 519.6152  -200   0   0   0   0
6   Free   23.8325 41.2791 -114.23 0 0 0  0
7   vessel -4.65  8.054  -90 0  0   0   0
8   vessel -4.65  -8.054 -90 0  0   0   0
9   vessel 9.3 0  -90 0  0   0   0
10  vessel -4.65  8.054  -90 0  0   0   0
11  vessel -4.65  -8.054 -90 0  0   0   0
12  vessel 9.3 0  -90 0  0   0   0

---------------------- LINES ------------------------------------
ID  LineType AttachA AttachB UnstrLen NumSegs Outputs
(-)  (-)      (-)      (-)     (m)      (-)     (-)
1   CHAIN  1   2   565 15 -
2   CHAIN  2   7   50  2   -
3   CHAIN  2   11  50  2   -
4   CHAIN  3   4   565 15 -
5   CHAIN  4   8   50  2   -
```

```
6   CHAIN  4   12  50  2   -
7   CHAIN  5   6   565 15  -
8   CHAIN  6   10  50  2   -
9   CHAIN  6   9   50  2   -

---------------------- SOLVER OPTIONS ---------------------------------------
0.01    dtM      - time step to use in mooring integration (s)
3.0e5   kbot     - bottom stiffness (Pa/m)
3.0e4   cbot     - bottom damping (Pa-s/m)
2.0     dtIC     - time interval for analyzing convergence during IC gen (s)
60.0    TmaxIC   - max time for ic gen (s)
4.0     CdScaleIC - factor by which to scale drag coefficients during dynamic relaxation (-)
0.01    threshIC - threshold for IC convergence (-)
------------------------ OUTPUTS ----------------------------------------------
LINE2N2FZ
LINE3N2FZ
LINE5N2FZ
LINE6N2FZ
LINE8N2FZ
LINE9N2FZ
END
------------------------- need this line ------------------------------------
```

F.0.8. ServoDyn file

```
   ------- SERVODYN v1.05.* INPUT FILE ------------------------------------------
IEA 15 MW WindCrete Gran Canaria COREWIND

---------------------- SIMULATION CONTROL --------------------------------------
False               Echo      - Echo input data to <RootName>.ech (flag)
"default"           DT        - Communication interval for controllers (s) (or "default")
---------------------- PITCH CONTROL -------------------------------------------
0                   PCMode    - Pitch control mode {0: none, 3: user-defined from routine PitchCntrl, 4:
    user-defined from Simulink/Labview, 5: user-defined from Bladed-style DLL} (switch)
0.0                 TPCOn     - Time to enable active pitch control (s) [unused when PCMode=0]
9999.9              TPitManS(1) - Time to start override pitch maneuver for blade 1 and end standard pitch
     control (s)
9999.9              TPitManS(2) - Time to start override pitch maneuver for blade 2 and end standard pitch
     control (s)
9999.9              TPitManS(3) - Time to start override pitch maneuver for blade 3 and end standard pitch
     control (s) [unused for 2 blades]
2.0                 PitManRat(1) - Pitch rate at which override pitch maneuver heads toward final pitch
    angle for blade 1 (deg/s)
2.0                 PitManRat(2) - Pitch rate at which override pitch maneuver heads toward final pitch
    angle for blade 2 (deg/s)
2.0                 PitManRat(3) - Pitch rate at which override pitch maneuver heads toward final pitch
    angle for blade 3 (deg/s) [unused for 2 blades]
0.0                 BlPitchF(1) - Blade 1 final pitch for pitch maneuvers (degrees)
0.0                 BlPitchF(2) - Blade 2 final pitch for pitch maneuvers (degrees)
0.0                 BlPitchF(3) - Blade 3 final pitch for pitch maneuvers (degrees) [unused for 2 blades]
---------------------- GENERATOR AND TORQUE CONTROL ----------------------------
0                   VSContrl  - Variable-speed control mode {0: none, 1: simple VS, 3: user-defined from
    routine UserVSCont, 4: user-defined from Simulink/Labview, 5: user-defined from Bladed-style DLL} (
    switch)
2                   GenModel  - Generator model {1: simple, 2: Thevenin, 3: user-defined from routine
    UserGen} (switch) [used only when VSContrl=0]
96.55               GenEff    - Generator efficiency [ignored by the Thevenin and user-defined generator
    models] (%)
True                GenTiStr  - Method to start the generator {T: timed using TimGenOn, F: generator
    speed using SpdGenOn} (flag)
True                GenTiStp  - Method to stop the generator {T: timed using TimGenOf, F: when generator
    power = 0} (flag)
9999.9              SpdGenOn  - Generator speed to turn on the generator for a startup (HSS speed) (rpm)
    [used only when GenTiStr=False]
9999.9              TimGenOn  -  GeneratorTime to turn on the generator for a startup (s) [used only when
    GenTiStr=True]
9999.9              TimGenOf  - Time to turn off the generator (s) [used only when GenTiStp=True]
---------------------- SIMPLE VARIABLE-SPEED TORQUE CONTROL --------------------
7.559987120819503   VS_RtGnSp - Rated generator speed for simple variable-speed generator control (HSS
    side) (rpm) [used only when VSContrl=1]
```

```
19624046.66639      VS_RtTq    - Rated generator torque/constant generator torque in Region 3 for simple variable-speed generator control (HSS side) (N-m) [used only when VSContrl=1]
343357.4355671095   VS_Rgn2K   - Generator torque constant in Region 2 for simple variable-speed generator control (HSS side) (N-m/rpm^2) [used only when VSContrl=1]
2.                  VS_SlPc    - Rated generator slip percentage in Region 2 1/2 for simple variable-speed generator control (%) [used only when VSContrl=1]
---------------------- SIMPLE INDUCTION GENERATOR ------------------------------
9999.9              SIG_SlPc   - Rated generator slip percentage (%) [used only when VSContrl=0 and GenModel=1]
9999.9              SIG_SySp   - Synchronous (zero-torque) generator speed (rpm) [used only when VSContrl=0 and GenModel=1]
9999.9              SIG_RtTq   - Rated torque (N-m) [used only when VSContrl=0 and GenModel=1]
9999.9              SIG_PORt   - Pull-out ratio (Tpullout/Trated) (-) [used only when VSContrl=0 and GenModel=1]
---------------------- THEVENIN-EQUIVALENT INDUCTION GENERATOR -----------------
9999.9              TEC_Freq   - Line frequency [50 or 60] (Hz) [used only when VSContrl=0 and GenModel=2]
9998                TEC_NPol   - Number of poles [even integer > 0] (-) [used only when VSContrl=0 and GenModel=2]
9999.9              TEC_SRes   - Stator resistance (ohms) [used only when VSContrl=0 and GenModel=2]
9999.9              TEC_RRes   - Rotor resistance (ohms) [used only when VSContrl=0 and GenModel=2]
9999.9              TEC_VLL    - Line-to-line RMS voltage (volts) [used only when VSContrl=0 and GenModel=2]
9999.9              TEC_SLR    - Stator leakage reactance (ohms) [used only when VSContrl=0 and GenModel=2]
9999.9              TEC_RLR    - Rotor leakage reactance (ohms) [used only when VSContrl=0 and GenModel=2]
9999.9              TEC_MR     - Magnetizing reactance (ohms) [used only when VSContrl=0 and GenModel=2]
---------------------- HIGH-SPEED SHAFT BRAKE ----------------------------------
0                   HSSBrMode - HSS brake model {0: none, 1: simple, 3: user-defined from routine UserHSSBr, 4: user-defined from Simulink/Labview, 5: user-defined from Bladed-style DLL} (switch)
9999.9              THSSBrDp   - Time to initiate deployment of the HSS brake (s)
0.6                 HSSBrDT    - Time for HSS-brake to reach full deployment once initiated (sec) [used only when HSSBrMode=1]
28116.2             HSSBrTqF   - Fully deployed HSS-brake torque (N-m)
---------------------- NACELLE-YAW CONTROL --------------------------------------
0                   YCMode     - Yaw control mode {0: none, 3: user-defined from routine UserYawCont, 4: user-defined from Simulink/Labview, 5: user-defined from Bladed-style DLL} (switch)
9999.9              TYCOn      - Time to enable active yaw control (s) [unused when YCMode=0]
0                      YawNeut           - Neutral yaw position--yaw spring force is zero at this yaw (degrees)
8458453511.0        YawSpr     - Nacelle-yaw spring constant (N-m/rad)
28561762.0          YawDamp    - Nacelle-yaw damping constant (N-m/(rad/s))
9999.9              TYawManS   - Time to start override yaw maneuver and end standard yaw control (s)
0.25                YawManRat  - Yaw maneuver rate (in absolute value) (deg/s)
0.0                 NacYawF    - Final yaw angle for override yaw maneuvers (degrees)
---------------------- Aerodynamic Flow Control --------------------------------
0                   AfCmode    - Airfoil control mode {0- none, 1- cosine wave cycle, 4- user-defined from Simulink/Labview, 5- user-defined from Bladed-style DLL}
0.0                 AfC_Mean   - Mean level for sinusoidal cycling or steady value (-) [used only with AfCmode==1]
0.0                 AfC_Amp    - Amplitude for for cosine cycling of flap signal (AfC = AfC_Amp*cos(Azimuth+phase)+AfC_mean) (-) [used only with AfCmode==1]
0.0                 AfC_phase  - Phase relative to the blade azimuth (0 is vertical) for for cosine cycling of flap signal (deg) [used only with AfCmode==1]
---------------------- STRUCTURAL CONTROL ---------------------------------------
0                   NumBStC    - Number of blade structural controllers (integer)
"unused"            BStCfiles  - Name of the file for blade tuned mass damper (quoted string) [unused when CompNTMD is false]
0                   NumNStC    - Number of nacelle structural controllers (integer)
"unused"            NStCfiles  - Name of the file for nacelle tuned mass damper (quoted string) [unused when CompNTMD is false]
0                   NumTStC    - Number of tower structural controllers (integer)
"unused"            TStCfiles  - Name of the file for tower tuned mass damper (quoted string) [unused when CompNTMD is false]
0                   NumSStC    - Number of sbustructure structural controllers (integer)
"unused"            SStCfiles  - Name of the file for sbustructure tuned mass damper (quoted string) [unused when CompNTMD is false]
---------------------- CABLE CONTROL --------------------------------------------
0                   CCmode     - Cable control mode {0- none, 4- user-defined from Simulink/Labview, 5- user-defineAfC_phased from Bladed-style DLL}
---------------------- BLADED INTERFACE ---------------------------------------- [used only with Bladed Interface]
```

```
"D:/Thesis/Optimization_Project/openFAST/openfast/ServoData/DISCON.dll" DLL_FileName - Name/location of the dynamic library {.dll [Windows] or .so [Linux]} in the Bladed-DLL format (-) [used only with Bladed Interface]
"D:/Thesis/Optimization_Project/openFAST/openfast/DISCON.IN" DLL_InFile - Name of input file sent to the DLL (-) [used only with Bladed Interface]
"DISCON"           DLL_ProcName - Name of procedure in DLL to be called (-) [case sensitive; used only with DLL Interface]
"default"          DLL_DT    - Communication interval for dynamic library (s) (or "default") [used only with Bladed Interface]
True               DLL_Ramp  - Whether a linear ramp should be used between DLL_DT time steps [introduces time shift when true] (flag) [used only with Bladed Interface]
9999.9             BPCutoff  - Cuttoff frequency for low-pass filter on blade pitch from DLL (Hz) [used only with Bladed Interface]
0.0                NacYaw_North - Reference yaw angle of the nacelle when the upwind end points due North (deg) [used only with Bladed Interface]
0                  Ptch_Cntrl - Record 28: Use individual pitch control {0: collective pitch; 1: individual pitch control} (switch) [used only with Bladed Interface]
0.0                Ptch_SetPnt - Record 5: Below-rated pitch angle set-point (deg) [used only with Bladed Interface]
0.0                Ptch_Min  - Record 6: Minimum pitch angle (deg) [used only with Bladed Interface]
0.0                Ptch_Max  - Record 7: Maximum pitch angle (deg) [used only with Bladed Interface]
0.0                PtchRate_Min - Record 8: Minimum pitch rate (most negative value allowed) (deg/s) [used only with Bladed Interface]
0.0                PtchRate_Max - Record 9: Maximum pitch rate (deg/s) [used only with Bladed Interface]
0.0                Gain_OM   - Record 16: Optimal mode gain (Nm/(rad/s)^2) [used only with Bladed Interface]
0.0                GenSpd_MinOM - Record 17: Minimum generator speed (rpm) [used only with Bladed Interface]
0.0                GenSpd_MaxOM - Record 18: Optimal mode maximum speed (rpm) [used only with Bladed Interface]
0.0                GenSpd_Dem - Record 19: Demanded generator speed above rated (rpm) [used only with Bladed Interface]
0.0                GenTrq_Dem - Record 22: Demanded generator torque above rated (Nm) [used only with Bladed Interface]
0.0                GenPwr_Dem - Record 13: Demanded power (W) [used only with Bladed Interface]
---------------------- BLADED INTERFACE TORQUE-SPEED LOOK-UP TABLE -------------
0                  DLL_NumTrq - Record 26: No. of points in torque-speed look-up table {0 = none and use the optimal mode parameters; nonzero = ignore the optimal mode PARAMETERs by setting Record 16 to 0.0} (-) [used only with Bladed Interface]
GenSpd_TLU          GenTrq_TLU
(rpm)               (Nm)
---------------------- OUTPUT --------------------------------------------------
True               SumPrint  - Print summary data to <RootName>.sum (flag) (currently unused)
1                  OutFile   - Switch to determine where output will be placed: {1: in module output file only; 2: in glue code output file only; 3: both} (currently unused)
True               TabDelim  - Use tab delimiters in text tabular output file? (flag) (currently unused)
"ES10.3E2"         OutFmt    - Format used for text tabular output (except time). Resulting field should be 10 characters. (quoted string) (currently unused)
30.0               TStart    - Time to begin tabular output (s) (currently unused)
            OutList    - The next line(s) contains a list of output parameters. See OutListParameters.xlsx for a listing of available output channels, (-)
"GenPwr"
"GenTq"
END of input file (the word "END" must appear in the first 3 columns of this last OutList line)
---------------------------------------------------------------------------------------
```

G

Structural maximum loadings distribution

G.1. Rigid Spar Model

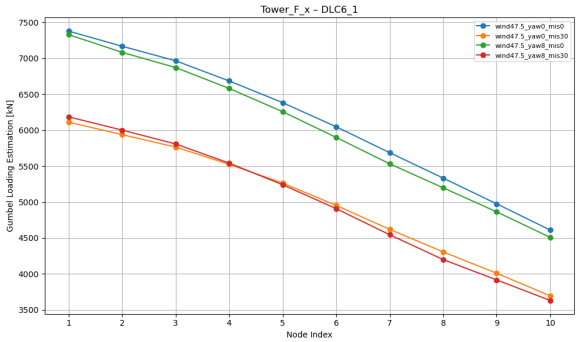

(a) Tower Force F_x - DLC 6.1

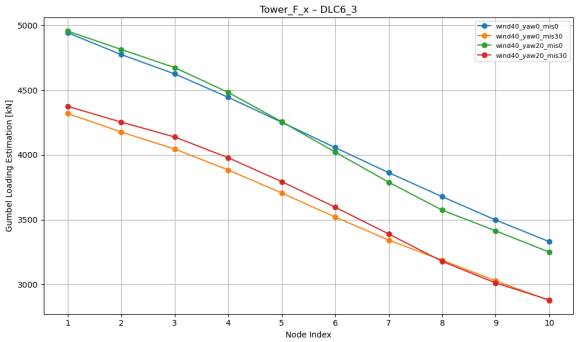

(b) Tower Force F_x - DLC 6.3

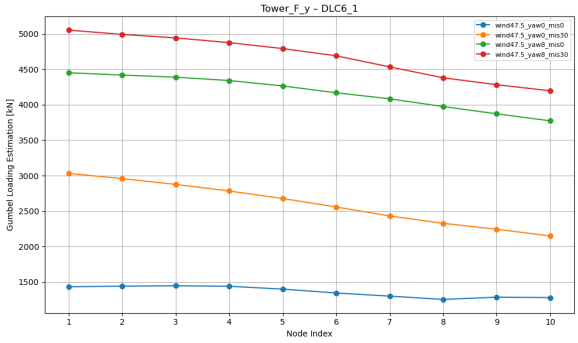

(c) Tower Force F_y - DLC 6.1

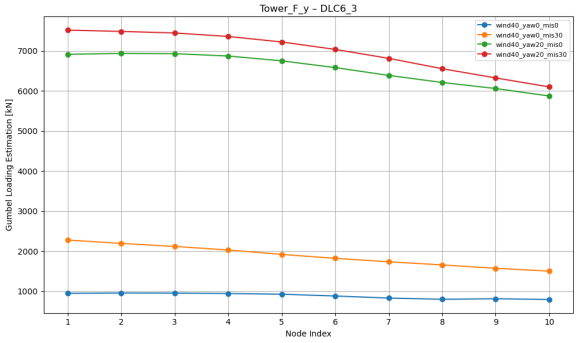

(d) Tower Force F_y - DLC 6.3

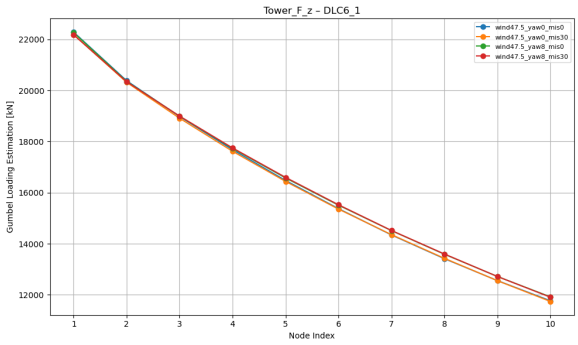

(e) Tower Force F_z - DLC 6.1

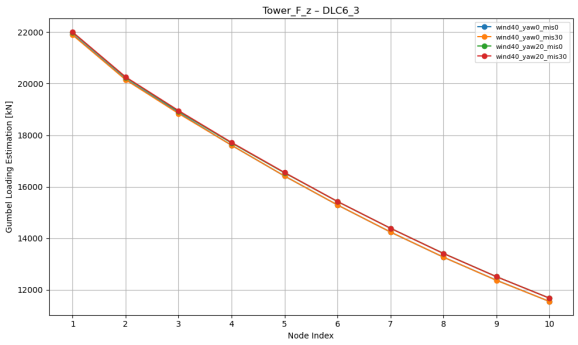

(f) Tower Force F_z - DLC 6.3

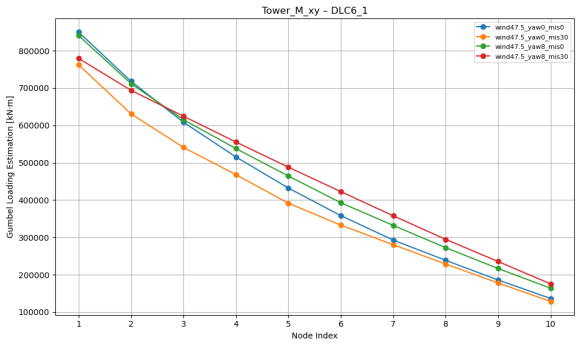

(g) Tower Bending Moments M_{xy} - DLC 6.1

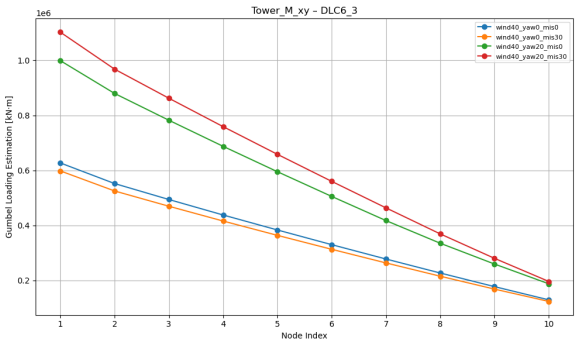

(h) Tower Bending Moments M_{xy} - DLC 6.3

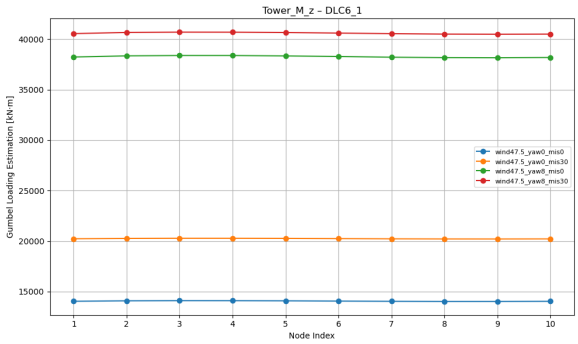

(i) Tower Bending Moments M_z - DLC 6.1

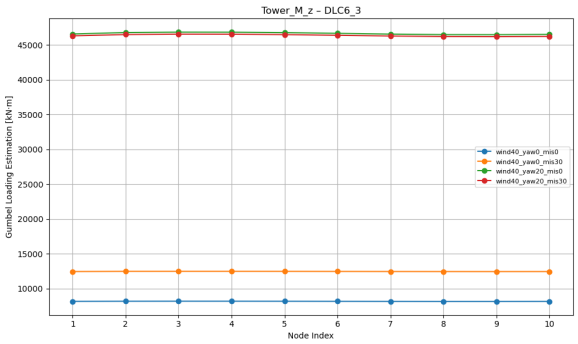

(j) Tower Bending Moments M_z - DLC 6.3